TECHNISCHE UNIVERSITÄT MÜNCHEN

Lehrstuhl II für Technische Chemie

Dry reforming- From understanding the elementary steps to better catalysts

Yu Lou

Vollständiger Abdruck der von der Fakultät für Chemie der Technischen Universität München zur Erlangung des akademischen Grades eines

Doktors der Naturwissenschaften (Dr. rer. nat.)

genehmigten Dissertation.

Vorsitzender: Univ.-Prof. Dr. Kai-Olaf Hinrichsen

Prüfer der Dissertation:

1. Univ.-Prof. Dr. Johannes A. Lercher
2. Univ.-Prof. Dr. Tom Nilges

Die Dissertation wurde am 15.02.2017 bei der Technischen Universität München eingereicht und durch die Fakultät für Chemie am 16.03.2017 angenommen.

Statutory Declaration

I declare that I have authored this thesis independently and that I have solely used the declared (re)sources and that I have marked all material, which has been quoted either literally or by content from the used sources. At the end of each chapter all collaborators are named and their specific contribution is addressed. Published content of this thesis is clearly marked.

_____ , _____ _____

One needs 3 things to be truly happy living in the world: something to do, someone to love, something to hope for.

Acknowledgements

Completion of this doctoral dissertation was possible with the support of several people.

First, I am very grateful to Professor Johannes A. Lercher, the supervisor of my doctoral work. Thank you for offering me the position in this international group and giving me the opportunity to work on this interesting project. It has been a real pleasure to do this thesis under your supervision and I would thank you for your insightful guidance and support throughout this project.

I am also grateful to Professor Andreas Jentys. The discussions with you throughout my doctoral work are really memorable. Thank you for giving me the freedom to pursue my own ideas that I have been interested in and for your valuable scientific advice.

I am also very thankful to Dr. Yue Liu for his insightful thoughts during the numerous times of discussion in the final stage of my graduation study.

Next, I would like to thank the members of CO_2 group. I thank Edith Berger for the organization of TGA measurements and schlenk system. And special thanks to my co-worker Matthias Steib, who has contributed to the EXAFS measurements and shared his knowledge with me.

I would like to thank all the technical and administrative staffs for their kind assistance. I thank Xaver Hecht for the BET and hydrogen chemisorption measurements and for solving technical problems. Martin Neukamm is acknowledged for his support in the order of chemicals and labware and AAS measurements. I also thank Andreas Marx for his efforts with all the electronic devices. Stefanie Seibold, Helen Brenner, Bettina Federmann, Karen Schulz and Ulrike Sanwald are acknowledged for their administrative assistance.

My colleagues, Dr. Elisabeth Hanrieder and Dr. Sebastian Grundner, who spared their time to perform TEM measurements for my samples, I acknowledge your contributions. My officemates, Yuanshuai Liu, Ruixue Zhao, Andreas Ehrmaier, Sebastian Eckestein, Dr. Yulia Martynova, Dr. Christian Gärtner, Dr. Linus Schulz and Dr. Wenhao Luo are acknowledged for a friendly and cooperative work environment. I am very grateful to all the members of this international group for sharing their time with me. Prof. Dr. Xuebing Li, Dr. Hui Shi, Dr. Yongzhong Zhu, Prof. Dr. Chen Zhao, Dr. Oliver Y. Gutiérrez, Dr. Maricruz Sanchez, Dr. Eszter Baráth, Dr. Erika E. Ember, Dr. Yanzhe Yu, Dr. Xianyong Sun, Dr. Jiayue He, Dr. Baoxiang Peng, Dr. Robin Kolvenbach, Dr. Yuchun Zhi, Dr. Vishnuvarthan Muthusamy, Dr. Eva Schachtl, Dr. Tobias Berto, Sebastian Foraita, Dr. Stanislav Kasakov, Dr. John Ahn, Dr. Bo Peng, Dr. Wenji Song, Dr. Sebastian Müller, Dr. Maximilian Hahn, Dr. Jennifer Hein, Dr. Jeongnam Kim, Dr. Luis Francisco Gonzalez Peña, Manuel Wagenhofer, Martina Braun, Guoju Yang, Yang Song, Yang Zhang, Peter Hintermeier, Sylvia Albersberger, Daniel Melzer, Wanqiu Luo, Takaaki Ikuno and Ferdinand Vogelgsang, Claudia B. Himmelsbach, Moritz Schreiber, Marco Peroni, Kai Sanwald, Martin Baumgärtl, Xi Chen, Guanhua Cheng, Christoph Denk, Takaaki Ikuno, Felix M. Kirchberger as well as other members whose names are not mentioned here, for their friendship and all the great times that we have shared.

Furthermore, I would like to express my gratitude to our research partners from TU Wien (TUW) and Institute of isotopes (IoI). Prof. Dr. G. Rupprechter, Asst. Prof. Dr. K. Föttinger, Dipl. A. Wolfbeisser and Dr. A. Horvath are acknowledged for their scientific advice and insightful discussions.

Last but not least, I owe a great debt of thanks to my family for their love, encouragement and understanding years by years. My parents have offered me unconditional support during my master degree and further PhD study in Germany. To my lovely wife Yanping, who inspired me, provided constant encouragement during the entire process and gave me the most precious gift that I've ever received during my life, my lovely daughter Lucy.

Thanks to all of you

Yu Lou

Feb. 2017

Abbreviations

Å	Angstrom
AAS	Atomic absorption spectroscopy
BET	Brunauer-Emmett-Teller
CO	Carbon monoxide
DP	Deposition-precipitation
DRM	Dry reforming of methane
EXAFS	Extended X-ray absorption fine structure
g	Gram
GC	Gas chromatography
h	Hour
IR	Infrared
K	Kelvin
(k)J	(Kilo) joule
(k)Pa	(Kilo) pascals
MS	Mass spectrometry
(m)L	(Milli) liter
min	Minute
nm	Nanometer
NMR	Nuclear magnetic resonance
NP(s)	Nanoparticle(s)
OSC	Oxygen storage capacity
POM	Partial oxidation of methane
RDS	Rate determining step
RWGS	Reverse water gas reaction
R/P	Reserves-to-production
SRM	Steam reforming of methane
TEM	Transmission electron microscopy
TGA	Thermogravimetric analysis

TOF	Turn over frequency
TPR	Temperature programmed reduction
wt%	Weight percent
XRD	X-ray diffraction
XANES	X-ray absorption near edge structure
XAS	X-ray absorption spectroscopy

Abstract

The activity of Ni/ZrO_2 catalysts for dry reforming and its thermal stability are significantly enhanced by activation and regeneration in presence of CO_2. The exposure to CO_2 mitigates the decoration of ZrO_2 on nickel surface and creates a large ZrO_2-Ni interface. Small and well-defined Ni particles supported on SiO_2 and ZrO_2 were prepared by a novel approach via self-assembled nano-capsules. Ni/ZrO_2 with small metal nanoparticles contains a high fraction of perimeter Ni, which is better accessible to surface O species facilitating carbon removal and which leads to enhanced DRM stability.

Kurzzusammenfassung

Die Aktivität von Ni/ZrO_2 für das Trockenreformieren und seine thermische Stabilität wird durch Aktivierung und Regenerierung in Gegenwart von CO_2 deutlich erhöht. Die CO_2 Behandlung vergrößert die Grenzfläche zwischen Ni und ZrO_2. Kleine, einheitliche Ni-Partikel wurden durch einen neuen Ansatz der selbstorganisierenden Nanokapseln geträgert. Dieser Katalysator besitzt kleine, stabile Ni-Partikel geträgert auf ZrO_2. Dies erleichtert die Entfernung des Kohlenstoffs von der Ni-Oberfläche und führt so zu einer stablien katalytischen Aktivität für das Reformieren von Methan mit CO_2.

Table of contents

ACKNOWLEDGEMENTS ..... **I**

ABBREVIATIONS ..... **IV**

ABSTRACT ..... **VI**

KURZZUSAMMENFASSUNG ..... **VI**

TABLE OF CONTENTS ..... **VII**

CHAPTER 1 ..... **- 1 -**

1.1. General background 2

1.2. Syngas production and reforming technology 4

1.3. Dry reforming 7

1.3.1. Reaction networks *7*

1.3.2. Effect of temperature *8*

1.3.3. Effect of pressure *10*

1.4. Mechanism of dry reforming of methane 11

1.5. Catalysts for dry reforming of methane 17

1.6. Recent development in catalyst preparation methods 21

1.6.1. Plasma technology *21*

1.6.2. Stabilization of Ni nanoparticles within well-defined structure *22*

1.7. Scope of this thesis 27

1.8. Associated Content 29

1.9. References 30

CHAPTER 2 ..... **36**

2.1. Introduction 37

2.2. Experimental section 39

2.2.1. Chemicals *39*

2.2.2. Catalyst preparation *39*

2.2.3. Catalyst characterization *39*

2.2.4. Catalytic measurements ... *40*
2.3. Results and discussion ... 42
2.3.1. Deactivation of Ni/ZrO_2 catalyst ... *42*
2.3.2. In situ activation and stabilization of Ni/ZrO_2 with CO_2. ... *45*
2.3.3. Reaction parameters for in situ activation by CO_2. ... *48*
2.3.4. Mechanism of in situ activation by CO_2 regeneration. ... *56*
2.4. Conclusions ... 61
2.5. Associated Content ... 63
2.6. Appendix ... 64
2.7. References ... 65
CHAPTER 3 ... 69
3.1. Introduction ... 70
3.2. Experimental and theoretical methods ... 74
3.2.1. Chemicals ... *74*
3.2.2. Catalyst preparation ... *74*
3.2.3. Catalyst testing ... *74*
3.2.4. Catalyst characterization ... *75*
3.3. Results and discussion ... 77
3.3.1. Estimation of particle size threshold for stable DRM catalysts ... *77*
3.3.2. Synthesis of small nickel and platinum particles via metal colloidal solution ... *79*
3.3.3. Characterization of particle size ... *84*
3.3.4. Catalytic performance ... *87*
3.3.5. Influence of particle size on the DRM activity and stability ... *89*
3.4. Conclusions ... 99
3.5. Associated Content ... 100
3.6. Appendix ... 102
3.7. References ... 109
CHAPTER 4 ... 112
CHAPTER 5 ... 115

Curriculum Vitae ……..…….…… 117

List of Publications…… 119

Chapter 1

Introduction

1.1. General background

During the course of global economic sustainable development, human beings are confronted with immense pressures in population, resources and the environment. The energy problem has received much attention in recent years. In view of depletion in stock of petroleum reserves, a more widespread use of natural and renewable energy sources have been recognized as an important contribution to a sustainable development.

Methane is the most abundant hydrocarbon on our planet, which exists in enormous quantity in natural gas and biogas and also in the form of gas hydrate at the continental slopes and in permafrost areas.[1] The total reserves of natural gas was proved in 2015, with a total storage capacity of 186.9×10^{12} m^3,[2] which is sufficient to meet 52.8 years of current production. Estimates of the amount of methane increased from 125.7×10^{12} m^3 in the last 25 years (shown in Figure 1-1), as a consequence of the improved production technology allowing access to unconventional sources, i.e. shale gas fracking.[3]

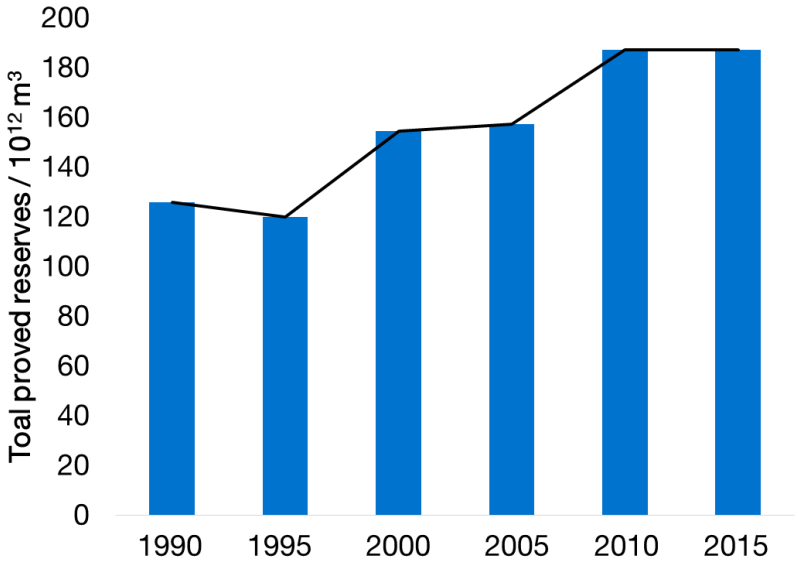

Figure 1-1. Total reserves of natural gas in the last 25 years. The amount of natural gas in crystalline hydrates is excluded from this estimates.

Additionally, the reserves-to-production (R/P) ratio decreased sharply in the past 10 years, as the increased natural gas production from 2.79 × 10^{12} m^3 to 3.54 × 10^{12} m^3 (shown in Figure 1-2). It is worth noting that enormous amount of natural gas in crystalline hydrates is excluded from this estimate, which varies from 1000 × 10^{12} m^3 to 5000 × 10^{12} m^3.[4] Consequently, the utilization of methane is getting more economically attractive in terms of its enormous reserves.

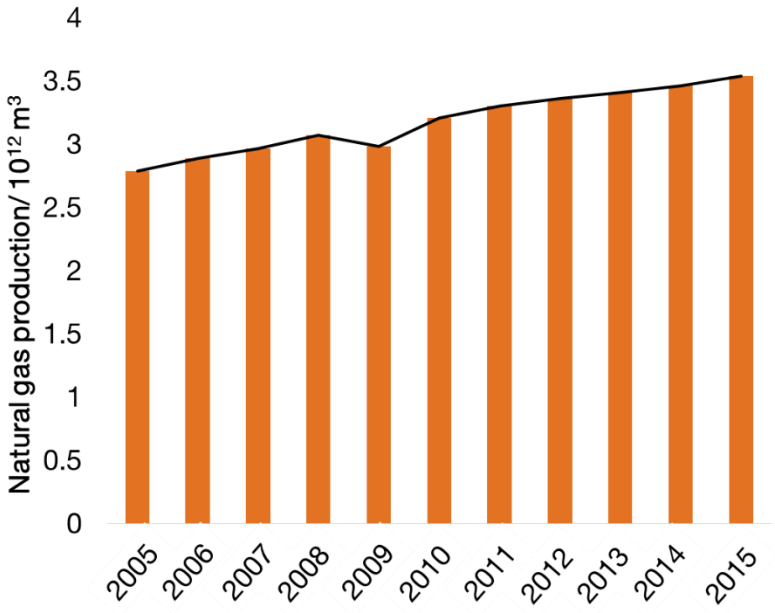

Figure 1-2. Natural gas production in the last 10 years.

However, instead of use as chemical feedstock, the majority of methane is consumed for heating and electrical generation.[5] It is reported that less than 10 % of natural gas was used as input for producing chemicals.[1] Thus, a more efficient use of the natural gas, especially methane, is becoming more attractive.

1.2. Syngas production and reforming technology

Syngas is a mixture of carbon monoxide and hydrogen, which can be produced from a variety of sources, including natural gas, coal, biomass, or virtually any hydrocarbon feedstock via steam reforming, partial oxidation and gasification.[6] Syngas is used as a versatile intermediate resource for production of hydrogen, ammonia, methanol, and synthetic hydrocarbon fuels.

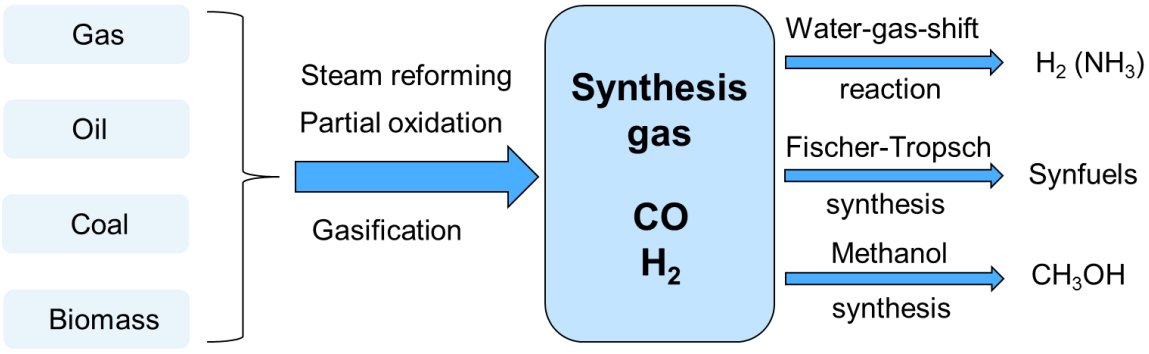

Figure 1-3. Schematic representation of natural gas production from a variety of sources and of its transformation to chemicals and fuels.[6]

Until now, hydrocarbon reforming, particularly steam reforming of methane (SRM) (Equation 1-1), is generally the largest and widely used method in industry to produce hydrogen and carbon monoxide. The steam reforming reaction is an endothermic process, which requires energy input to meet the endothermicity of the reaction.[7,8] During this process, CO_2 is produced along with syngas. However, the removal and disposal of CO_2 is a major issue in the petrochemical industrial.[9]

$$CH_{4(g)} + H_2O_{(g)} \rightleftharpoons CO_{(g)} + 3\ H_{2(g)} \qquad \Delta H^0_{298\ k} = 206\ kJ\ mol^{-1}$$

(**Equation 1-1**)

The partial oxidation of methane (POM) is a mildly exothermic process, which however, can result in hot-spot formation at high space velocity, leading to higher risks and greater difficulties for process control.

$$CH_{4(g)} + 1/2\ O_{2(g)} \rightleftharpoons CO_{(g)} + 2\ H_{2(g)} \qquad \Delta H^{0}_{298\ k} = -37\ kJ\ mol^{-1}$$

(**Equation 1-2**)

Hence, during the last several years, in addition to steam reforming and partial oxidation, there has been renewed interest in the dry reforming of methane (DRM) for the production of synthesis gas. Compared to SRM and POM, DRM has many advantages. It produces syngas with a H_2/CO ratio close to 1, which is a preferable feed for Fischer-Tropsch synthesis.[10] Syngas with high H_2/CO ratio, i.e. those from SRM with a H_2/CO ratio of 3 and from POM with a H_2/CO ratio of 2, favors methanation and suppress chain growth in Fischer-Tropsch synthesis.[11,12] Furthermore, the separation of CO_2 from natural gas are not required since many remote natural gas fields contain significant amounts of CO_2. Additionally, dry reforming also provide a pathway to reduce the CO_2 and CH_4, which are regarded as important greenhouse gases.

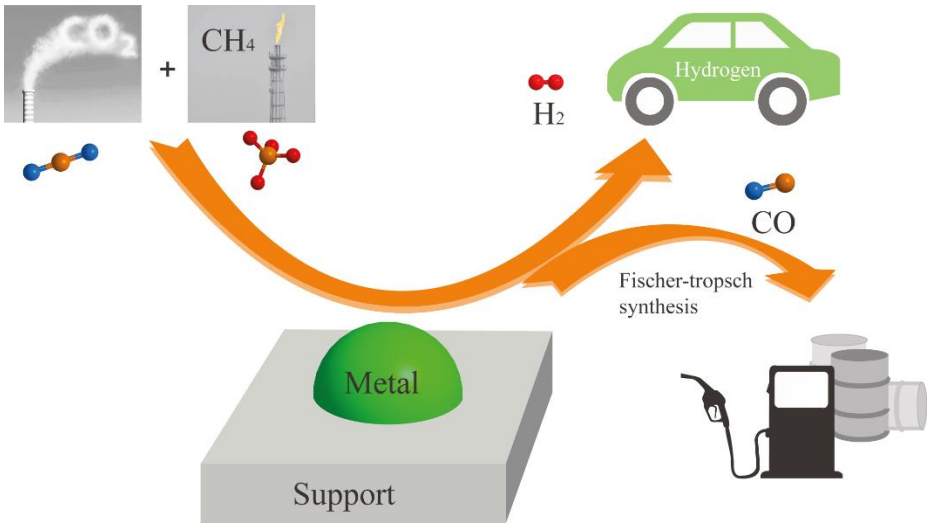

Figure 1-4. Schematic representation of dry reforming to form syngas and its transformation into fuels via Fischer-Tropsch synthesis

The main problem for the DRM reaction is the rapid deactivation of supported metal catalysts caused by sintering of metal particles and coke formation. In order to reach acceptable conversion levels, high temperatures above 900 K are required.[13] Therefore, a significant challenge to stabilize dry reforming catalyst is reducing the sintering of the active metal.[14] Furthermore, deactivation of the catalysts by coke formation is also serious during DRM reaction. Coke formation on catalysts and walls of the reactor pipes are serious problems in many industrial reactors. In severe cases, it leads to blockage of reactor tubes. Thus, many efforts have recently been made in this area in developing suitable DRM catalysts, which is stable against sintering and coke formation.

1.3. Dry reforming

1.3.1. Reaction networks

In dry reforming reaction, CH_4 reacts with CO_2 to form CO and H_2 (Equation 1-3). This reaction is highly endothermic, thus, high temperature is required in order to reach an acceptable conversion. The minimum operating temperature for DRM reaction at atmospheric pressure was thermodynamically determined,[15] which showed that the DRM become thermodynamically favorable at the temperature above 913 K with a feed ratio of CH_4 : CO_2 = 1:1.

$$CO_{2(g)} + CH_{4(g)} \rightleftharpoons 2\ CO_{(g)} + 2\ H_{2(g)} \qquad \Delta H^0_{298\ k} = 247\ kJ\ mol^{-1}$$

(**Equation 1-3**)

The reverse water gas reaction (RWGS) (Equation 1-4), which occurs during DRM reaction, is slightly endothermic. In this reaction, the consumption of H_2 leads to a H_2/CO ratio less than unity, and the generated H_2O can further react with CH_4 in the steam reforming (Equation 1-1). At the temperature higher than 1093 K, the RWGS will not take place.

$$CO_{2(g)} + H_{2(g)} \rightleftharpoons CO_{(g)} + H_2O_{(g)} \qquad \Delta H^0_{298\ k} = 41\ kJ\ mol^{-1}$$

(**Equation 1-4**)

DRM reaction suffers from coke deposition on the catalysts, which is formed predominantly via the Boudouard reaction (Equation 1-5) and methane decomposition (Equation 1-6).[16-18] The Boudouard reaction is an exothermic process, which shows a greater preference towards carbon deposition at low temperature. It was reported that at the temperature above 973 K,[15] this reaction lies completely on the side of carbon monoxide and, thus, no carbon is formed via CO disproportion reaction.

$$2\ CO \rightleftharpoons C + CO_2 \qquad \Delta H^0_{298\ k} = -\ 171\ kJ\ mol^{-1}$$

(**Equation 1-5**)

Methane decomposition reaction (Equation 1-6) is also an endothermic reaction and thermodynamically favored at high temperatures. The lower limiting temperature of 830 K[15] was determined at atmospheric pressure.

$$CH_4 \rightleftharpoons C + 2\ H_2 \qquad \Delta H^0_{298\ k} = 75\ kJ\ mol^{-1}$$

(**Equation 1-6**)

Besides, the reverse carbon gasification reaction (Equation 1-7) also forms carbon, which is considered to have less influence on the carbon formation than methane decomposition and Boudouard reaction.

$$CO + H_2 \rightleftharpoons C + H_2O \qquad \Delta H^0_{298\ k} = -\ 131\ kJ\ mol^{-1}$$

(**Equation 1-7**)

Thus, as aforementioned reaction networks, DRM is thermodynamically preferable at the temperature above 1000 K[19], at which the carbon formation via CO disproportion reaction is kinetically inhibited and the DRM reaction is simultaneously facilitated.

1.3.2. Effect of temperature

The reaction equilibrium constants of aformentioned reactions as a function of temperature was summaried in Figure 1-5.[20] Lower reaction temperature, i.e. below 873 K, has a significantly greater preference for carbon formation via Boudouard reaction (Equation 1-5) and reverse carbon gasification reaction (Equation 1-7). At the temperature above 1023 K, the equilibrium constant of the DRM reaction (Eq. 1-3) increased dramatically than that of the side reactions

(Equation 1-4 and 1-6). Therefore, in order to minimize the impact of coke formation during DRM reaction, high reaction temperatures are more favorable.

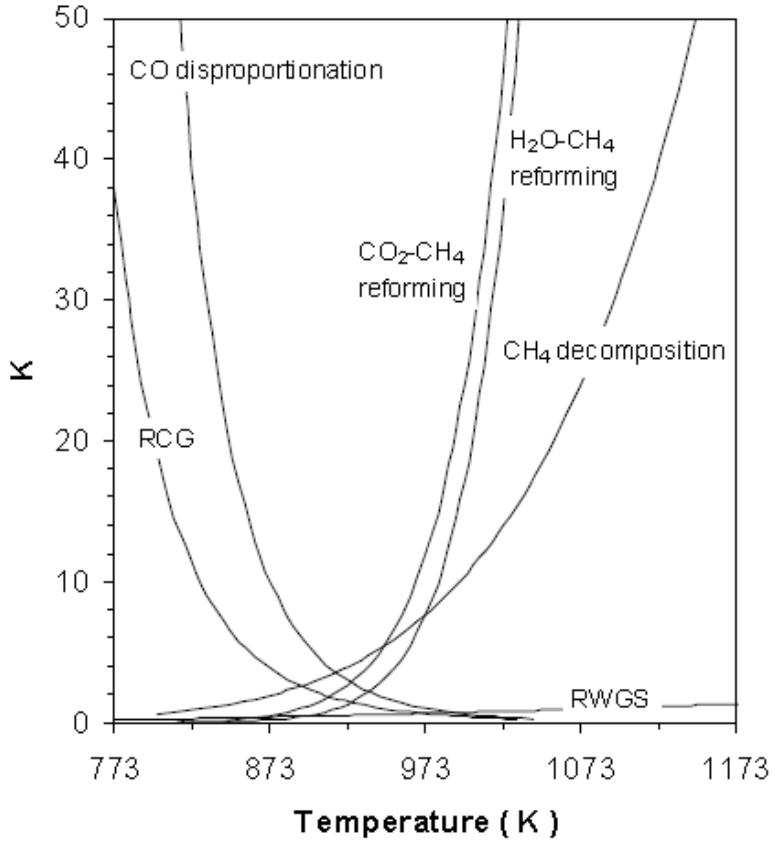

Figure 1-5. Equilibrium constants of reactions involved in networks of DRM as a function of temperature.[20]

Furthermore, the variation of equilibrium composition as a function of reaction temperature is shown in Figure 1-6.[21] The equilibrium composition is calculated at total pressure of 1 atm and initial CH_4/CO_2 ratio of 1/1. As shown in Figure 1-6, the composition of H_2 and CO increases while the fractions of H_2O, CH_4 and CO_2 decreases. The molar ratio of H_2 to CO becomes closer to unity at higher temperatures. Thus, DRM is preferable at a higher temperature to achieve high conversion of CH_4 and CO_2 and to minimize the impact of RWGS on the H_2/CO ratio.

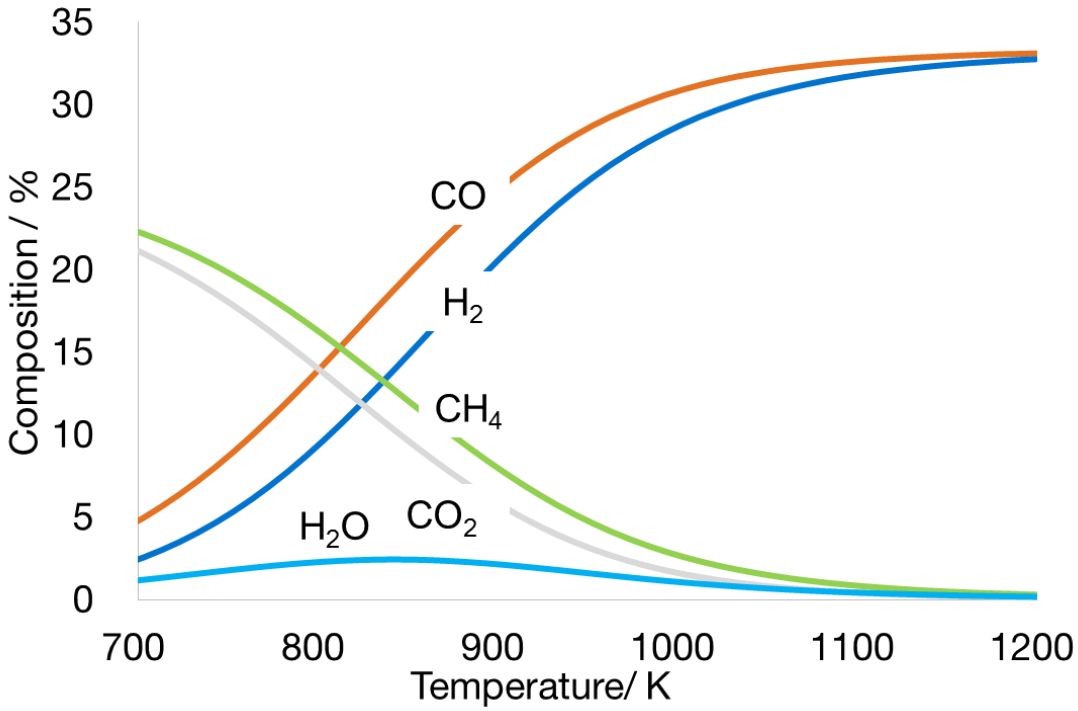

Figure 1-6. Variation of equilibrium composition with temperatures.

1.3.3. Effect of pressure

In the DRM reaction, the number of gaseous molecules increases and the pressure also increases. The influence of the pressure on the equlibrium compositions was illustrated in Figure 1-7, which showed that lower pressure favor the complete conversion of CH_4 and CO_2 to form CO and H_2. Nonetheless, in view of the industrial process, high pressure allow to minimize the reactor size and energy use.[22]

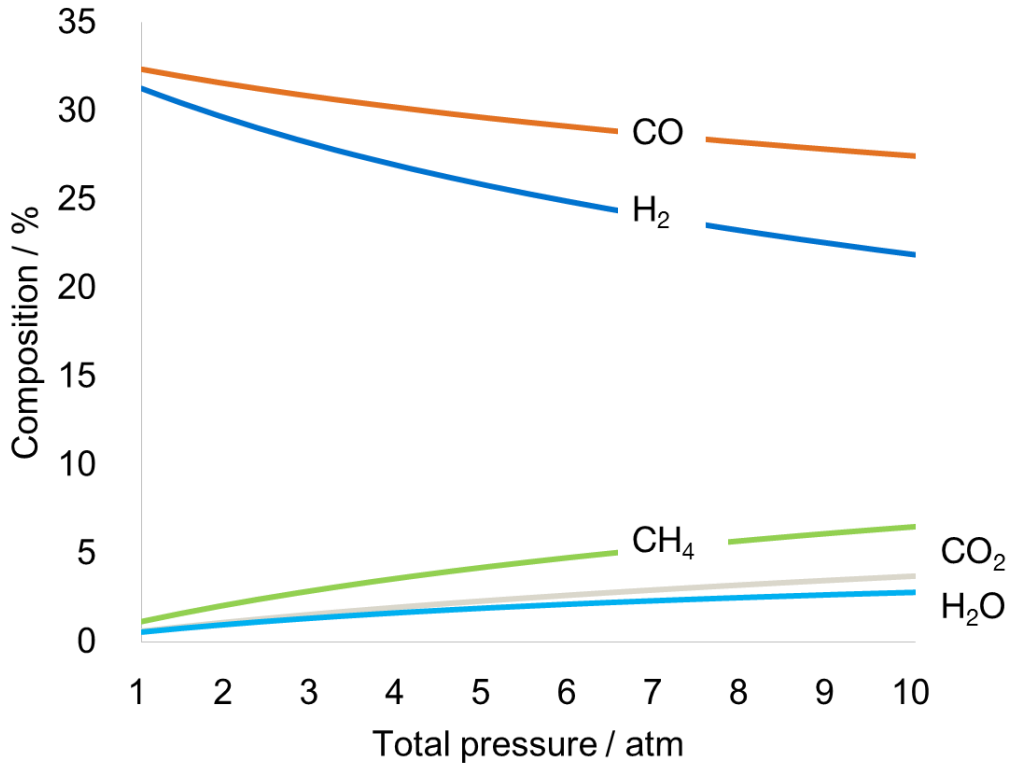

Figure 1-7. Variation of equilibrium compositons with increasing reaction pressure at 1073 K.

1.4. Mechanism of dry reforming of methane

Carbon dioxide reforming of methane has been studied over the years by a large number of research groups and many contributions have been made in this area, both on the theoretical side[23-29] and on the applications to the industrial process[30-32]. Nevertheless, little research has been focus on the reaction kinetics and its mechanism. Until now, no generally accepted kinetic model has been published yet.

Nonetheless, it is widely accepted that the dissociative chemisorption of CH_4 denote the initial step of the reforming reaction, which occurs on the active metal surface[33-37]. The stepwise decomposition of CH_4 and formed H and CH_x species have been confirmed by Osaki et al.[38]:

$$CH_4 + 2\ M \rightleftharpoons CH_3\text{-}M + H\text{-}M$$

(**Equation 1-8**)

$$CH_3\text{-}M + M \rightleftharpoons CH_2\text{-}M + H\text{-}M$$

(**Equation 1-9**)

$$CH_2\text{-}M + M \rightleftharpoons CH\text{-}M + H\text{-}M$$

(**Equation 1-10**)

$$CH\text{-}M + M \rightleftharpoons C\text{-}M + H\text{-}M$$

(**Equation 1-11**)

where M stands for the surface metal active sites. The CH_x intermediates formed during dry reforming of methane were determined in situ via pulse surface reaction rate analysis (PSRA).[39] The value of x varied from 0 to 3 on supported Ni catalysts[10,40,41] and 0.75 on supported Co catalyst[42]. In the 1970s Matsumoto and his coworkers have proved that different CH_x species was formed on Ni catalysts after adsorption of hydrocarbons and CH_x intermediates with lower values of x were more likely to form carbonaceous deposits.[43-45] Furthermore, the cleavage of the first C-H bond was concluded to be the rate determining step for all reforming and decomposition reactions of methane on noble metals as well as on metallic Ni.[33-37]

Nevertheless, there are mainly two different reaction pathways proposed for CO_2 activation on dry reforming catalysts. Wei and Iglesia proposed in their research that methane and CO_2 are activated on the metal surface through a Langmuir-Hinshelwood mechanism.[33-37] The main steps involved are illustrated in Figure 1-8.[28]

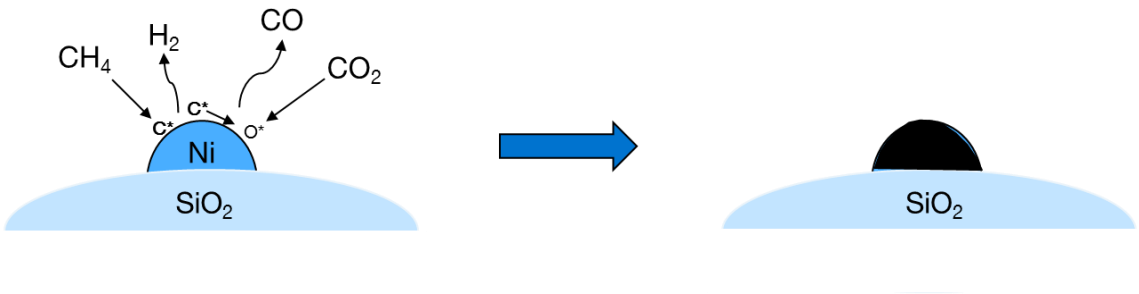

Figure 1-8. Schematic representation of dry reforming via a mono-functional mechanism. The section shaded in black represented coke formation on the metal surface

As aforementioned, the CH_4 is adsorbed and dissociated on the metal surfaces, forming H and CH_x intermediates. The H species can then recombine with another H species to form H_2 molecule. CO_2 is also activated on the metal surface by the formation of CO and surface O species, which react further with CH_x species to form CO molecule to inhibit the deposition of inactive coke on the metal surface. However, as the reaction proceeds, the active metal surface is covered with highly dehydrogenated carbon deposits, which eventually undergoes ageing and graphitization on the metal surface.[28] Thus, the increasing amount of carbonaceous residues continuously covered the active metal site for CH_4 and CO_2 activation, leading to an ongoing deactivation of DRM catalysts by coke deposition. The main steps are summarized as follows[28]:

CH_4 and CO_2 activation on the metal surface:

$$CH_4 \rightleftharpoons CH_{x\,(metal)} + (4\text{-}x)\ H_{(metal)}$$

$$2\ H_{(metal)} \rightleftharpoons H_{2\,(gas)}$$

$$CO_{2\,(gas)} \rightleftharpoons CO_{2\,(metal)}$$

$$CO_{2\,(metal)} \rightleftharpoons CO_{(metal)} + O_{(metal)}$$

$$O_{(metal)} + CH_{x\,(metal)} \rightleftharpoons CO_{(metal)} + x\ H_{(metal)}$$

$$CO_{(metal)} \rightleftharpoons CO_{(gas)}$$

$$H_{(metal)} + O_{(metal)} \rightleftharpoons HO_{(metal)}$$

$$H_{(metal)} + HO_{(metal)} \rightleftharpoons H_2O_{(gas)}$$

$$OH_{(metal)} \rightleftharpoons HO_{(support)}$$

On the other side, a bifunctional mechanism was proposed for the dry reforming reaction, in which the support participates in the reaction behavior. Lercher and his coworkers[46-49] showed in a series of papers that the CO_2 molecule is predominantly adsorbed and activated on the support by the formation of carbonates. Other groups have shown the similar results of dry reforming over metal catalysts supported on Al_2O_3[28], La_2O_3[50], TiO_2 and MgO[51,52] that the support plays an important role in activating and converting CO_2 . The main mechanism are illustrated in Figure 1-9.

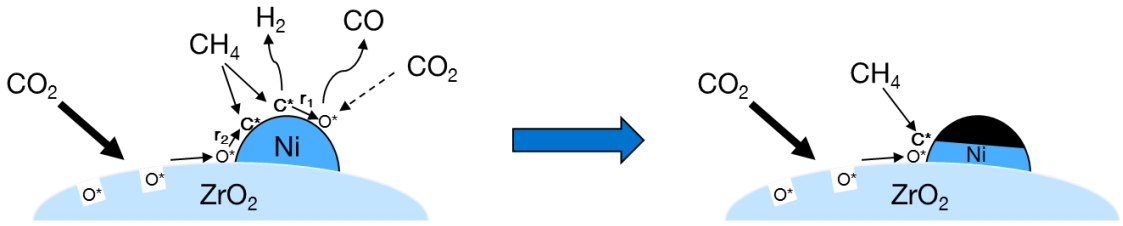

Figure 1-9. Schematic representation of dry reforming via a bifunctional mechanism. The section shaded in black represented coke formation on the metal surface. The surface oxygen species in the form of (hydrogen) carbonate was illustrated as O*.

As mentioned above, the methane molecule is activated on the metal surface, forming H and CH_x species, which is similar as the mono-functional mechanism. Netherless, CO_2 is supposed to be adsorbed by the Lewis base center of the oxide support. The (hydrogen) carbonates formed during the CO_2 activation react subsequently at the interface between metal and support with the carbon species.

Thus, two reaction pathways exist in eliminating surface carbon species formed from methane decomposition, which is on the metal particles and on the boundary of metal and support. It is supposed that carbon removal reaction at the perimerter is much more faster than the carbon formation, while the carbon removal rate on the metal surface is lower than the CH_4 decompostion rate.[49] After a certain time, the metal surface was covered by a monolayer of coke to a large extent, but the perimeter is still available for the reaction. The main steps are summarized as follows[28]:

CH_4 activation on the metal surface:

$$CH_4 \rightleftharpoons CH_{x\,(metal)} + (4\text{-}x)\,H_{(metal)}$$

$$2\,H_{(metal)} \rightleftharpoons H_{2\,(gas)}$$

$$O_{(metal)} + CH_{x\,(metal)} \rightleftharpoons CO_{(metal)} + x\,H_{(metal)}$$

$$CO_{(metal)} \rightleftharpoons CO_{(gas)}$$

$$H_{(metal)} + O_{(metal)} \rightleftharpoons HO_{(metal)}$$

$$H_{(metal)} + HO_{(metal)} \rightleftharpoons H_2O_{(gas)}$$

$$OH_{(metal)} \rightleftharpoons HO_{(support)}$$

CO_2 activation on the support:

$$CO_{2\,(gas)} \rightleftharpoons CO_{2\,(support)}$$

$$CO_{2\,(support)} + O^{2-}_{(support)} \rightleftharpoons CO_3^{2-}{}_{(support)} + O_{(metal)}$$

$$CO_{2\,(support)} + OH^-_{(support)} \rightleftharpoons HCO_3^-{}_{(support)}$$

$$H_{(metal)} \rightleftharpoons H_{(support)}$$

$$CO_3^{2-}\ (support) + 2\ H\ (support) \rightleftharpoons HCO_2^{-}\ (support) + OH^{-}\ (support)$$

$$HCO_3^{2-}\ (support) + 2\ H\ (support) \rightleftharpoons HCO_2^{-}\ (support) + H_2O\ (support)$$

$$HCO_2^{-}\ (support) \rightleftharpoons CO\ (support) + OH^{-}\ (support)$$

$$CO\ (support) \rightleftharpoons CO\ (gas)$$

Hence, as discussed, Ni catalysts supported on oxide with higher concentration of oxygen vacancy and mobility of surface oxygen promote the removal of surface carbon deposition. In addition, the rate of carbon removal reaction increases with reducing metal particle size in terms of larger metal-support interface (shown in Scheme 1-10).

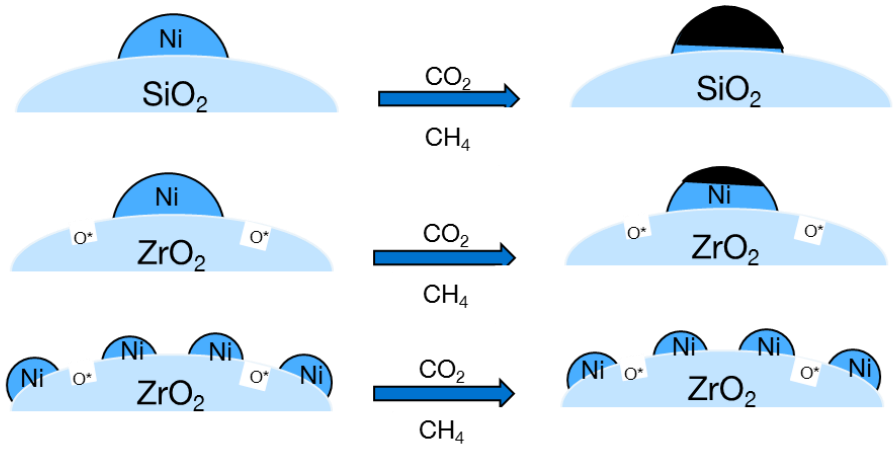

Figure 1-10. Schematic representation of influence of support and metal particle size on the coke formation during DRM reaction.

1.5. Catalysts for dry reforming of methane

A lot of studies have been dedicated to developing highly active and stable catalysts for DRM reaction, which include metal oxides, monometallic and bimetallic catalysts, and supported metal catalysts. Typically the DRM catalysts reported consist of a metal, i.e. Ni, Co, Ru, Rh, Pd and Pt, on an oxide support, such as SiO_2, Al_2O_3, MgO, TiO_2, CaO, CeO_2, ZrO_2 or La_2O_3.[53] These two components play an important role in the DRM reaction.[32]

In general, the metal used for DRM reaction includes noble metals (Ru, Rh and Pt) and transition metals (Co and Ni). The catalyst based on noble metals are reported to have high catalytic activity and coke tolerance and excellent resistance towards agglomeration. Nevertheless, the high cost and low availability limits the industrial application of noble metal. Due to the lower price and higher availability, supported Ni catalysts have been widely investigated in recent research. However, compared to noble catalysts, nickel catalysts are generally more prone to form cokes under reaction condition and to sinter at high temperature.[54] Therefore, current focus of research is to improve the stability of DRM catalysts, with regard to different oxide support, preparation method, addition of promoter and bimetallic catalysts.

The oxide support itself is relatively catalytically inactive, however, there is strong evidence that the support have a significant effect on the stability of DRM catalyst. Bitter et al. reported the effect of Al_2O_3, ZrO_2 and TiO_2 and found that the stability of the catalysts increased in the order $Pt/A1_2O_3 < Pt/TiO_2 < Pt/ZrO_2$.[55] Zhang et al. also demonstrated the following influence of support on the initial DRM activity: $Rh/ZrO_2 > Rh/TiO_2 \geqq Rh/Al_2O_3 > Rh/La_2O_3 \approx Rh/SiO_2 > Rh/MgO$.[56] Briefly, the support with a high oxygen storage capacity and mobility facilitate the carbon removal reaction, which leads to higher stability during DRM reaction.

In recent years, the addition of alkali and alkaline earth metals or metal oxide to enhance the activity and stability of DRM catalysts has also been investigated.[32] Chang[57] et al. reported in 1996 that coke deposition on the catalysts was

remarkably eliminated by the addition of alkaline promoters such as K and Ca oxides, leading to the formation of carbonate species on alkaline promoters in the vicinity of Ni. Furthermore, the dissociative adsorption of CO_2 on the Ni surface was also facilitated with the addition of alkaline promoters. The addition of CaO also lead to an increased thermal stability. Dias and his coworker found that the impregnation of Ni and Ca on alumina increases the sintering resistance of the support and offer good catalytic performance during DRM reaction.[58] Pan et al. found that Ni/SiO_2-Ga_2O_3 catalyst showed a higher stability and coke resistance than the Ni/SiO_2 catalyst.[59] CO_2 is adsorbed physically onto SiO_2 and is activated on Ga_2O_3, resulting in surface carbonate and bicarbonate species, which react more easily with deposit carbon than reaction with linearly bonded or physically adsorbed CO_2.

CeO_2[60-62] was also suggested to be an efficient promoter for DRM catalysts. Ni catalysts with CeO_2 promoters reduced the chemical interaction between nickel and support, resulting in an increase in reducibility and higher dispersion of nickel particles. Beside, CeO_2 have high oxygen storage capacity (OSC), which provides positive effect on the activation of CO_2 during DRM, leading to an enhanced ability to remove coke in the vicinity of metal and support.

Additionally, instead of investigation of monometallic catalysts with various support modification, alloying with a second metal to form bimetallic catalysts have received much attention in recent years. The advantages of activity, selectivity and stability of the second metal was transferred on the first metal, leading to a modification of the catalyst properties through a synergistic effect between two metals.[63,64] Frusteri et al. investigated potassium-promoted Ni/MgO catalyst in the dry reforming of methane.[65] Bare Ni/MgO system showed remarkable deactivation during DRM reaction in terms of sintering and formation of large amounts of whisker carbon. K addition lowered the reactivity of the catalyst, but, strongly improved its resistance to both coking and sintering processes. Osaki and Mori[38] concluded that K plays an important role in dividing the nickel surface into smaller ensembles, thus, suppressing carbon deposition.

Moreover, Chen et al. developed a long-term stable Cu-Ni/SiO_2 catalyst for CO_2 reforming of methane[66]. They proved that the incorporation of Copper stabilized the structure of the active site on Ni surface for CH_4 decomposition and hindered the deactivation of the Ni catalyst caused by sintering or by loss of nickel crystallites. Lee et al. found that the addition of just 1% Cu could modify the Ni ensemble environment, resulting an enhanced stability for the DRM reaction.[67] Vanadium has also been investigated as promoter for DRM reaction.[68] It was found that the addition of V suppress the formation of $NiAl_2O_4$, which is inactive for DRM reaction. Tomishige et al. reported that the addition of Sn can effectively minimize carbon deposition.[69] The synergetic effect of Ni-Co based bimetallic catalysts also lead to highly active and stable reaction behavior.[16,70-75] Alloying Ni with Co decreases the apparent Ni particle size to the size which is too small for carbon nucleation and growth.

Table 1-1. Recently reported catalysts for dry reforming of methane

Metal	Support	References
Ni	La_2O_3	50
Ni	ZrO_2	54
Ni	MgO	76
Ni	Al_2O_3-CeO_2	60-62,77
Ni	Al_2O_3-CaO	58
Ni	SiO_2-Ga_2O_3	59
Ni-K	MgO-K_2O	65
Ni-K	Al_2O_3	38
Ni-Cu	SiO_2	66
Ni-Cu	Al_2O_3	67
Ni-V	Al_2O_3	68
NiO-Sn	MgO	69
Ni-Co	Al_2O_3	75
NiO-CoO	MgO	70

Ni-Co	$MgO\text{-}ZrO_2$	71,72,74
Ni-Co	TiO_2	73
Ni-Co	$MgAl_2O_4$	16
Ni-Co	$Al_2O_3\text{-}ZrO_2$	78
Co	TiO_2	79
Pt	Al_2O_3	48,49,55
Pt	TiO_2	48,49,55
Pt	ZrO_2	48,49,55
Ru	SiO_2	28
Ru	Al_2O_3	28
Rh	ZrO_2	56
Rh	TiO_2	56,80,81
Rh	Al_2O_3	56,80-82
Rh	La_2O_3	56,82
Rh	SiO_2	56,80,81
Rh	MgO	56,81
Rh	CeO_2	82
Rh	La_2O_3	82

1.6. Recent development in catalyst preparation methods

Recently, several innovative developments for the stabilization of supported nickel catalysts are reported. Most of them focus on the improved thermal stability at high reaction temperature and resistance to coke deposition during DRM reaction, including plasma treatment of Ni catalysts or stabilization of Ni nanoparticles within composite metal oxide, mesoporous structure and microporous zeolitic frameworks.

1.6.1. Plasma technology

In the last few years there has been an increasing use of plasma technology for catalyst synthesis as an improved resistance towards coke deposition.[83,84] Compared to the conventional thermal method, the structure of the Ni nanoparticles can be easily controlled,[85] leading to an enhanced dispersion and surface concentration of the active metal phase. The energetic species in plasmas, electrons, ions and radicals can modify the metal particle size, morphology and metal-support interaction, leading to some specific catalytic properties.[86] In addition, the trace impurities in the gas stream, which is sensitive to the catalyst, can be also removed via plasma treatment.[87] Zhu et al. treated the Ni/Al_2O_3 with argon glow discharge plasma, displaying an excellent resistance to formations of filamentous carbon and encapsulating carbon for CO_2 reforming of methane than conventional thermally calcined Ni/Al_2O_3.[88] It was proved that the plasma treated Ni/Al_2O_3 has a high concentration of close packed plane and improved Ni dispersion.

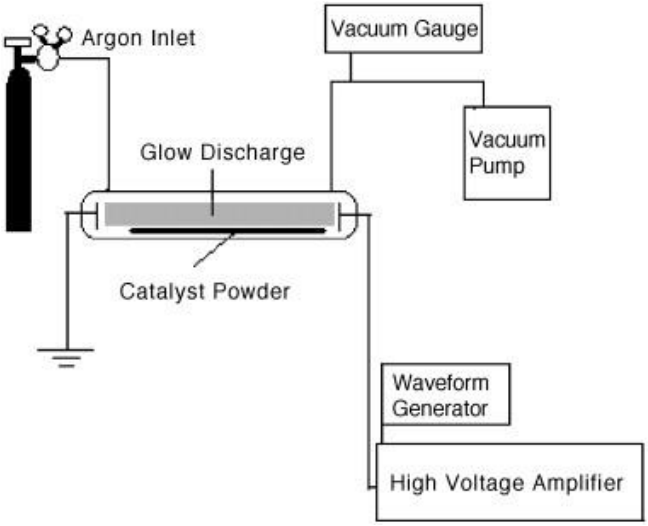

Figure 1-11. Schematic representation of plasma treatment setup.[88]

Wang et al. reported a similar preparation method using a plasma-assisted technique. Ni nanoparticles were confined within the pore channels of mesoporous Mg-SBA15.[89] It was proved that the plasma-treated catalyst exhibited a better stability against sintering than those of the untreated catalyst. In contrast to the calcined Ni catalyst, the plasma-treated catalyst showed excellent resistance to the deposition of filamentous carbon and encapsulating carbon. Similarly, this conventional treatment has been extended to synthesize Ni catalysts on various oxide supports, i.e. Ni/MgO[76] Ni/Al_2O_3-CeO_2[77] and Ni-Co/Al_2O_3-ZrO_2[78].

1.6.2. Stabilization of Ni nanoparticles within well-defined structure

Many recent investigation have been made to confine Ni particles in nickel precursors with well-defined structure. Halliche et al. investigated a series of Ni-based catalysts on HZSM-5 and USY zeolites, suggesting a better catalytic performance of Ni/USY than Ni/Al_2O_3.[90] Frontera et al. studied the influence of zeolite support on the overall catalyst performance. A high amount of silanol groups on the surface of silicalite-1 improve the CH_4 and CO_2 conversion but also reduce the deactivation of the catalyst due to coke deposition.[91] However, in terms

of the requirement for operating at high temperature above 873 K, it is crucial to improve the thermal stability of the zeolite.[92]

In another series of studies, nickel particles were stabilized on carbon/carbide support. Liu et al. reported a Ni containing mesoporous silica Ni-KIT-6, which was prepared by one-spot self-assembly method, resulting highly dispersed Ni species in the mesoporous silica (shown in Figure 1-12).[93] Compared with conventionally impregnated Ni catalysts, Ni-KIT-6 exhibits extremely smaller Ni particles and stronger interaction of Ni with silica matrix, which leads to high DRM activity and stability. Wang et al. also presented a one-pot evaporation-induced self-assembly method to synthesize mesoporous $NiO\text{-}CeO_2\text{-}Al_2O_3$ catalysts with high DRM stability.[94,95]

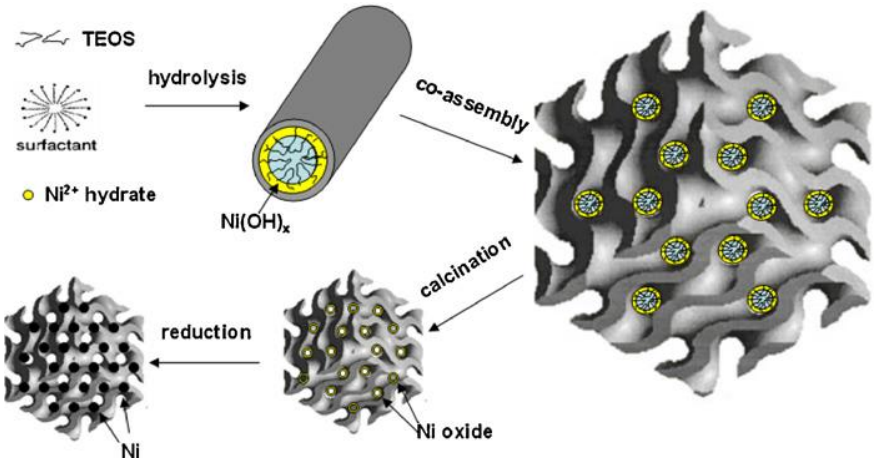

Figure 1-12. Schematic diagram of the preparation of the Ni-KIT-6 catalyst.[93]

Furthermore, Coperet and his coworkers published a versatile method for the preparation of small Ni nanoparticle through nickel–silicide colloid, with sizes of 1.3 ± 0.2 and 2.1 ± 0.2 nm (shown in Figure 1-13).[96] The resulting catalysts showed high activity in low temperature dry reforming reaction.

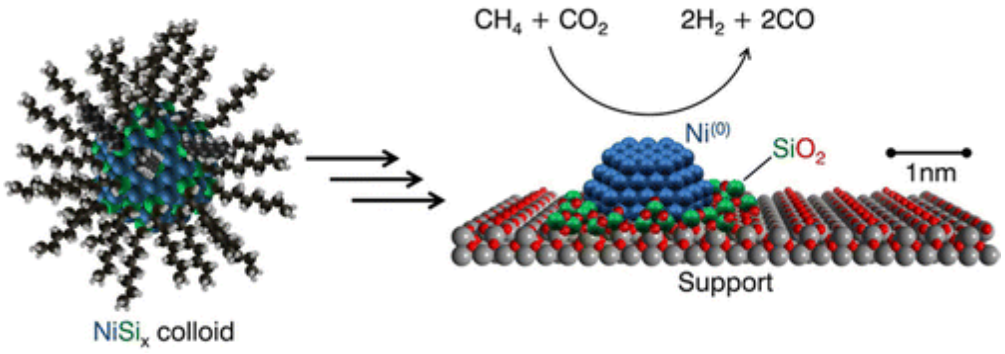

Figure 1-13. Conversion of nickel−silicide colloids into supported Ni catalysts and dry reforming reaction under its catalysis.[96]

Recently, Han et al. reported highly coke-resistant Ni catalysts by immobilizing premade Ni nanoparticles onto functionalized silica supports.[97] The Ni/SiO_2 catalyst was then coated with silica overlayer, resulting a uniform distribution of Ni particles on the support (shown in Figure 1-14). The silica-coated Ni catalysts showed highly stable activity during 170 h of DRM reaction at 1073 K. In contrast, Ni catalysts without silica coating show severe sintering after DRM reaction, and the formation of filamentous carbon was observed.

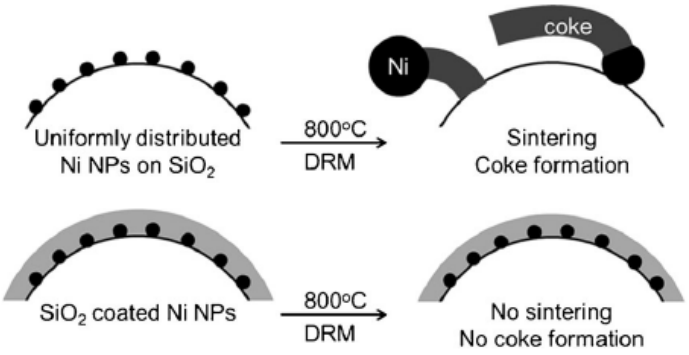

Figure 1-14. DRM reaction over conventional supported Ni/SiO_2 and silica-coated nickel nanoparticle (NP) catalysts.[97]

In this dissertation, we report a novel method to prepare small and well defined Ni nanoparticles supported on metal oxides under mild conditions. The synthesis of metal colloids uses metal salts (M^{n+}) as precursor, which are self-assembled in host molecular capsules to protect metal particles against sintering during calcination at high temperature, resulting metal particles with a size of 1-2 nm on the support.

Molecular capsules[98-101] formed via a spontaneous self-assembly process have been of great interest during the past decades. These capsule molecules consist of 6 resorcin[4]arene molecules connected via hydrogen bonds. The particularly interesting feature of these nanospheroid architectures for synthesis of catalytically active materials is the ability to encapsulate neutral and charged guest species within the well-defined cavity[98,101] or to the formation of metal coordinated nanocapsules[102]. Thus, these structure can be regard as an ideal candidate for encapsulating positive charged metal ion. Zhang et al. reported that the resorcin[4]arene hexamer can encapsulate protonated tertiary amines which is used as an efficient enzyme-like catalyst for Wittig reaction.[99]

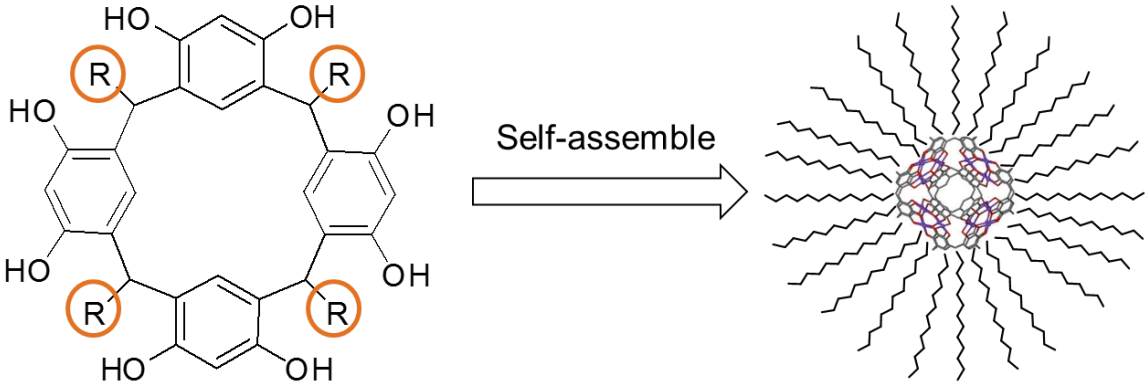

Figure 1-15. Schematic representation of the hexameric resorcin[4]arene molecule and its self-assemble process to capsule molecule. The R group in red designates the alkyl group of resorcinarene molecule.

Furthermore, the size of a colloidal particles could be adjusted via modification of alkyl group of resorcinarene. Increasing the C number of the alkyl chain leads to an increased steric hindrance, which is more suitable for synthesis of well dispersed metal colloidal solution. In this dissertation, pyrogallol[4]arene molecule was used in the synthesis, leading to well-dispersed metal particles on the support after high temperature calcination and reduction.

1.7. Scope of this thesis

The main task of this dissertation is to differentiate between reactions on the metal surface and at the metal support interface during DRM and to use this knowledge for developing a new generation of highly active and stable catalysts. The insight required for designing catalysts includes the knowledge of the nature and geometrical properties of the metal particles and the way they are anchored to and interact with the support.

In the second chapter of this thesis, a detailed experiment study has been carried out to study the regeneration effect of CO_2 on the DRM reaction over Ni/ZrO_2 catalysts. Combining the experimental results from kinetic analysis, IR spectroscopy and XAS measurements under *operando* conditions, it was shown that after reduction the Ni particles were covered to a certain extent with partially reduced ZrO_2. The exposure to CO_2 at temperatures above 873 K resulted in the removal of the ZrO_2 decoration and additional sites for CO_2 activation at the interface between the support and the metal particles, thus enhancing the activity of the Ni/ZrO_2 catalysts for dry reforming of methane.

Based on the results described so far, it is evident that well dispersed on metal particles on a partially reducible support such as ZrO_2 will be essential to maintain the activity in the DRM reaction. Thus, in the following chapter, a new synthetic method via host colloidal solutions as metal precursors was shown to synthesize Ni and Pt catalysts. The particle sizes have been characterized by TEM and EXAFS measurements. The ZrO_2 supported Pt and Ni particles synthesized by this new method showed stable activities under DRM condition over a prolonged period. The amount of carbon deposition on the spent catalysts was quantified by the TGA measurement, indicating the same reaction rate of C-H bond activation (formation of CH_x species) and coke removal reaction. We proposed that the higher stability of these two catalysts is mainly due to the presence of small metal particles, which enlarges the metal-support interface and kinetically inhibits the deposition of inactive coke.

In the following discussion, two different pathways and active sites for H consumption was studied via the H_2 and H_2O formation. It is interesting to note that the H_2O formation is much more resistant against deactivation than H_2 formation on all catalyst for DRM reaction, which corresponds to the non-perimeter metal and perimeter metal. This allows us to monitor the catalyst deactivations for different active sites and reaction pathways. Furthermore, a H_2 and H_2O formation rate in a ratio of 2.5 ± 0.4 on Ni/ZrO_2 catalysts was observed under DRM condition, while on all other oxide supported catalyst the initial formation rate of H_2 was much higher, indicating the disbalance of the CH_x formation and coke removal reaction.

The final chapter concludes the summary and conclusion of this dissertation.

1.8. Associated Content

Figure 1-5 reprinted with permission from (Zhang, J.; Wang, H.; Dalai, A. K. *Journal of Catalysis* **2007**, *249*, 300). License number: 4047100008056

Figure 1-11 reprinted with permission from (Zhu, X. L.; Huo, P. P.; Zhang, Y. P.; Cheng, D. G.; Liu, C. J. *Applied Catalysis B-Environmental* **2008**, *81*, 132.). License number: 4047091111760

Figure 1-12 reprinted with permission from (Liu, Z. C.; Zhou, J.; Cao, K.; Yang, W. M.; Gao, H. X.; Wang, Y. D.; Li, H. X. *Applied Catalysis B-Environmental* **2012**, *125*, 324.). License number: 4047090804201

Figure 1-13 reprinted with permission from (Baudouin, D.; Szeto, K. C.; Laurent, P.; De Mallmann, A.; Fenet, B.; Veyre, L.; Rodemerck, U.; Coperet, C.; Thieuleux, C. *Journal of the American Chemical Society* **2012**, *134*, 20624.). Copyright (2012) American Chemical Society.

Figure 1-14 reprinted with permission from (Han, J. W.; Kim, C.; Park, J. S.; Lee, H. *Chemsuschem* **2014**, *7*, 451.). License number: 4047090104805

1.9. References

(1) Horn, R.; Schlogl, R. *Catal Lett* **2015**, *145*, 23.

(2) BP *Tech. rep., BP* **2016**.

(3) Scotchman, I. C. *P Geologist Assoc* **2016**, *127*, 535.

(4) Milkov, A. V. *Earth-Sci Rev* **2004**, *66*, 183.

(5) Tang, P.; Zhu, Q. J.; Wu, Z. X.; Ma, D. *Energ Environ Sci* **2014**, *7*, 2580.

(6) Schlögl, R. *Chemical Energy Storage* **2013**, 443.

(7) Rezaei, M.; Alavi, S. M.; Sahebdelfar, S.; Bai, P.; Liu, X. M.; Yan, Z. F. *Applied Catalysis B-Environmental* **2008**, *77*, 346.

(8) Choudhary, T. V.; Choudhary, V. R. *Angewandte Chemie-International Edition* **2008**, *47*, 1828.

(9) Ross, J. R. H. *Catalysis Today* **2005**, *100*, 151.

(10) Bradford, M. C. J.; Vannice, M. A. *Applied Catalysis a-General* **1996**, *142*, 73.

(11) Gadalla, A. M.; Sommer, M. E. *Chem Eng Sci* **1989**, *44*, 2825.

(12) Gadalla, A. M.; Bower, B. *Chem Eng Sci* **1988**, *43*, 3049.

(13) Therdthianwong, S.; Siangchin, C.; Therdthianwong, A. *Fuel Process Technol* **2008**, *89*, 160.

(14) Liu, Z. Y.; Grinter, D. C.; Lustemberg, P. G.; Nguyen-Phan, T. D.; Zhou, Y. H.; Luo, S.; Waluyo, I.; Crumlin, E. J.; Stacchiola, D. J.; Zhou, J.; Carrasco, J.; Busnengo, H. F.; Ganduglia-Pirovano, M. V.; Senanayake, S. D.; Rodriguez, J. A. *Angewandte Chemie-International Edition* **2016**, *55*, 7455.

(15) Wang, S. B.; Lu, G. Q. M.; Millar, G. J. *Energ Fuel* **1996**, *10*, 896.

(16) Zhang, J. G.; Wang, H.; Dalai, A. K. *Journal of Catalysis* **2007**, *249*, 300.

(17) Ginsburg, J. M.; Pina, J.; El Solh, T.; de Lasa, H. I. *Ind Eng Chem Res* **2005**, *44*, 4846.

(18) Majewski, A. J.; Wood, J.; Bujalski, W. *International Journal of Hydrogen Energy* **2013**, *38*, 14531.

(19) Bradford, M. C. J.; Vannice, M. A. *Catal. Rev.-Sci. Eng.* **1999**, *41*, 1.

(20) Zhang, J.; Wang, H.; Dalai, A. K. *Journal of Catalysis* **2007**, *249*, 300.

(21) Zhang, J. G. *PhD thesis University of Saskatchewan* **2008**.

(22) Shamsi, A.; Johnson, C. D. *Catalysis Today* **2003**, *84*, 17.

(23) Wang, C.; Sun, N.; Zhao, N.; Wei, W.; Zhang, J.; Zhao, T.; Sun, Y.; Sun, C.; Liu, H.; Snape, C. E. *Chemcatchem* **2014**, *6*, 640.

(24) Wang, C. Z.; Sun, N. N.; Kang, M.; Wen, X.; Zhao, N.; Xiao, F. K.; Wei, W.; Zhao, T. J.; Sun, Y. H. *Catal Sci Technol* **2013**, *3*, 2435.

(25) Baudouin, D.; Rodemerck, U.; Krumeich, F.; de Mallmann, A.; Szeto, K. C.; Menard, H.; Veyre, L.; Candy, J. P.; Webb, P. B.; Thieuleux, C.; Coperet, C. *Journal of Catalysis* **2013**, *297*, 27.

(26) Guczi, L.; Stefler, G.; Geszti, O.; Sajo, I.; Paszti, Z.; Tompos, A.; Schay, Z. *Applied Catalysis a-General* **2010**, *375*, 236.

(27) Juan-Juan, J.; Roman-Martinez, M. C.; Illan-Gomez, M. J. *Applied Catalysis a-General* **2009**, *355*, 27.

(28) Ferreira-Aparicio, P.; Rodriguez-Ramos, I.; Anderson, J. A.; Guerrero-Ruiz, A. *Applied Catalysis a-General* **2000**, *202*, 183.

(29) Choudhary, T. V.; Goodman, D. W. *Journal of Molecular Catalysis a-Chemical* **2000**, *163*, 9.

(30) Serrano-Lotina, A.; Daza, L. *Applied Catalysis a-General* **2014**, *474*, 107.

(31) Kahle, L. C. S.; Roussiere, T.; Maier, L.; Delgado, K. H.; Wasserschaff, G.; Schunk, S. A.; Deutschmann, O. *Ind Eng Chem Res* **2013**, *52*, 11920.

(32) Fan, M.-S.; Abdullah, A. Z.; Bhatia, S. *Chemcatchem* **2009**, *1*, 192.

(33) Yamaguchi, A.; Iglesia, E. *Journal of Catalysis* **2010**, *274*, 52.

(34) Ramallo-Lopez, M. A.; Requejo, F. G.; Craievich, A. F.; Wei, J.; Avalos-Borja, M.; Iglesia, E. *Journal of Molecular Catalysis a-Chemical* **2005**, *228*, 299.

(35) Wei, J. M.; Iglesia, E. *Journal of Physical Chemistry B* **2004**, *108*, 4094.

(36) Wei, J. M.; Iglesia, E. *Journal of Catalysis* **2004**, *225*, 116.

(37) Wei, J. M.; Iglesia, E. *Journal of Catalysis* **2004**, *224*, 370.

(38) Osaki, T.; Mori, T. *Journal of Catalysis* **2001**, *204*, 89.

(39) Osaki, T.; Masuda, H.; Mori, T. *Catal Lett* **1994**, *29*, 33.

(40) Rostrupnielsen, J. R.; Hansen, J. H. B. *Journal of Catalysis* **1993**, *144*, 38.

(41) Bradford, M. C. J.; Vannice, M. A. *Applied Catalysis a-General* **1996**, *142*, 97.

(42) Osaki, T.; Masuda, H.; Horiuchi, T.; Mori, T. *Catal Lett* **1995**, *34*, 59.

(43) Matsumoto, H. *Shokubai* **1974**, *16*, 122.

(44) Matsumoto, H. *Shokubai* **1976**, *18*, 71.

(45) Matsumoto, H. *Hyomen* **1977**, *15*, 226.

(46) Bitter, J. H.; Seshan, K.; Lercher, J. A. *Journal of Catalysis* **1997**, *171*, 279.

(47) Bitter, J. H.; Seshan, K.; Lercher, J. A. *Journal of Catalysis* **1998**, *176*, 93.

(48) Bitter, J. H.; Seshan, K.; Lercher, J. A. *Journal of Catalysis* **1999**, *183*, 336.

(49) Nagaoka, K.; Seshan, K.; Aika, K.; Lercher, J. A. *Journal of Catalysis* **2001**, *197*, 34.

(50) Zhang, Z. L.; Verykios, X. E.; MacDonald, S. M.; Affrossman, S. *J Phys Chem-Us* **1996**, *100*, 744.

(51) Bradford, M. C. J.; Vannice, M. A. *Catal Lett* **1997**, *48*, 31.

(52) Bradford, M. C. J.; Vannice, M. A. *Abstr Pap Am Chem S* **1997**, *214*, 44.

(53) Rostrupnielsen, J. R. *Catalysis Today* **1993**, *18*, 305.

(54) Hally, W.; Bitter, J. H.; Seshan, K.; Lercher, J. A.; Ross, J. R. H. *Studies in Surface Science and Catalysis*, 1994; Vol. 88.

(55) Bitter, J. H.; Hally, W.; Seshan, K.; vanOmmen, J. G.; Lercher, J. A. *Catalysis Today* **1996**, *29*, 349.

(56) Zhang, Z. L.; Tsipouriari, V. A.; Efstathiou, A. M.; Verykios, X. E. *Journal of Catalysis* **1996**, *158*, 51.

(57) Chang, J. S.; Park, S. E.; Chon, H. Z. *Applied Catalysis a-General* **1996**, *145*, 111.

(58) Dias, J. A. C.; Assaf, J. M. *Catalysis Today* **2003**, *85*, 59.

(59) Pan, Y. X.; Kuai, P. Y.; Liu, Y. A.; Ge, Q. F.; Liu, C. J. *Energ Environ Sci* **2010**, *3*, 1322.

(60) Wang, S. B.; Lu, G. Q. *Applied Catalysis B-Environmental* **1998**, *19*, 267.

(61) Xu, G. L.; Shi, K. Y.; Gao, Y.; Xu, H. Y.; Wei, Y. D. *Journal of Molecular Catalysis a-Chemical* **1999**, *147*, 47.

(62) Mondal, K. C.; Choudhary, V. R.; Joshi, U. A. *Applied Catalysis a-General* **2007**, *316*, 47.

(63) Sankar, M.; Dimitratos, N.; Miedziak, P. J.; Wells, P. P.; Kiely, C. J.; Hutchings, G. J. *Chem Soc Rev* **2012**, *41*, 8099.

(64) Muraza, O.; Galadima, A. *Int J Energ Res* **2015**, *39*, 1196.

(65) F. Frusteri, F. A., G. Calogero, T. Torre, A. *Catalysis Communications* **2001**, *2*.

(66) Chen, H. W.; Wang, C. Y.; Yu, C. H.; Tseng, L. T.; Liao, P. H. *Catalysis Today* **2004**, *97*, 173.

(67) Lee, J. H.; Lee, E. G.; Joo, O. S.; Jung, K. D. *Applied Catalysis a-General* **2004**, *269*, 1.

(68) Valentini, A.; Carreno, N. L. V.; Probst, L. F. D.; Lisboa-Filho, P. N.; Schreiner, W. H.; Leite, E. R.; Longo, E. *Applied Catalysis a-General* **2003**, *255*, 211.

(69) Tomishige, K.; Himeno, Y.; Matsuo, Y.; Yoshinaga, Y.; Fujimoto, K. *Ind Eng Chem Res* **2000**, *39*, 1891.

(70) Choudhary, V. R.; Mamman, A. S. *J Chem Technol Biot* **1998**, *73*, 345.

(71) Fan, M. S.; Abdullah, A. Z.; Bhatia, S. *International Journal of Hydrogen Energy* **2011**, *36*, 4875.

(72) Fan, M. S.; Abdullah, A. Z.; Bhatia, S. *Chemsuschem* **2011**, *4*, 1643.

(73) Takanabe, K.; Nagaoka, K.; Nariai, K.; Aika, K. *Journal of Catalysis* **2005**, *232*, 268.

(74) Fan, M. S.; Abdullah, A. Z.; Bhatia, S. *Applied Catalysis B-Environmental* **2010**, *100*, 365.

(75) You, X. J.; Wang, X.; Ma, Y. H.; Liu, J. J.; Liu, W. M.; Xu, X. L.; Peng, H. G.; Li, C. Q.; Zhou, W. F.; Yuan, P.; Chen, X. H. *Chemcatchem* **2014**, *6*, 3377.

(76) Hua, W.; Jin, L. J.; He, X. F.; Liu, J. H.; Hu, H. Q. *Catal Commun* **2010**, *11*, 968.

(77) Rahemi, N.; Haghighi, M.; Babaluo, A. A.; Jafari, M. F.; Estifaee, P. *J Nanosci Nanotechno* **2013**, *13*, 4896.

(78) Rahemi, N.; Haghighi, M.; Babaluo, A. A.; Jafari, M. F.; Khorram, S. *J Appl Phys* **2013**, *114*.

(79) Takanabe, K.; Nagaoka, K.; Nariai, K.; Aika, K. *Journal of Catalysis* **2005**, *230*, 75.

(80) Nakamura, J.; Aikawa, K.; Sato, K.; Uchijima, T. *Catal Lett* **1994**, *25*, 265.

(81) Erdohelyi, A.; Cserenyi, J.; Solymosi, F. *Journal of Catalysis* **1993**, *141*, 287.

(82) Basini, L.; Sanfilippo, D. *Journal of Catalysis* **1995**, *157*, 162.

(83) Liu, C. J.; Zou, J. J.; Yu, K. L.; Cheng, D. G.; Han, Y.; Zhan, J.; Ratanatawanate, C.; Jang, B. W. L. *Pure Appl Chem* **2006**, *78*, 1227.

(84) Chu, W.; Wang, L. N.; Chernavskii, P. A.; Khodakov, A. Y. *Angewandte Chemie-International Edition* **2008**, *47*, 5052.

(85) Zhao, B. R.; Yan, X. L.; Zhou, Y.; Liu, C. J. *Ind Eng Chem Res* **2013**, *52*, 8182.

(86) Bo, Z.; Yan, J. H.; Li, X. D.; Chi, Y.; Cen, K. F. *International Journal of Hydrogen Energy* **2008**, *33*, 5545.

(87) Chen, H. L.; Lee, H. M.; Chen, S. H.; Chao, Y.; Chang, M. B. *Applied Catalysis B-Environmental* **2008**, *85*, 1.

(88) Zhu, X. L.; Huo, P. P.; Zhang, Y. P.; Cheng, D. G.; Liu, C. J. *Applied Catalysis B-Environmental* **2008**, *81*, 132.

(89) Wang, N.; Shen, K.; Yu, X. P.; Qian, W. Z.; Chu, W. *Catal Sci Technol* **2013**, *3*, 2278.

(90) Halliche, D.; Cherifi, O.; Auroux, A. *Thermochim Acta* **2005**, *434*, 125.

(91) Frontera, P.; Macario, A.; Aloise, A.; Crea, F.; Antonucci, P. L.; Nagy, J. B.; Frusteri, F.; Giordano, G. *Catalysis Today* **2012**, *179*, 52.

(92) Kawi, S.; Kathiraser, Y.; Ni, J.; Oemar, U.; Li, Z. W.; Saw, E. T. *Chemsuschem* **2015**, *8*, 3556.

(93) Liu, Z. C.; Zhou, J.; Cao, K.; Yang, W. M.; Gao, H. X.; Wang, Y. D.; Li, H. X. *Applied Catalysis B-Environmental* **2012**, *125*, 324.

(94) Wang, N.; Xu, Z. X.; Deng, J.; Shen, K.; Yu, X. P.; Qian, W. Z.; Chu, W.; Wei, F. *Chemcatchem* **2014**, *6*, 1470.

(95) Wang, N.; Shen, K.; Huang, L. H.; Yu, X. P.; Qian, W. Z.; Chu, W. *Acs Catal* **2013**, *3*, 1638.

(96) Baudouin, D.; Szeto, K. C.; Laurent, P.; De Mallmann, A.; Fenet, B.; Veyre, L.; Rodemerck, U.; Coperet, C.; Thieuleux, C. *Journal of the American Chemical Society* **2012**, *134*, 20624.

(97) Han, J. W.; Kim, C.; Park, J. S.; Lee, H. *Chemsuschem* **2014**, *7*, 451.

(98) MacGillivray, L. R.; Atwood, J. L. *Nature* **1997**, *389*, 469.

(99) Zhang, Q.; Tiefenbacher, K. *Journal of the American Chemical Society* **2013**, *135*, 16213.

(100) McKinlay, R. M.; Thallapally, P. K.; Cave, G. W. V.; Atwood, J. L. *Angewandte Chemie-International Edition* **2005**, *44*, 5733.

(101) Zhang, Q.; Tiefenbacher, K. *Nat Chem* **2015**, *7*, 197.

(102) Dalgarno, S. J.; Power, N. P.; Atwood, J. L. *Coordin Chem Rev* **2008**, *252*, 825.

Chapter 2

Enhanced activity in methane dry reforming by CO_2 induced surface restructuring of Ni/ZrO_2

The activity of Ni/ZrO_2 catalysts for dry reforming of methane and its thermal stability are largely enhanced by activation and regeneration in presence of CO_2 above 873 K. After reduction in H_2, Ni particles are partly covered with Zr-suboxides. The exposure to CO_2 reduces this coverage and creates a larger ZrO_2-Ni interface. Being equilibrated with the metal surface, the Zr-suboxide acts as catalyst by accepting and later transferring one oxygen of CO_2 to the Ni surface, releasing CO in the decomposition of transiently formed carbonates. This leads to an additional channel of CO_2 dissociation in addition to the direct CO_2 dissociation on Ni. The higher, kinetically controlled availability of atomic oxygen on Ni is concluded to reduce the carbon concentration on the surface, leading to less refractory carbon deposition.

2.1. Introduction

Dry reforming of methane (DRM) leads to synthesis gas with H_2/CO ratios close to 1 and is frequently used to decrease this ratio in combined CH_4 reforming processes. To reach acceptable conversion levels, temperatures around 900 K are required.[1-5] Therefore, a significant challenge for the stability of reforming catalysts is to relieve sintering of the active metal.[6] The other major challenge is to prevent coke deposition since the composition of reactants in dry reforming thermodynamically favors formation of carbon deposits.[7,8]

To minimize sintering, metal particles have been stabilized on supports that prevent growth by limiting both transport of individual atoms, as well as coalescence of metal particles.[5,9-15] In literature there is a controversial discussion on the role of the metal support interface on the activity and stability of a catalyst in dry reforming of methane. Iglesia et al. proposed that the activity is only related to the active metal and the particle size of the active metal, independent of the support.[16-20] Bitter et al. proposed a bifunctional pathway for dry reforming of methane over Pt/ZrO_2[21-28], where CO_2 is adsorbed and reacts in the vicinity of metal and support, whereas CH_4 is only decomposed at the metal surface. Therefore, they proposed that a catalyst is stable when the rates of CO_2 reduction and CH_4 activation are in balance. Montoya et al. used a Ce doped ZrO_2 support to demonstrate that the oxygen mobility at the metal support interface is crucial for a stable catalyst.[29] They have shown that the metal particles were partially covered with support under reducing conditions being therefore, not accessible for dry reforming.

As the ratio between carbon, oxygen and hydrogen in the feed gas allows carbon formation during methane dry reforming, the rate of carbon formation has to be minimized, either by limiting the formation itself via the synthesis and stabilization of nanoparticles[9,12,13,15,30,31] or by preventing routes to form stable refractory carbon.[5,13,29,32-34] Although great effort has been made in developing stable Ni

based dry reforming catalysts, carbon deposits still need to be removed periodically by oxidative treatments, which pose a challenge in itself, as the highly exothermic reaction with oxygen may lead to metal particle growth.

We report here a new approach overcoming above mentioned limitations via utilizing three principles of stabilizing catalysts for dry reforming. We combine (i) a lower rate of coke formation on a partially reducible support that (ii) stabilizes small metal particles with (iii) an endothermic, thermally less taxing regeneration of the coked catalyst. The combination of CO_2 as oxidant for carbon and of a support, which creates an active interface to the metal atoms and enables a more facile use of one of the oxygen atoms in CO_2 will be shown to combine high activity with high stability. Sites at the interface between Ni and the partially reduced Zr-support are the key for this additional pathway in methane dry reforming, providing oxygen for the reforming process itself as well as for regeneration of the coked catalyst. Oxygen vacancies at the interface between Ni and the ZrO_2 support will be shown to transiently convert CO_2 to carbonates, which in turn decompose, releasing CO and liberating one oxygen of the carbonate to diffuse to the metal surface and to regenerate the oxygen vacancy. Combining steady state and transient kinetic measurements with X-ray absorption spectroscopy the role of the individual steps of reactions for this new pathway will be elucidated.

Figure 2-1. Schematic representation of the DRM reaction over CO_2 treated Ni/ZrO_2 catalyst.

2.2. Experimental section

2.2.1. Chemicals

All chemicals were obtained from commercial suppliers and used as received. Nickel(II) nitrate hexahydrate (Sigma–Aldrich, ≥ 98.5%), zirconium hydroxide (Mel chemicals, XZO1501/03), silicon dioxide (Evonik, Aerosil 200), aluminum oxide (Evonik, Aeroxide AIUC)

2.2.2. Catalyst preparation

Zirconium hydroxide was calcined in air (flow rate 30 ml·min^{-1}) at 1073 K for 15 h with a heating rate of 0.5 K·min^{-1}. Ni-based catalysts supported on SiO_2, Al_2O_3 and ZrO_2 were prepared by incipient wetness impregnation using nickel(II) nitrate hexahydrate ($Ni(NO_3)_2{\cdot}6H_2O$) as Ni precursor. Typically, $Ni(NO_3)_2{\cdot}6H_2O$ was dissolved in doubly distilled water to form a transparent green solution, and then the aqueous solution was slowly dropped onto support with continuous stirring at ambient temperature for 1 h. After impregnation at room temperature for further 20 h, the catalysts were dried at 373 K for 12 h. Afterwards, the catalyst was calcined in air at 673 K (heating rate 0.5 K·min^{-1}) for 2 h (flow rate 100 mL·min^{-1}) and reduced with pure H_2 at 873 K (heating rate 0.5 K·min^{-1}) for 2 h (flow rate 100 mL·min^{-1}).

2.2.3. Catalyst characterization

Elemental analysis was performed with atomic absorption spectroscopy (AAS) on a UNICAM 939 AA-Spectrometer. The BET specific surface area was determined from N_2 adsorption-desorption isotherms measured at 77 K on a PMI automatic BET-Sorptometer. Before measurement, the sample was activated in vacuum at 473 K for 2 h.

IR spectra of adsorbed CO was measured on a Bruker Vertex 70 spectrometer at a resolution of 4 cm^{-1} collecting 128 scans in transmission absorption mode. The samples were pressed into self-supporting wafers and activated in flowing H_2 (p = 1 bar) at 923 K for 1 h (heating rate 10 $K \cdot min^{-1}$) and then outgassed at 923 K for 0.5 h ($p < 10^{-4}$ mbar) to remove H_2. After lowering the temperature to 313 K, the catalysts were exposed to CO (p = 5 mbar) for 0.5 h. Then, the catalysts were evacuated at 313 K for 30 min to remove the physically adsorbed CO. IR spectra of adsorbed CO on Ni/ZrO_2 were measured afterwards. Subsequently, Ni/ZrO_2 was treated in flowing CO_2 (p = 1 bar) at 923 K for 1 h, cooled to 313 K in CO_2 (p = 10 mbar). Then, the Ni/ZrO_2 catalyst was reduced in flowing H_2 (p = 1 bar) at 923 K for 1 h (heating rate 10 $K \cdot min^{-1}$). After outgassing at 923 K for 0.5 h ($p < 10^{-4}$ mbar), the temperature was lowered to 313 K. CO was adsorbed at 313 K with pressure of 5 mbar followed by evacuation. Afterwards, the IR spectra of adsorbed CO were recorded until no further changes in the spectra were observed.

2.2.4. Catalytic measurements

The catalytic activities of prepared catalysts (20 mg catalyst diluted in 480 mg SiC) were studied in a fix bed flow reactor at 873 K and atmospheric pressure. The catalysts were loaded in a quartz tube (7 mm diameter) and reduced in situ with 20 vol% H_2 in N_2 (total flow rate 100 $mL \cdot min^{-1}$) at 873 K for 2 h. Then, the catalysts were heated to 1073 K in N_2 and the DRM reaction was carried out afterwards. The reactant gases consisted of 25 vol% CH_4 (99.995 vol%), 25 vol% CO_2 (99.995 vol%) and 50 vol% N_2 (99.999 vol%) with a total flow of 100 mL/min. N_2 was used as inert internal standard. The reaction products were analyzed online by Shimadzu GC-MS and GC fitted with TCD and FID. Reaction rate was expressed as methane consumption rate and calculated using following equations:

$$\text{Reaction rate} = \frac{Conversion_{CH_4} \times CH_{4\,in}}{n_{Ni}}$$

(**Equation 2-1**)

in which $CH_{4\ in}$ is the CH_4 amount in feed gas, and n_{Ni} is total amount of Ni on the catalysts. The conversion of CH_4 during DRM reaction was calculated as follows:

$$\text{Conversion}_{CH_4} = \frac{CH_{4\ in} - CH_{4\ out}}{CH_{4\ in}} \times \frac{N_{2\ in}}{N_{2\ out}} \times 100\%$$

(**Equation 2-2**)

in which $CH_{4\ out}$ is the CH_4 amount in outlet gas. The conversion of methane was normalized to the amount of N_2 in feed gas ($N_{2\ in}$) and outlet gas ($N_{2\ out}$).

The CO_2 regeneration reaction was carried out in situ at 1073 K. After 100 mins of DRM, the reaction was stopped and the catalysts were exposed to a stream of 100 % N_2 or CO_2 (flow rate 50 mL·min^{-1}) at 1073 K for 100 minutes. Subsequently, CH_4 and CO_2 were introduced into the reactor again and DRM reaction was produced directly after CO_2 regeneration. Two subsequent cycles of CO_2 treatment and DRM reaction were produced under the same condition, which was shown in Figure 2-2. The N_2 interruption test was carried out under the same condition by using N_2 instead of CO_2.

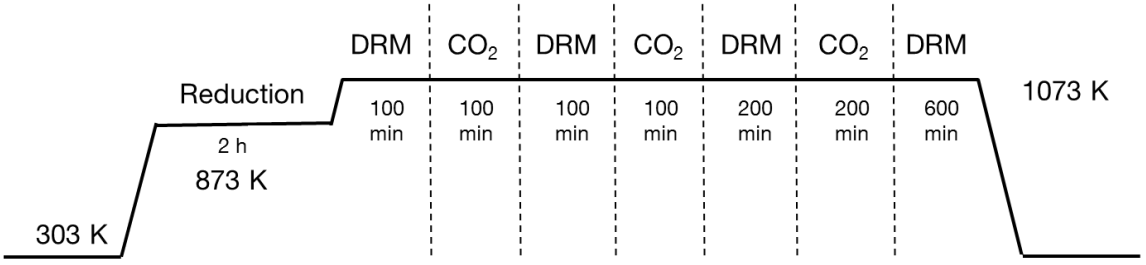

Figure 2-2. Schematic representation of in situ CO_2 regeneration and DRM reaction at 1073 K and atmospheric pressure.

2.3. Results and discussion

2.3.1. Deactivation of Ni/ZrO_2 catalyst

As aforementioned, the main problem for the DRM reaction is the deactivation of DRM catalysts caused by sintering of metal particles and coke formation.[2-5,7] Thus, it is necessary to find out which factor is more essential for the stability of DRM catalysts. In view of this, a N_2 interruption test was planned to study the effect of sintering and coke formation on the reaction behavior. As shown in Figure 2-3(a), Ni/ZrO_2 catalyst showed decreased activity during 20 h of DRM reaction as the most DRM catalysts. A parallel experiment was carried out by treating the DRM catalyst with N_2 in situ at reaction temperature. As shown in Figure 2-3(b), after 100 minutes of DRM reaction the reaction was stopped and the catalysts were exposed to pure N_2 for 100 minutes. Thus, no DRM reaction was carried out during this period. After this step the rate on Ni/ZrO_2 did not decreased after switching back to reaction conditions, indicating the same amount of active site for dry reforming reaction. Two subsequent cycles with N_2 exposure followed by DRM reaction confirmed the unchanged concentration of surface nickel for methane activation during this N_2 treatment. Therefore, we concluded that no sintering occurred during this N_2 treatment at the temperature for DRM reaction. In contrast, as the DRM proceeds, Ni/ZrO_2 showed decreased activity, which is mainly due to the formation of inactive carbon species on the catalyst.

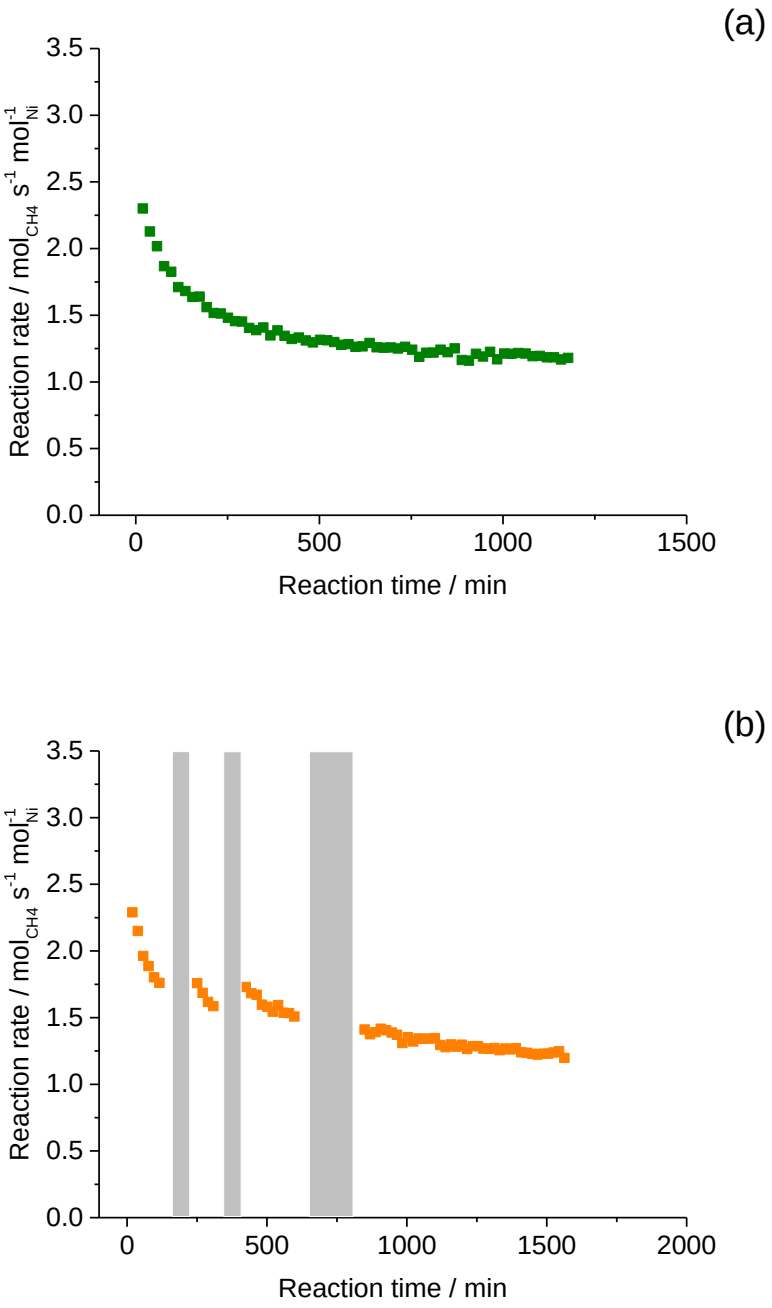
(a)
Reaction rate / mol_{CH4} s^{-1} mol_{Ni}^{-1}
3.5
3.0
2.5
2.0
1.5
1.0
0.5
0.0
0
500
1000
1500
Reaction time / min
(b)
Reaction rate / mol_{CH4} s^{-1} mol_{Ni}^{-1}
3.5
3.0
2.5
2.0
1.5
1.0
0.5
0.0
0
500
1000
1500
2000
Reaction time / min

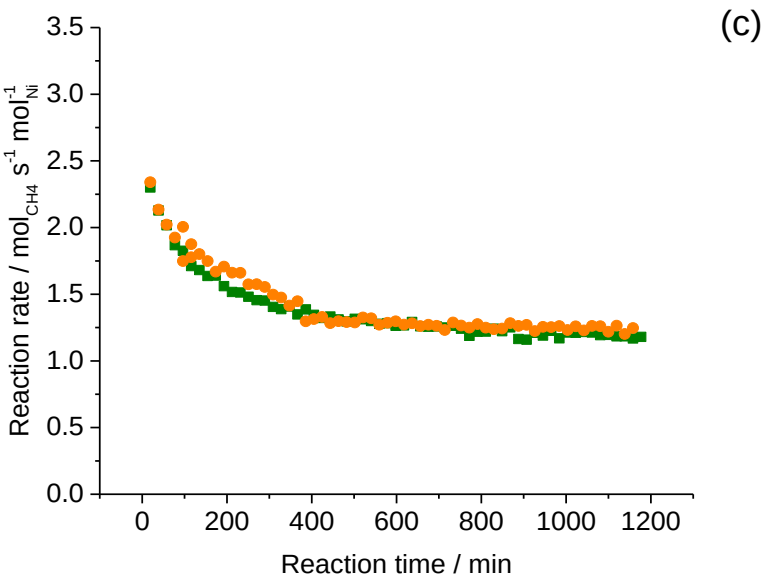

Figure 2-3. DRM rates for Ni/ZrO_2 (Zr8SNi17) at 1073 K at atmospheric pressure without interruption (a) and with N_2 interruption (b). The catalysts were treated in 100 % N_2 in the sections indicated. (c) Plots of DRM rates for Ni/ZrO_2 without interruption (green) and with N_2 interruption (orange) by excluding the section of N_2 treatment.

To further explain the unchanged DRM reactivity of Ni/ZrO_2 catalyst during N_2 treatment, Figure 2-3 (b) was rearranged to exclude the section of N_2 treatment. It is interesting to note that the pattern of CH_4 consumption rate with TOS during DRM reaction were almost identical over N_2 treated and non-treated Ni/ZrO_2 (as shown in Figure 2-3 (c)), which further proved that sintering at high reaction temperature has almost no effect on the deactivation of Ni/ZrO_2 during DRM reaction. As a consequence, formation of inactive coke during DRM reaction was proved to be the critical reason for the deactivation of Ni/ZrO_2 catalyst. For this reason, we focused on the removal of inactive carbon and in situ regeneration of ZrO_2 supported nickel catalyst in the following chapter.

2.3.2. In situ activation and stabilization of Ni/ZrO_2 with CO_2.

Coke deposition on the DRM catalysts can be removed via oxidative treatment using O_2, H_2O and CO_2.[35] However, compared to CO_2 and H_2O, treating Ni catalyst with O_2 at high temperature also lead to sintering of nickel particles. Thus, in this work, Ni/ZrO_2 was regenerated with CO_2 in situ under DRM condition at 1073 K, which showed increased DRM activity after CO_2 treatment.

The turnover rates for CH_4 conversion on ZrO_2 supported Ni catalysts at 1073 K are shown as a function of time on stream in Figure 2-4. In the first 100 minutes these three Ni/ZrO_2 catalysts showed relatively lower DRM activity. After 100 minutes, the reaction was stopped and the catalysts were exposed to a stream of 100 % CO_2 at 1073 K for 100 minutes. After this step the rate on all Ni/ZrO_2 increased markedly after switching back to reaction conditions. The Zr8SNi17 (1.18 wt% Ni/ZrO_2 synthesized by sol gel method) and Ni/ZrO_2 had initial DRM activities of 2.43 and 1.59 $mole_{CH4}\ s^{-1}\ mole_{Ni}^{-1}$, which increased to 3.43 and 3.24 $mole_{CH4}\ s^{-1}\ mole_{Ni}^{-1}$, respectively (shown in Figure 2-4 (a) and (b)). The Zr8Ni1imp (1 wt% Ni/ZrO_2 synthesized by incipient wetness impregnation) exhibits the strongest CO_2 regeneration effect among these three Ni/ZrO_2 catalysts, which increased from 0.38 to 2.76 $mole_{CH4}\ s^{-1}\ mole_{Ni}^{-1}$ (shown in Figure 2-4 (c)). Two subsequent cycles with intermediate CO_2 exposure followed by DRM reaction confirmed the re-activation of the Ni/ZrO_2 catalyst.

(a)

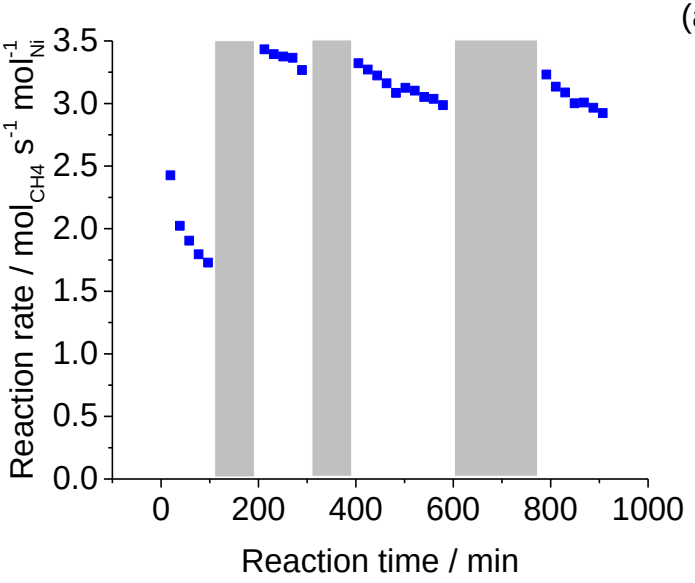
Reaction rate / mol_{CH4} s^{-1} mol_{Ni}^{-1}
3.5
3.0
2.5
2.0
1.5
1.0
0.5
0.0
0
200
400
600
800
1000
Reaction time / min

(b)

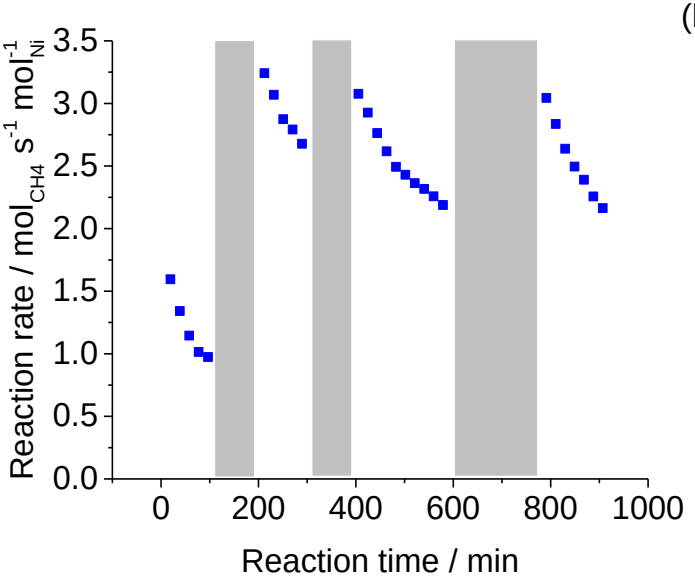
Reaction rate / mol_{CH4} s^{-1} mol_{Ni}^{-1}
3.5
3.0
2.5
2.0
1.5
1.0
0.5
0.0
0
200
400
600
800
1000
Reaction time / min

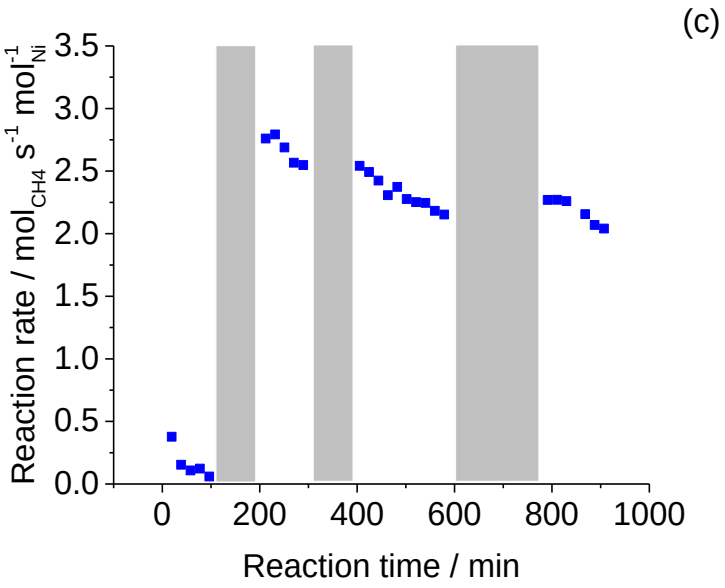

Figure 2-4. DRM rates for (a) Zr8SNi17 (1.18 wt% Ni/ZrO_2 synthesized by sol gel method), (b) 1 wt% Ni/ZrO_2 and (c) Zr8Ni1imp (1 wt% Ni/ZrO_2 synthesized by incipient wetness impregnation). The catalysts were treated in 100 % CO_2 in the sections indicated.

To test the stability of the CO_2 treated catalyst, a reaction with longer TOS was carried out with 1 wt% Ni/ZrO_2. After 100 min of DRM at 1073 K, Ni/ZrO_2 was treated with CO_2 for 100 min and the activity for DRM was monitored for 130 h. As shown in Figure 2-5, the initial reaction rate of methane was 1.59 mol_{CH4} mol_{Ni}^{-1} s^{-1} and decreased to 0.97 mol_{CH4} mol_{Ni}^{-1} s^{-1} after 100 min of DRM. After CO_2 treatment it increased to 3.24 mol_{CH4} mol_{Ni}^{-1} s^{-1}. During the following 130 h of reaction time the reaction rate decreased to 2.12 mol_{CH4} mol_{Ni}^{-1} s^{-1}, which was still above the initial activity before CO_2 activation.

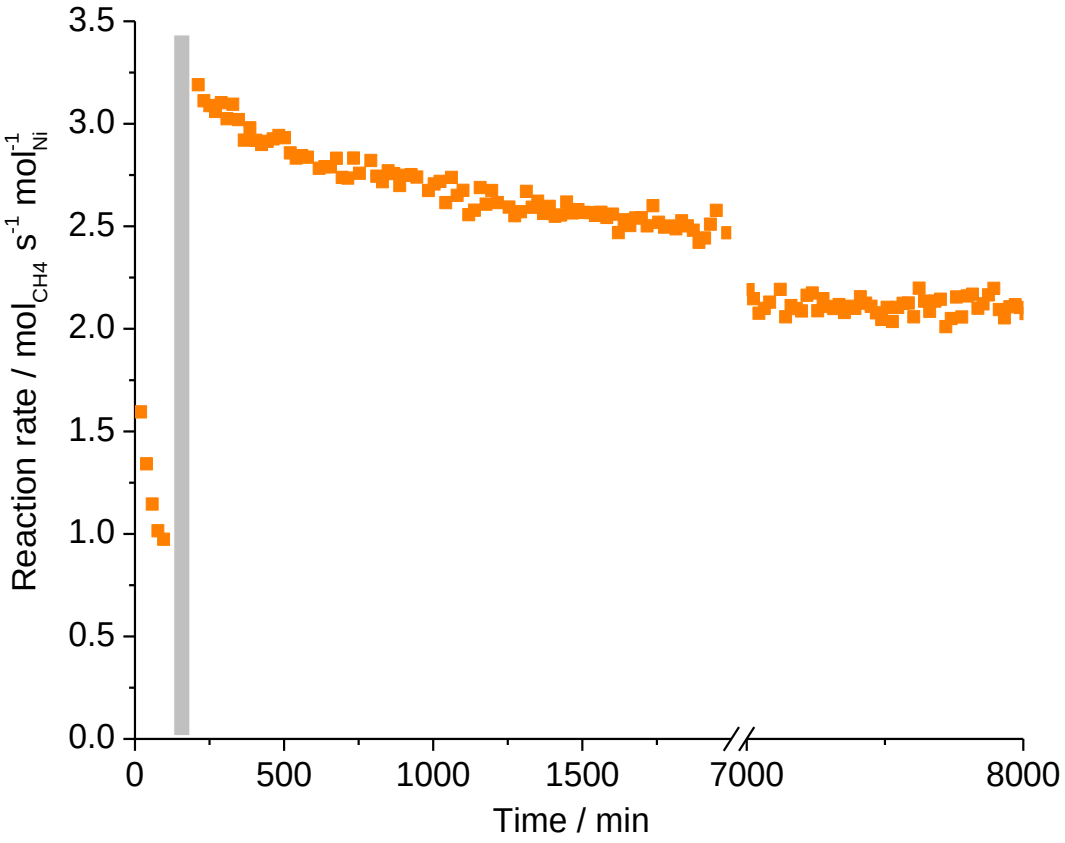

Figure 2-5. DRM rates over a 1% Ni/ZrO_2 during a long term test. The catalysts were treated in 100 % CO2 in the section shaded in grey for 100 min.

2.3.3. Reaction parameters for in situ activation by CO_2.

The changes in the activity demonstrate that Ni/ZrO_2 underwent a chemical or physical transformation by exposure to CO_2. Thus, Pt/ZrO_2 was treated with CO_2 under the same conditions to study the effect of metal on the *in situ* activation. As shown in Figure 2-6, Pt/ZrO_2 showed decreased activity in the first 100 minutes of DRM reaction. Afterwards, Pt/ZrO_2 was treated with pure CO_2 at 1073 K for 100 minutes. However, compared to ZrO_2 supported nickel catalysts, the DRM activity of Pt/ZrO_2 did not increase after CO_2 treatment. Two further in situ CO_2 treatment followed by DRM reaction confirmed that the DRM activity of Pt/ZrO_2 would not be affected by the CO_2 treatment.

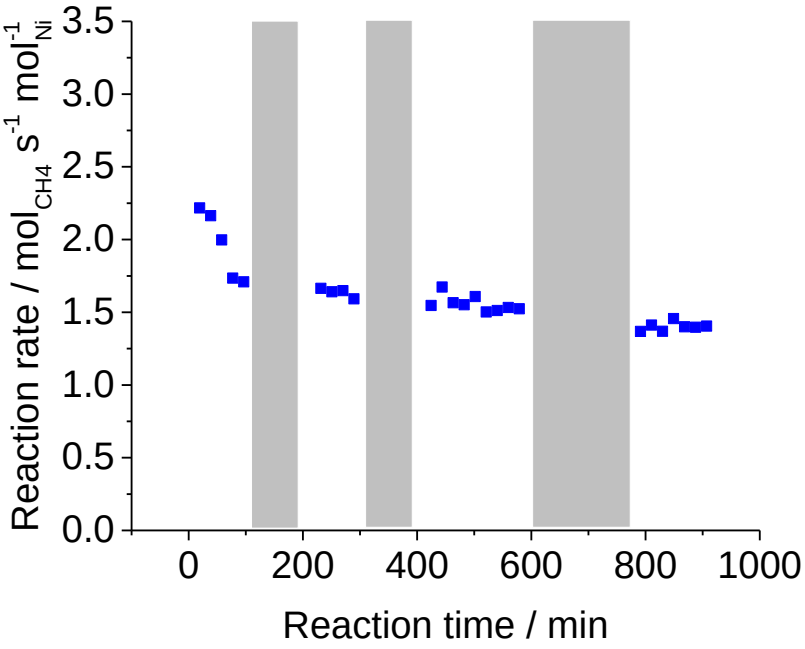

Figure 2-6. DRM rates for Pt/ZrO_2. The catalyst was treated in 100 % CO_2 in the sections indicated.

SiO_2 and Al_2O_3 were also included in this work to demonstrate the effect of support on the CO_2 regeneration. The turnover rates for CH_4 conversion on Ni supported on SiO_2, Al_2O_3 and ZrO_2 at 1073 K are shown as a function of time on stream in Figure 2-7. In the first 100 minutes the rates on the three catalysts were similar. At this point, the reaction was stopped and the catalysts were exposed to a stream of 100 % CO_2 at 1073 K for 100 minutes. After this step the rate on Ni/ZrO_2 increased markedly. It is important to emphasize that for Ni/Al_2O_3, the exposure to CO_2 did not affect the course of deactivation, while Ni/SiO_2 was strongly deactivated. Two subsequent cycles with CO_2 exposure followed by DRM demonstrate that periodical reactivation of Ni/ZrO_2 with CO_2 restitutes the activity of Ni/ZrO_2. It is interesting to note that treatment with CO_2 at 1073 K before DRM increased the reaction rate to the level it reached otherwise after regeneration, i.e., it increased by somewhat less than a factor of three for Ni/ZrO_2. Exposure to He at 1073 K did not affect the activity.

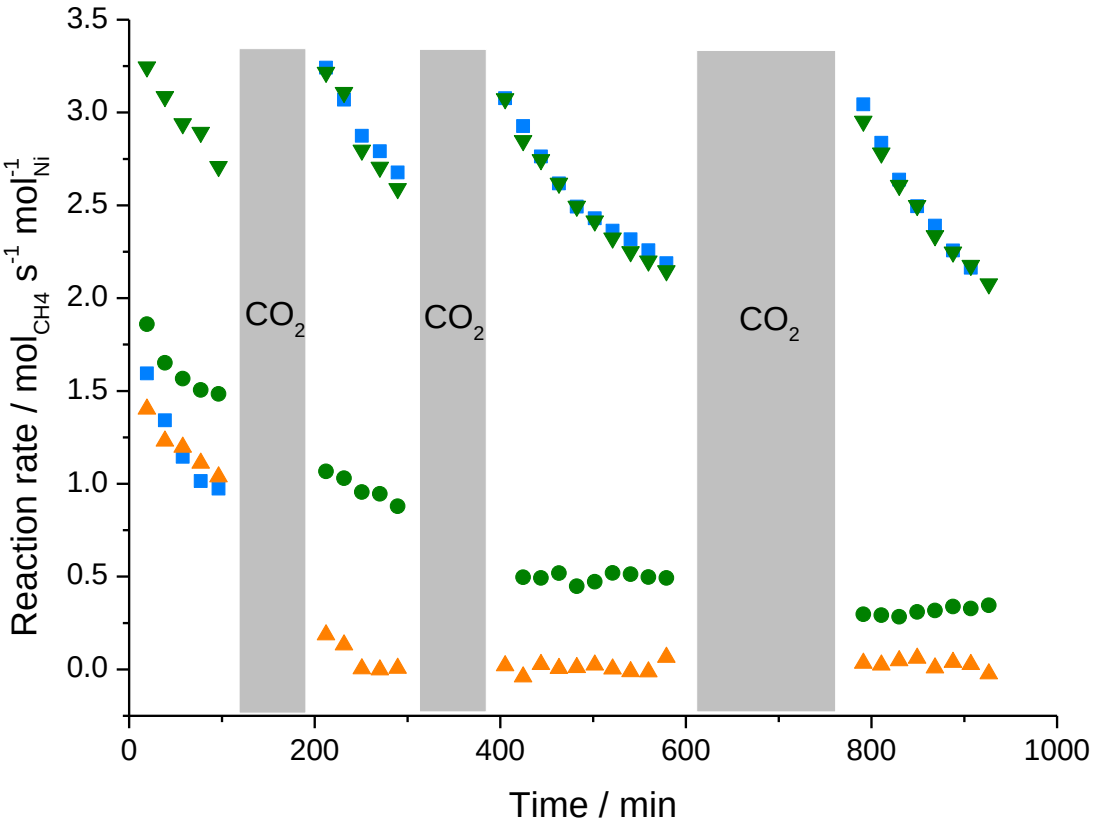

Figure 2-7. DRM rates for (■) Ni/ZrO_2, (●) Ni/Al_2O_3, (▲) Ni/SiO_2 and (▼) CO_2 treated Ni/ZrO_2 at 1073 K before reaction. The catalysts were treated in 100 % CO_2 in the sections indicated. The dotted red line designates the initial reaction rate for CH_4 decomposition at 1073 K.

To differentiate between a chemical reaction of CO_2 with the catalyst and the removal of coke by oxidation, the Ni/ZrO_2 catalyst was treated with O_2 (10 vol% O_2 in N_2) instead of CO_2 between two DRM reaction cycles (as shown in Figure 2-8). In contrast to the CO_2 treatment, the DRM activity did not increase after O_2 treatment as if the DRM reaction would have continued, which can be attributed to a combined effect of coke removal and metal sintering during O_2 treatment. This was also confirmed by a control experiment using O_2 as regeneration gas and the catalyst was treated with CO_2 directly after DRM reaction over O_2 treated Ni/ZrO_2 (as shown in Figure 2-8). The similar initial activities after CO_2 and O_2 treatment

suggested that CO_2 treatment did not change the particle size of Ni on the ZrO_2. Note that during the treatment with CO_2, the oxidation of previously formed carbon deposits as well as that of the metal particles is endothermic (Table 2-1), while the oxidation with oxygen is highly exothermic. Hence, compared to O_2, CO_2 is regarded as a mild oxidizing and regeneration agent.

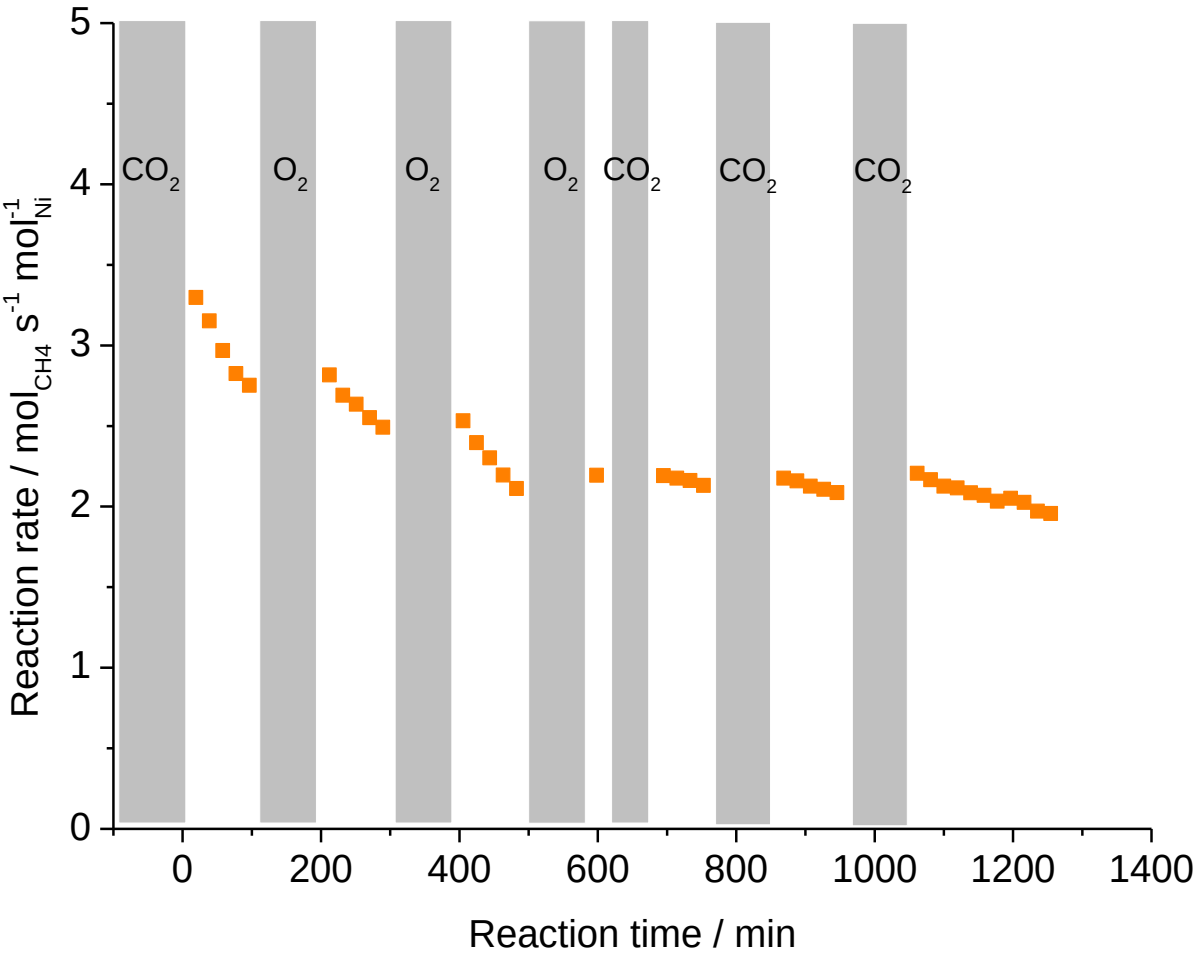

Figure 2-8. DRM rates over a 1% Ni/ZrO_2. The catalysts were treated in situ at 1073 K with 100 % CO_2 or 10 % O_2 in N_2 in the sections indicated.

Table 2-1. Reaction equations and corresponding reaction enthalpies for different oxidation reactions of Ni and carbon.

1.	$CO_2 + C \rightleftharpoons 2CO$	$\Delta H^0 = 169.9$ kJ mol^{-1}
2.	$Ni + CO_2 \rightleftharpoons NiO + CO$	$\Delta H^0 = 47.1$ kJ mol^{-1}
3.	$C + O_2 \rightleftharpoons CO_2$	$\Delta H^0 = -394.8$ kJ mol^{-1}
4.	$2Ni + O_2 \rightleftharpoons 2NiO$	$\Delta H^0 = -235.2$ kJ mol^{-1}

Additionally, the effect of partial pressure of CO_2 during regeneration on the in situ activation was directly observed by flushing the Ni/ZrO_2 catalyst with different concentration of CO_2 in the gas phase. As shown in Figure 2-9, exposing the catalyst during the break in reaction with 5 vol% CO_2 did not affect the course of deactivation. Notably, treating Ni/ZrO_2 with 100 vol%CO_2 led to a strong increase of the activity of Ni/ZrO_2. Thus, the re-activation cannot happen during reaction due to a too low partial pressure of CO_2.

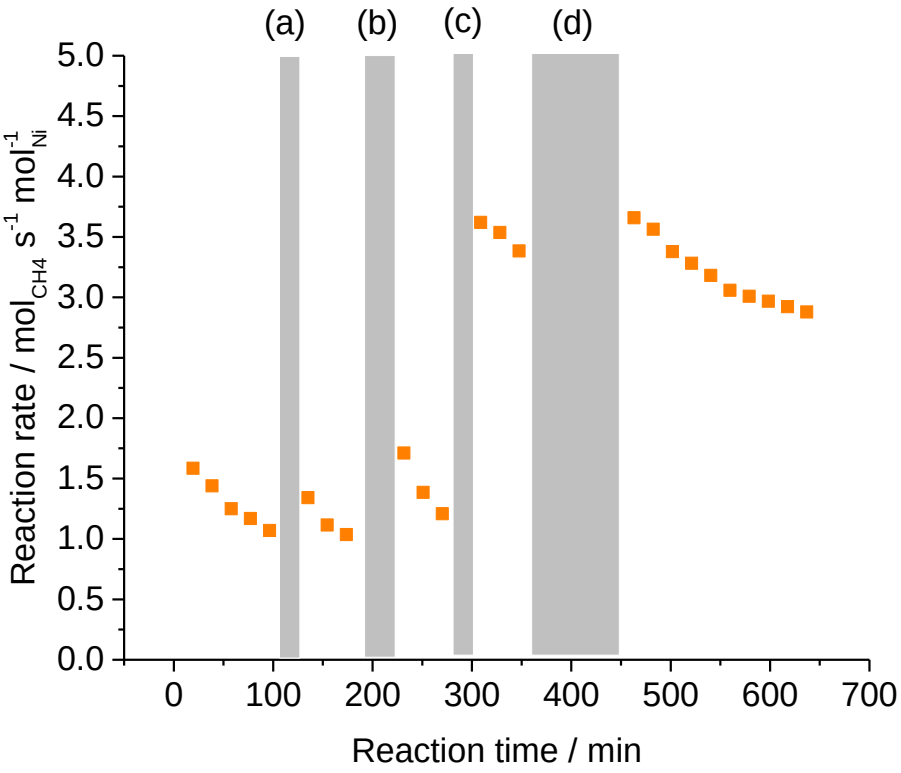

Figure 2-9. Regeneration as a function of CO_2 partial pressure: (a) 5 vol% CO_2 in N_2 for 20 min, (b) 5 vol% CO_2 in N_2 for 40 min,(c) 100 % CO_2 for 20 min and (d) 100 % CO_2 for 40 min.

To further study the influence of the temperature on the in situ activation, the initial activities of CH_4 during DRM reaction were measured over CO_2 treated and untreated Ni/ZrO_2 between 823 and 1073 K. Firstly, Ni/ZrO_2 was in situ reduced in H_2 at 873 K and then the temperature was changed to the reaction temperature. Afterwards, DRM reaction and CO_2 regeneration were produced at the same temperature. As shown in Figure 2-10(a), the exposure of Ni/ZrO_2 to CO_2 at 823 K did not affect the reaction activity, while the initial activities of Ni/ZrO_2 increased after CO_2 treatment at temperature above 873 K. In addition, CO_2 treated nickel catalysts shows more stable reaction behavior in comparison with dry reforming over untreated nickel catalysts, indicating the stabilization and maintenance of the reaction activity after treating with CO_2.

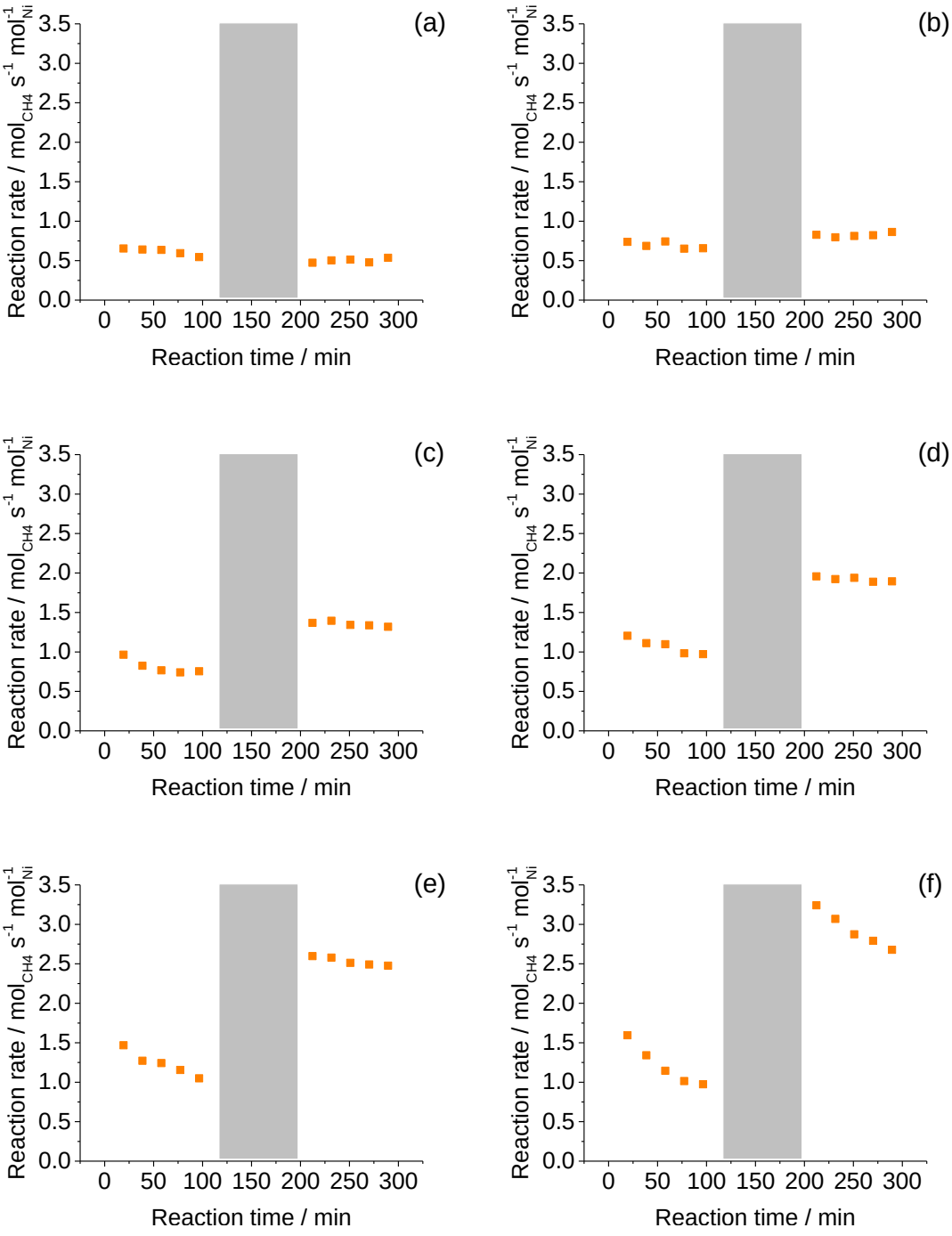

Figure 2-10. DRM rates over a 1% Ni/ZrO_2. The catalysts were treated in situ at (a) 823 K, (b) 873 K, (c) 923 K, (d) 973 K, (e) 1023 K and (f) 1073 K, with 100 % CO_2 in the sections indicated. The DRM reactions were carried out at the same temperature as the temperature for CO_2 treatment.

Furthermore, it is interesting to note that the difference of DRM activities before and after CO_2 regeneration become larger with increasing CO_2 treatment temperatures. The reaction rate and the ratio of initial DRM rate before and after CO_2 treatment was illustrated in Figure 2-11. At 823 K and 873 K, a comparable DRM reactivity before and after CO_2 treatment were observed, while above 873K the differences increased remarkably with increasing temperature. The results further demonstrated that high temperature facilitate the effect of CO_2 regeneration.

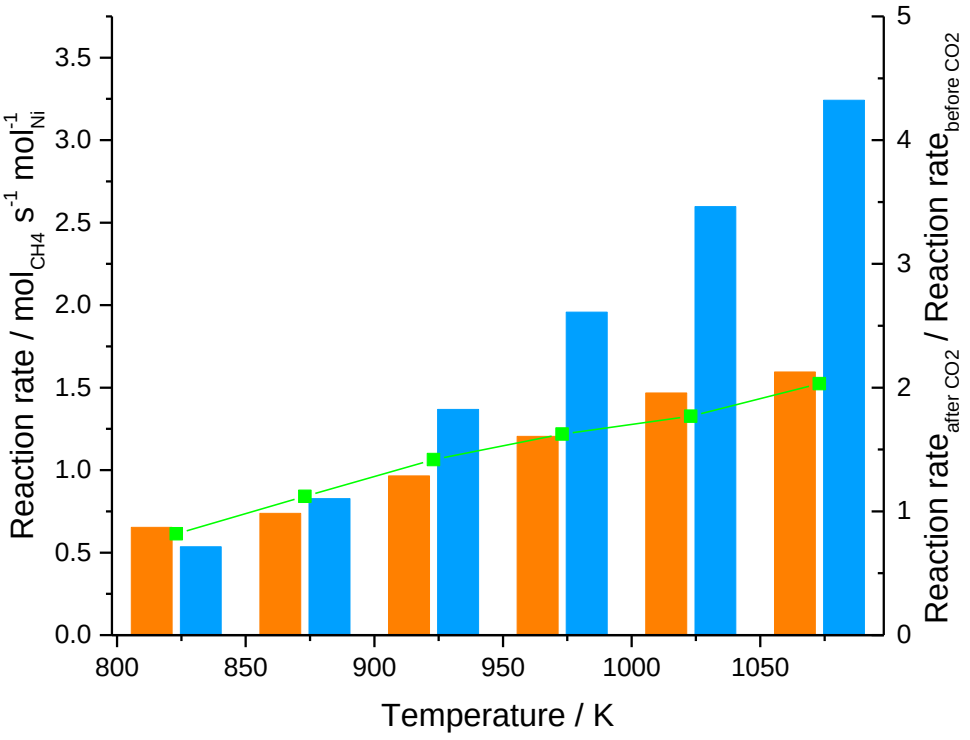

Figure 2-11. Initial DRM rate over 1 wt% Ni/ZrO_2 catalysts before(orange) and after (blue) CO_2 treatment. The green dot indicate the ratio of initial DRM activities over 1 wt% Ni/ZrO_2 catalysts before and after CO_2 treatment.

2.3.4. Mechanism of in situ activation by CO_2 regeneration.

It would be conceivable that the increase in the DRM rate after exposure to CO_2 is associated with the formation of smaller Ni particles formed during exposure to CO_2. As observed by Gonzalez, the exposure of a Ni/ZrO_2 catalyst to CO at high temperature increases the dispersion of the nickel metallic phase.[36] According to the DRIFTS results, $Ni(CO)_4$ complexes were formed via CO treatment, which corrodes the nickel particles and deposit nickel particles onto ZrO_2. Consequently, the size of nickel particles decreased after CO treatment. In our previous work, we have proved that CO_2 could be dissociated on Pt/ZrO_2, releasing oxygen and CO.[24] Thus, this leads us to hypothesize that CO plays a role in activation of Ni/ZrO_2 for DRM reaction.

For this reason, a control experiment with CO treatment was carried out at 1073 K, in which the Ni/ZrO_2 catalyst was treated with 20 vol% CO in N_2 and 100 % CO (total flow rate 100 $mL \cdot min^{-1}$) at 1073 K for 100 min directly after DRM reaction (shown in Figure 2-12). Nonetheless, the reaction activity did not change after in situ CO treatment under the same condition as the CO_2 treatment. Thus, the enhanced DRM activity would not be caused by the increases of nickel dispersion via $Ni(CO)_4$. Moreover, further treatment of Ni/ZrO_2 with pure CO_2 after 600 minutes of DRM lead to an enhanced reaction activity (as shown in Figure 2-14), with an identical reaction rate (3.29 mol_{CH4} mol_{Ni}^{-1} s^{-1}) as the rate after CO_2 regeneration. Consequently, we can exclude that the particle size of metallic nickel is affect by the CO treatment.

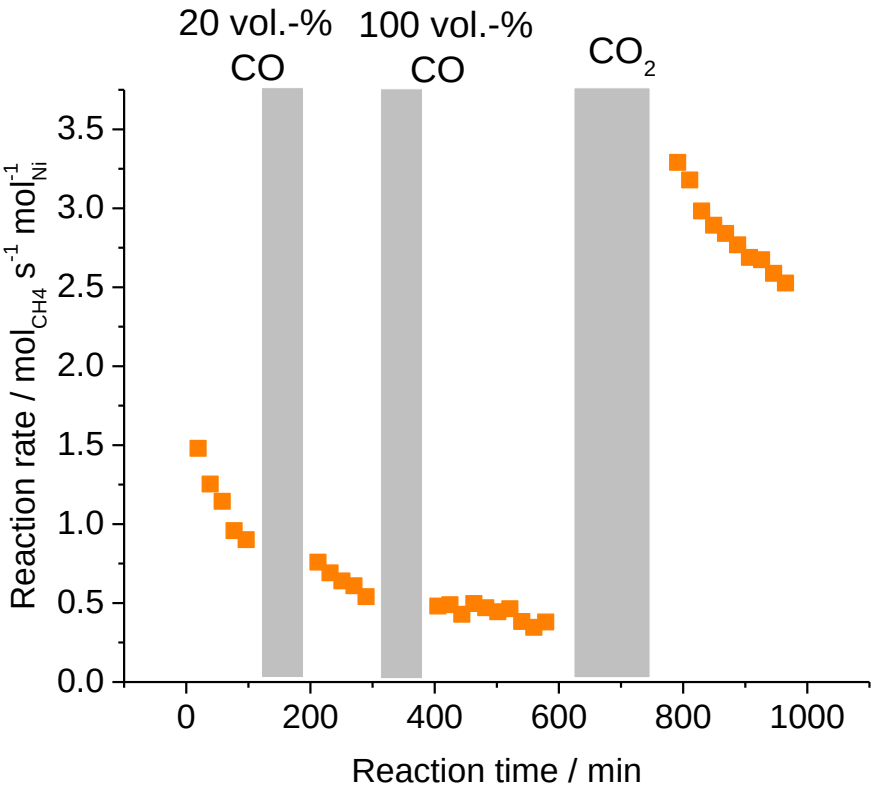

Figure 2-12. DRM rates over a 1% Ni/ZrO_2. The catalysts were treated in situ at 1073 K with 20 vol% CO in N_2, 100 % CO and 100 % CO_2 in the sections indicated, respectively.

The perfect linearity of the Arrhenius plot in Figure 2-13 shows that for both CO_2 treated and untreated catalyst DRM follows the same mechanism over the whole temperature range.[7] As it has been paradigmatically stated in literature [19,37,38] that C-H activation is rate determining, the identical activation energies of 89 and 85 kJ/mol for CO_2 treated and untreated Ni/ZrO_2 proof that the overall mechanism of methane dry reforming is not affected by the CO_2 treatment. The increase of the pre-exponential factor by 2.5 times, indicates that a higher concentration of metal sites was available for CH_4 conversion in the reactor after exposure to CO_2.

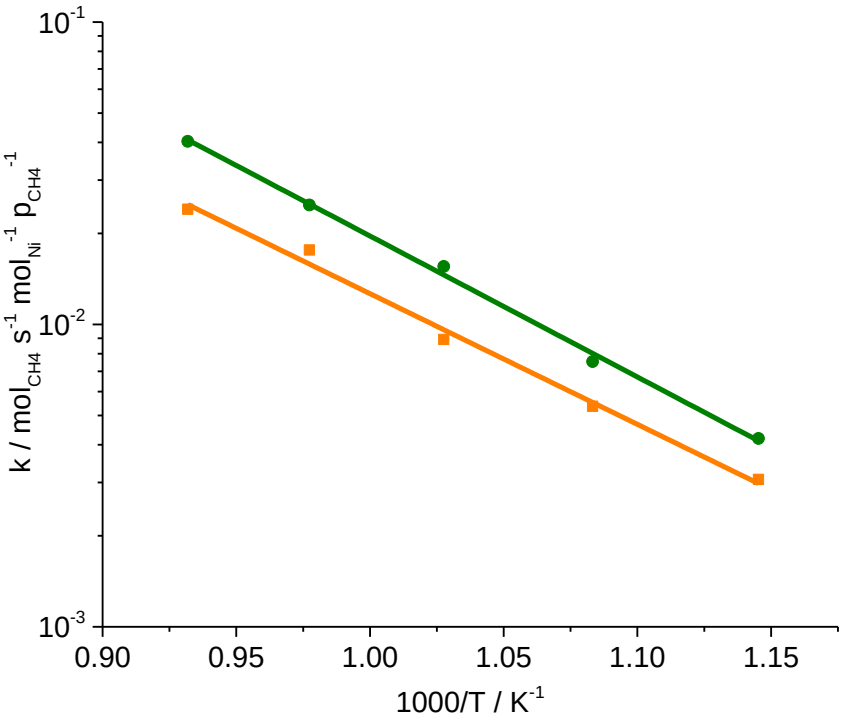

Figure 2-13. Arrhenius plots for dry reforming over CO_2 (●) treated and (●) untreated Ni/ZrO_2.

In order to independently determine the concentration of sites at the metal support interface we turn to IR spectroscopy of adsorbed CO (Figure 2-14 and Table 2A-1). The bands of adsorbed CO above 2000 cm^{-1} are typical for linearly bonded CO on Ni.[39] The shoulder observed above 2100 cm^{-1} is attributed to CO adsorbed on partially oxidized Ni.[39,40] In accordance to Goodman et al., we assign the band at 2085 cm^{-1} to CO adsorbed on Ni at the metal-support interface.[41] Note that this allows in principal to differentiate the undisturbed sites on the metal surface (bands below 2075 cm^{-1}) and sites in vicinity of the ZrO_2 support (band at 2085 cm^{-1}). After the CO_2 treatment, the intensity of the sum of the bands attributed to Ni surface sites increased 2.9 times (assuming that the adsorption coefficient of CO on Ni was identical in the two measurements), while the band at 2085 cm^{-1} increased nearly by a factor of 2. Most importantly the use of CO as probe molecule shows that the corresponding sites on Ni, i.e. the Ni sites adjacent to a defect vary in concentration exactly in proportion to the increase in rate of oxidation of Ni by CO_2 and the increase in rate of CO_2 reduction during DRM.

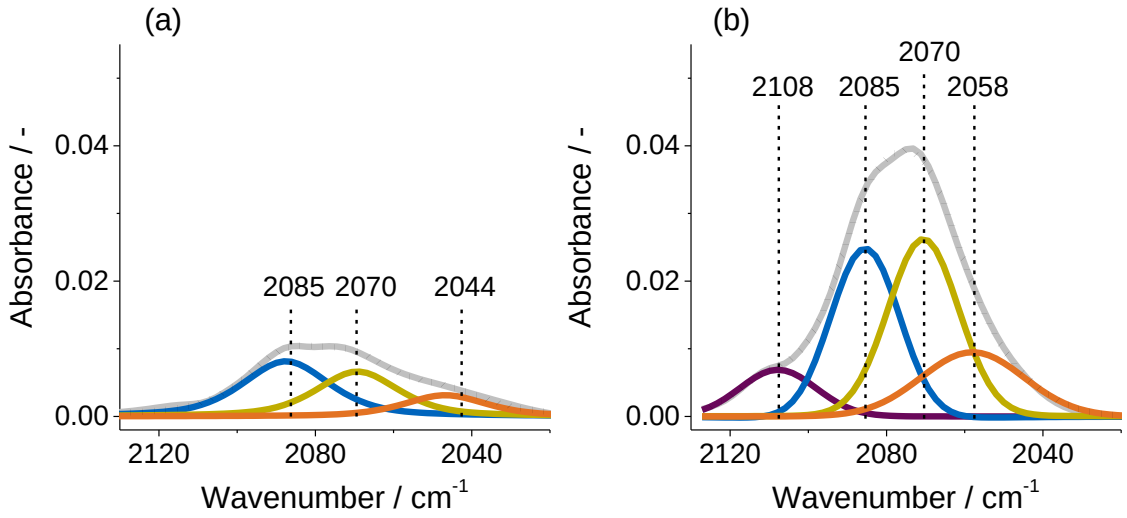

Figure 2-14. IR spectra of CO adsorbed at 5 mbar followed by evacuation on the untreated (a) and CO_2 treated (b) Ni/ZrO_2 catalyst.

The almost identical value of H_2/CO ratio before and after CO_2 regeneration over the whole temperature range further indicated the improved ability to resist coke formation. As shown in Figure 2-15, the initial H_2/CO ratios did not change after treating the Ni catalysts with CO_2 over the temperature range between 823 K and 1073 K. As aforementioned, the total amount of Ni surface sites increased 2.9 times after CO_2 treatment, indicating an enhanced CH_x and H formation rate (via CH_4 decomposition reaction). Thus, the rate of H_2 formation increased via recombination of H species. However, the ratio of H_2/CO did not change, suggesting that the rate of coke removal reaction by the formation of CO also increased after CO_2 activation. Consequently, the CO_2 treated Ni/ZrO_2 catalysts did not show an increased deactivation rate in spite of the increased amount of surface Ni species for CH_4 activation.

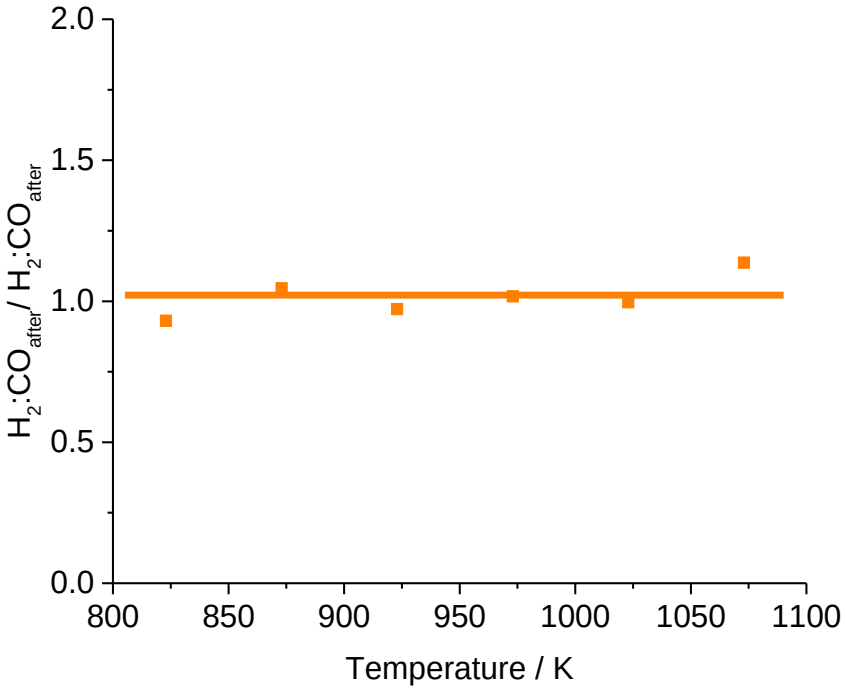

Figure 2-15. Ratio of initial H_2:CO value over 1 wt% Ni/ZrO_2 catalysts before and after CO_2 treatment.

The increased support metal interface was further proved by EXAFS measurement, which was carried out by my coworker Matthias Steib. The results showed that after reduction in H_2, Ni particles are partly covered with Zr-suboxides.[42-47] The exposure to CO_2 reduces the coverage by Zr-suboxides[48] and creates a larger ZrO_2-Ni interface, which is consistent with the result that H_2/CO ratio was not changed after CO_2 treatment. Being equilibrated with the metal surface, the Zr-suboxide acts as catalyst by accepting and later transferring one oxygen of CO_2 to Ni surface releasing CO in the decomposition of transiently formed carbonates. This leads to an additional channel of CO_2 dissociation in addition to the direct CO_2 dissociation on Ni. The higher kinetically controlled availability of atomic oxygen on Ni is hypothesized to reduce the carbon concentration on the surface, leading to less refractory carbon deposition.[35,49,50]

2.4. Conclusions

We have shown that exposure of Ni/ZrO_2 to CO_2 at high temperatures enhances the activity of the catalysts for DRM as well as the rate of oxidation of reduced Ni particles. The proposed reaction mechanism is illustrated in Figure 2-16. The increase in rate has been associated with a higher concentration of accessible Ni metal sites, while the stability is provided by the labile atomic oxygen being able to oxidize surface carbon formed during the dissociation of methane. The formation of this labile oxygen occurs through transiently formed carbonates at the metal support interface, which increases at the same time the fraction of accessible Ni surface sites. In DRM, this effect causes the approximately three-fold higher rate of CO formation by providing additional oxygen to remove carbon formed by the rate determining CH_4 dissociation. During regeneration the availability of oxygen via this route leads to the formation of CO via the (endothermic) Boudouard reaction, which is not as taxing with respect to heat evolution than the more conventional (exothermic) regeneration with O_2. While the nature of the ZrO_2 species at the Ni particles cannot be deduced from the current experiments, all observations are consistent with the fact that treatment with CO_2 maximizes the accessible ZrO_2 - Ni boundary as well as the concentration of metal surface sites. Overall, the results show that (inexpensive) Ni can be successfully used as catalyst in methane dry reforming, when ZrO_2 is used as support, generating a highly dynamic catalyst, which restructures itself during catalysis and regeneration by CO_2 on a nanoscopic level.

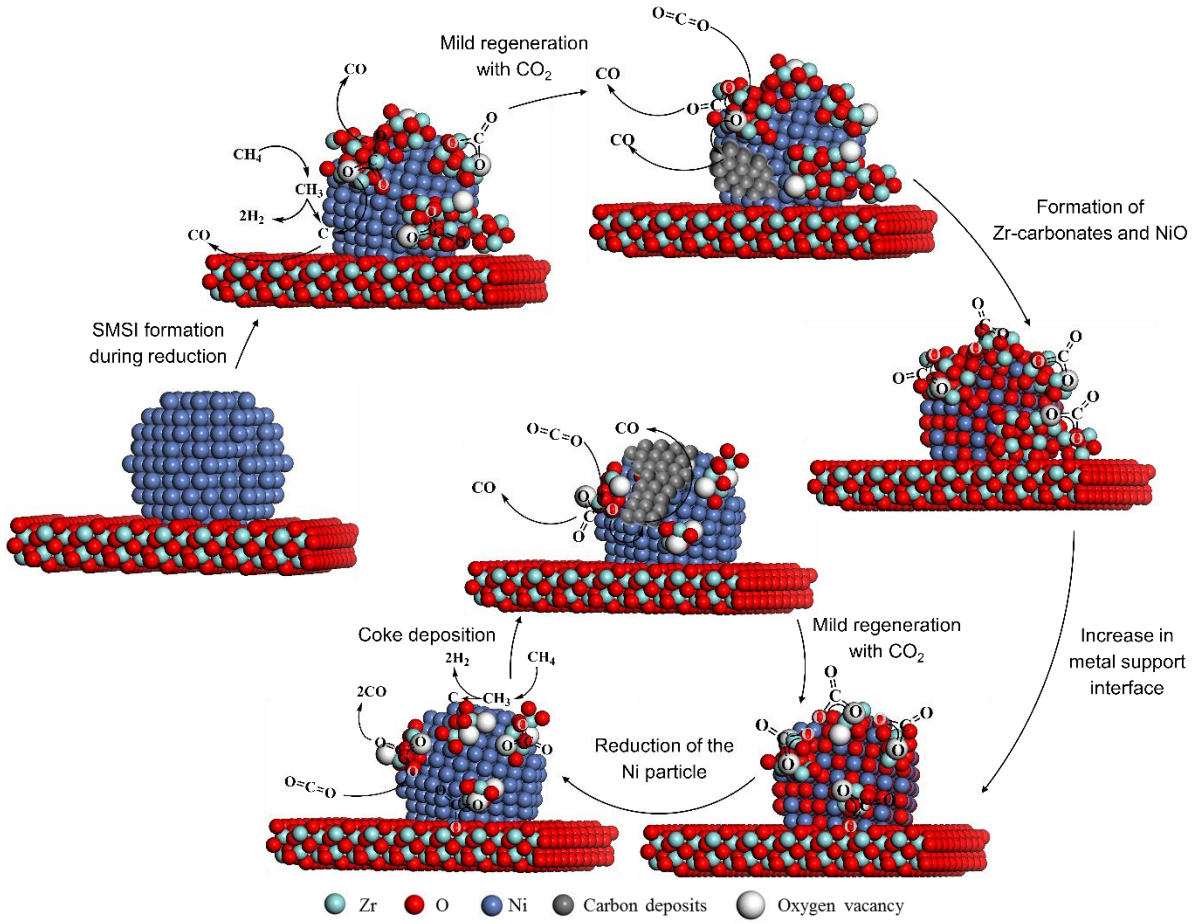

Figure 2-16. Schematic representation of the elementary steps during CO_2 treatment.

2.5. Associated Content

Publication

This chapter is based on the article of the same title as appeared to be submitted in Angewandte Chemie. The content and structure of Chapter 2 is different from this manuscript.

Contributions

Yu Lou did the main contributions in experimental design, kinetic experiments, IR spectroscopy, data analysis and manuscript preparation. Matthias Steib contributed with all EXAFS measurements, data analysis and manuscript preparation. Anita Horvath is responsible for the synthesis of Ni catalysts named Zr8SNi17 and Zr8Ni1imp. Andreas Jentys supervised the topic of CO_2 regeneration and was responsible for data analysis and manuscript preparation. Johannes A. Lercher is the principal investigator of this work.

Acknowledgments

This work was financially supported by the European Union under project ERA Chem and the BMBF under the project ZeitKatMat. The X-Ray absorption experiments were performed on the SuperXAS beamline at the Swiss Light Source, Paul Scherrer Institut, Villigen, Switzerland and at the CLAESS beamline at ALBA Synchrotron with the collaboration of ALBA staff. The authors gratefully acknowledge the beamline scientists Maarten Nachtegaal and Laura Simonelli for their help during the beamtime.

2.6. Appendix

Table 2A-1. Intensities of IR bands after CO adsorption.

Before CO_2 treatment		After CO_2 treatment	
Position / cm^{-1}	Area	Position / cm^{-1}	Area
		2108	0.168
2085	0.282	2085	0.516
2070	0.217	2070	0.603
2044	0.103	2058	0.313
∑	0.602	∑	1.600

2.7. References

(1) Therdthianwong, S.; Siangchin, C.; Therdthianwong, A. *Fuel Process Technol* **2008**, *89*, 160.

(2) Bradford, M. C. J.; Vannice, M. A. *Applied Catalysis a-General* **1996**, *142*, 73.

(3) Bradford, M. C. J.; Vannice, M. A. *Applied Catalysis a-General* **1996**, *142*, 97.

(4) Fan, M.-S.; Abdullah, A. Z.; Bhatia, S. *Chemcatchem* **2009**, *1*, 192.

(5) Liu, C. J.; Ye, J. Y.; Jiang, J. J.; Pan, Y. X. *Chemcatchem* **2011**, *3*, 529.

(6) Liu, Z. Y.; Grinter, D. C.; Lustemberg, P. G.; Nguyen-Phan, T. D.; Zhou, Y. H.; Luo, S.; Waluyo, I.; Crumlin, E. J.; Stacchiola, D. J.; Zhou, J.; Carrasco, J.; Busnengo, H. F.; Ganduglia-Pirovano, M. V.; Senanayake, S. D.; Rodriguez, J. A. *Angewandte Chemie-International Edition* **2016**, *55*, 7455.

(7) Bradford, M. C. J.; Vannice, M. A. *Catal. Rev.-Sci. Eng.* **1999**, *41*, 1.

(8) Kahle, L. C. S.; Roussiere, T.; Maier, L.; Delgado, K. H.; Wasserschaff, G.; Schunk, S. A.; Deutschmann, O. *Ind Eng Chem Res* **2013**, *52*, 11920.

(9) Gould, T. D.; Izar, A.; Weimer, A. W.; Falconer, J. L.; Medlin, J. W. *Acs Catal* **2014**, *4*, 2714.

(10) Liu, Z.; Zhou, J.; Cao, K.; Yang, W.; Gao, H.; Wang, Y.; Li, H. *Applied Catalysis B-Environmental* **2012**, *125*, 324.

(11) Du, X. J.; Zhang, D. S.; Gao, R. H.; Huang, L.; Shi, L. Y.; Zhang, J. P. *Chem Commun* **2013**, *49*, 6770.

(12) Xie, T.; Shi, L. Y.; Zhang, J. P.; Zhang, D. S. *Chem Commun* **2014**, *50*, 7250.

(13) Han, J. W.; Kim, C.; Park, J. S.; Lee, H. *Chemsuschem* **2014**, *7*, 451.

(14) Newnham, J.; Mantri, K.; Amin, M. H.; Tardio, J.; Bhargava, S. K. *International Journal of Hydrogen Energy* **2012**, *37*, 1454.

(15) Wu, T.; Cai, W. Y.; Zhang, P.; Song, X. F.; Gao, L. *Rsc Adv* **2013**, *3*, 23976.

(16) Yamaguchi, A.; Iglesia, E. *Journal of Catalysis* **2010**, *274*, 52.

(17) Ramallo-Lopez, M. A.; Requejo, F. G.; Craievich, A. F.; Wei, J.; Avalos-Borja, M.; Iglesia, E. *Journal of Molecular Catalysis a-Chemical* **2005**, *228*, 299.

(18) Wei, J. M.; Iglesia, E. *Journal of Physical Chemistry B* **2004**, *108*, 4094.

(19) Wei, J. M.; Iglesia, E. *Journal of Catalysis* **2004**, *224*, 370.

(20) Wei, J. M.; Iglesia, E. *Journal of Catalysis* **2004**, *225*, 116.

(21) Nagaoka, K.; Seshan, K.; Aika, K.; Lercher, J. A. *Journal of Catalysis* **2001**, *197*, 34.

(22) Bitter, J. H.; Seshan, K.; Lercher, J. A. *Journal of Catalysis* **1999**, *183*, 336.

(23) Seshan, K.; Bitter, J. H.; Lercher, J. A. In *Recent Advances in Basic and Applied Aspects of Industrial Catalysis*; Rao, T. S. R., Dhar, G. M., Eds. 1998; Vol. 113, p 187.

(24) Bitter, J. H.; Seshan, K.; Lercher, J. A. *Journal of Catalysis* **1998**, *176*, 93.

(25) Bitter, J. H.; Seshan, K.; Lercher, J. A. *Journal of Catalysis* **1997**, *171*, 279.

(26) Lercher, J. A.; Bitter, J. H.; Hally, W.; Niessen, W.; Seshan, K. *Design of stable catalysts for methane-carbon dioxide reforming*, 1996; Vol. 101.

(27) Bitter, J. H.; Hally, W.; Seshan, K.; vanOmmen, J. G.; Lercher, J. A. *Catalysis Today* **1996**, *29*, 349.

(28) Hally, W.; Bitter, J. H.; Seshan, K.; Lercher, J. A.; Ross, J. R. H. *Studies in Surface Science and Catalysis*, 1994; Vol. 88.

(29) Montoya, J. A.; Romero-Pascual, E.; Gimon, C.; Del Angel, P.; Monzon, A. *Catalysis Today* **2000**, *63*, 71.

(30) Han, J. W.; Kim, C.; Park, J. S.; Lee, H. *Chemsuschem* **2014**, *7*, 451.

(31) Baudouin, D.; Szeto, K. C.; Laurent, P.; De Mallmann, A.; Fenet, B.; Veyre, L.; Rodemerck, U.; Coperet, C.; Thieuleux, C. *Journal of the American Chemical Society* **2012**, *134*, 20624.

(32) Xu, B. Q.; Wei, J. M.; Yu, Y. T.; Li, Y.; Li, J. L.; Zhu, Q. M. *Journal of Physical Chemistry B* **2003**, *107*, 5203.

(33) Bachiller-Baeza, B.; Mateos-Pedrero, C.; Soria, M. A.; Guerrero-Ruiz, A.; Rodemerck, U.; Rodriguez-Ramos, I. *Applied Catalysis B-Environmental* **2013**, *129*, 450.

(34) Fan, M.-S.; Abdullah, A. Z.; Bhatia, S. *Applied Catalysis B-Environmental* **2010**, *100*, 365.

(35) Zheng, W. T.; Sun, K. Q.; Liu, H. M.; Liang, Y.; Xu, B. Q. *International Journal of Hydrogen Energy* **2012**, *37*, 11735.

(36) Gonzalez-Delacruz, V. M.; Pereniguez, R.; Temero, F.; Holgado, J. P.; Caballero, A. *Acs Catal* **2011**, *1*, 82.

(37) Bychkov, V. Y.; Krylov, O. V.; Korchak, V. N. *Kinet Catal+* **2002**, *43*, 86.

(38) Xu, B. Q.; Wei, J. M.; Yu, Y. T.; Li, J. L.; Zhu, Q. M. *Top Catal* **2003**, *22*, 77.

(39) Ko, C. S.; Gorte, R. J. *Surf Sci* **1985**, *155*, 296.

(40) Peri, J. B. *Abstr Pap Am Chem S* **1983**, *185*, 37.

(41) Coulter, K.; Xu, X. P.; Goodman, D. W. *J Phys Chem-Us* **1994**, *98*, 1245.

(42) Bernal, S.; Blanco, G.; Calvino, J. J.; Lopez-Cartes, C.; Perez-Omil, J. A.; Gatica, J. M.; Stephan, O.; Colliex, C. *Catal Lett* **2001**, *76*, 131.

(43) Bernal, S.; Calvino, J. J.; Cauqui, M. A.; Gatica, J. M.; Cartes, C. L.; Omil, J. A. P.; Pintado, J. M. *Catalysis Today* **2003**, *77*, 385.

(44) Baker, R. T.; Bernal, S.; Blanco, G.; Cordon, A. M.; Pintado, J. M.; Rodriguez-Izquierdo, J. M.; Fally, F.; Perrichon, V. *Chem Commun* **1999**, 149.

(45) Caballero, A.; Holgado, J. P.; Gonzalez-delaCruz, V. M.; Habas, S. E.; Herranz, T.; Salmeron, M. *Chem Commun* **2010**, *46*, 1097.

(46) Gonzalez-DelaCruz, V. M.; Holgado, J. P.; Pereniguez, R.; Caballero, A. *Journal of Catalysis* **2008**, *257*, 307.

(47) Bernal, S.; Botana, F. J.; Calvino, J. J.; Lopez, C.; PerezOmil, J. A.; RodriguezIzquierdo, J. M. *J Chem Soc Faraday T* **1996**, *92*, 2799.

(48) Mette, K.; Kuhl, S.; Tarasov, A.; Dudder, H.; Kahler, K.; Muhler, M.; Schlogl, R.; Behrens, M. *Catalysis Today* **2015**, *242*, 101.

(49) Ferreira-Aparicio, P.; Rodriguez-Ramos, I.; Anderson, J. A.; Guerrero-Ruiz, A. *Applied Catalysis a-General* **2000**, *202*, 183.

(50) Guczi, L.; Stefler, G.; Geszti, O.; Sajo, I.; Paszti, Z.; Tompos, A.; Schay, Z. *Applied Catalysis a-General* **2010**, *375*, 236.

Chapter 3

Stable Nickel based catalysts for dry reforming of methane

Novel approaches to synthesize highly dispersed nickel particles on ZrO_2 led to catalysts, which are active and stable for dry methane reforming. Successful catalysts had a particle size of around 1 nm and were stable against sintering and extensive carbon formation. Such catalysts had a H_2 and H_2O formation rate in a ratio of 2.5 ± 0.4, while on all others the initial formation rate of H_2 was much higher. On all but the stable Ni/ZrO_2 catalysts, deactivation of H_2 formation was much faster than that of H_2O formation. At longer time on stream the ratio of H_2 and H_2O formation rate was 2.5 ± 0.4 for all the Ni/ZrO_2 catalyst, no matter if they were stable from beginning or after deactivating to a stable level. At higher values, the catalyst underwent severe deactivation. We conclude that H_2 is formed on all surface Ni, while H_2O is preferentially formed close to the Ni-ZrO_2 interface only. As small Ni nanoparticles as observed for 1 wt% Ni/ZrO_2 contained a high fraction of all accessible Ni close to the Ni-ZrO_2 interface, the catalysts was highly stable.

3.1. Introduction

In recent years there has been growing interest in dry reforming reaction, which utilize the greenhouse gases, i.e. CH_4 and CO_2, to produce synthesis gas with H_2/CO ratio close to one[1,2]. Typical catalysts for this reaction include VIIIA metals and noble metals on oxide support. However, supported VIIIA metals catalysts for DRM, i.e. Ni and Co, suffer from strong deactivation as a result of metal sintering and coke deposition under H_2O free reaction conditions.[1,2] The excess rate in the reaction forming surface carbon (Equation 3-1) to the reaction removing surface carbon species (Equation 3-2) was found to be the reason for the coke deposition.

$$CH_4 \overset{Ni}{\rightleftharpoons} C_{Ni\text{-}ads} + 4\,H_{Ni\text{-}ads}$$

(**Equation 3-1**)

$$C_{Ni\text{-}ads} + O_{Ni\text{-}ads\ (from\ CO2)} \rightleftharpoons CO_{(gas)}$$

(**Equation 3-2**)

In our previous work[3] we have identified two reaction pathways for activating CO_2, i.e. on the metal particle and on the boundary between perimeter metal and support. The activation of CO_2 on the boundary is fast enough to transfer O onto the perimeter Ni which removes the surface carbon generated from CH_4 activation, forming CO. While the CO_2 activation on the metal surface is, however, much slower than the carbon deposition from CH_4. Thus, the utilization of transition metal oxides as support, i.e. ZrO_2[3-10] and CeO_2[11-14], have been extensively investigated to improve reactivity and stability due to the higher oxygen storage capacity on these oxide supports. In chapter 2, we have further proved the importance of the Ni-ZrO_2 perimeter in activating CO_2 during DRM reaction, which facilitates the CO_2 activation at the interface between Ni and ZrO_2 and kinetically inhibit the deposition of coke. Furthermore, it is interesting to note that the H_2O formation is much more resistant against deactivation than H_2 formation, indicating two different pathways

and active sites for H_2O and H_2 formation. This, consequently, leads to a continuously decreasing ratio between H_2 and H_2O with TOS during DRM reaction, and allow us to monitor the catalyst deactivations for different active sites and reaction pathways.

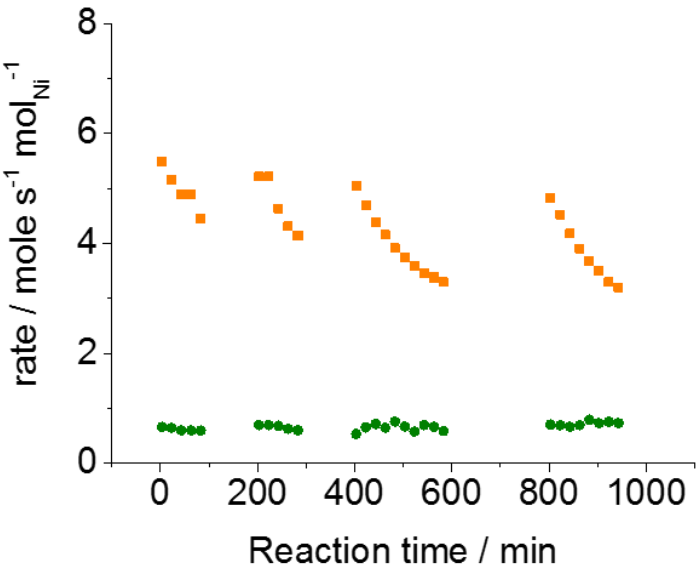

Figure 3-1. Rate of H_2 (orange) and H_2O (green) formation over a Ni/ZrO_2* catalyst at 1073 K during DRM reaction. Interval is treatment under 100 % CO_2 at 1073 K to regenerate catalyst by coke removing. *The catalyst was synthesized by conventional incipient wetness impregnation with metal loading of 1 wt%.

As shown in Figure 3-1, DRM over Ni/ZrO_2*, represented by the formation of H_2 and H_2O, underwent deactivation with TOS due to coke deposition on the catalyst. The rate decreased sharply for H_2 formation, suggesting the largely decreased number of accessible surface Ni (SNi) for both methane activation and H_2 formation (Equation 3-3).

$$2\ H_{\text{Ni-ads}} \rightleftharpoons H_{2\ (\text{gas})}$$

(on the SNi) (**Equation 3-3**)

In contrast, the rate for H_2O formation was much more stable compared to that of H_2 formation. In particular, removing the surface cokes via reverse Boudouard reaction under CO_2 (Equation 3-4), the H_2 formation activity was largely recovered while H_2O formation rate was unaffected. This result indicates that H_2 formation over Ni/ZrO_2 in DRM occurs on Ni sites that easily blocked by cokes while H_2O formation takes place dominantly on a different site that is hardly affected by cokes.

$$CO_2 + C_{\text{Ni-ads}} \rightleftharpoons 2\ CO_{(gas)}$$

(**Equation 3-4**)

The formation of H_2 takes place via the association of two H atoms on surface Ni (Equation 3-3), while the formation of H_2O requires an additional O atom, which is supplied by dissociation of CO_2.

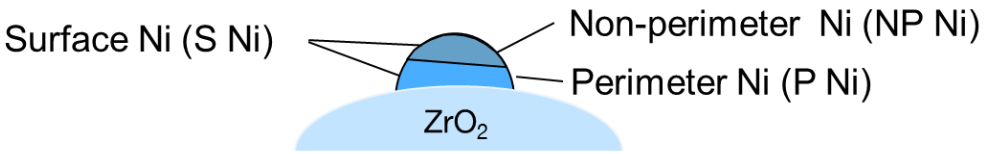

Figure 3-2. Schematic representation of perimeter Nickel (P Ni) and non-perimeter Nickel (NP Ni).

Thus, the evolution pattern of the H_2O formation rate with TOS is explained by the decreased number of surface Ni for CO_2 activation in the initial stage (Equation 3-5(a)) and a stable supply of oxygen via CO_2 activation on the $Ni\text{-}ZrO_2$ perimeter (Equation 3-5(b)).

$$2\ H_{\text{Ni-ads}} + O_{\text{Ni-ads}} \rightleftharpoons H_2O_{(gas)}$$

(on the NP Ni (minority)) (**Equation 3-5a**)

(on the P Ni (majority)) (**Equation 3-5b**)

Therefore, supported metal particles with smaller particle size provide larger metal-support interface and higher fraction of perimeter Ni, and thus promotes the removal of surface carbon species in the DRM reaction. To reduce the metal particle size after calcination and reduction at high temperature, various methods[15-22] have been dedicated to the design of metal catalysts with encapsulated structures. However, these methods require complicated synthesis procedures and rigorous preparation conditions during the synthesis and, therefore, synthesis of well dispersed metal nanoparticles with sizes down to nanometer scale, i.e. 1 nm, for DRM reaction is still a challenge.

In this context, we report a novel method to prepare small and well defined Ni nanoparticles supported on metal oxides under mild conditions. The synthesis of metal colloids uses metal salts (Ni^{2+}) as precursor, which are self-assembled in host capsules[23-26] to protect metal particles against sintering during calcination at high temperature. Ni catalysts synthesized by this new method showed small particle sizes on the support after calcination and reduction at high temperature. The 1 wt% Ni/ZrO_2 was found to be resistant to coke deposition during DRM in terms of larger Ni-ZrO_2 interface, which exhibits extremely high stability during DRM reaction.

3.2. Experimental and theoretical methods

3.2.1. Chemicals

All chemicals were obtained from commercial suppliers and used as received. Ni(II) nitrate hexahydrate (Sigma–Aldrich, ≥ 98.5%), zirconium hydroxide (Mel chemicals, XZO1501/03), silicon dioxide (Evonik, Aerosil 200), aluminum oxide (Evonik, Aeroxide AIUC), chloroform ($CHCl_3$) solution (Sigma, ≥ 99.9 %)

3.2.2. Catalyst preparation

Zirconium hydroxide ($Zr(OH)_4$) was calcined in air (flow rate 30 ml·min^{-1}) at 1073 K for 15 h with a heating rate of 0.5 K·min^{-1}. Ni based catalysts supported on SiO_2, Al_2O_3 and ZrO_2 were prepared using nickel colloidal solution as metal precursor. At first, H_2O saturated $CHCl_3$ solution was prepared by dropping H_2O into $CHCl_3$ and mixed by sonication as described in detail previously[26]. Then pyrogallol[4]arene was added into organic phase, forming a clear solution after gentle heating. Subsequently, $Ni(NO_3)_2{\cdot}6H_2O$ was added in the host molecule solution and the solution was stirred overnight until all $Ni(NO_3)_2{\cdot}6H_2O$ was dissolved. After a period of 20 h, the oxide support was added in the nickel colloidal solution before evaporation under reduced pressure. Afterwards, the as-prepared catalyst was dried at 373 K for 12 h, air-calcined at 673 K (heating rate 0.5 K·min^{-1}) for 2 h (flow rate 100 mL·min^{-1}) and reduced in pure H_2 at 873 K (heating rate 0.5 K·min^{-1}) for 2 h (flow rate 100 mL·min^{-1}).

3.2.3. Catalyst testing

DRM reactions were carried out in a fix bed reactor. Typically, 50 mg of catalysts were diluted with 450 mg SiC. The catalyst sample was loaded in a quartz reactor (7 mm diameter) and reduced with 20 vol% H_2 in N_2 (total flow rate 100 mL·min^{-1}) at 873 K for 2 h before DRM. Afterwards, 25 vol% CH_4 (99.995 vol%), 25 vol%

CO_2 (99.995 vol%) and 50 vol% N_2 (99.999 vol%) with a total flow of 100 mL/min were introduced into the reactor and the DRM reaction was carried out at the same temperature and atmospheric pressure. N_2 was used as calibration standards. The amount of reaction products were determined online by Shimadzu GC-MS and GC, using TCD and FID as detector. Conversion and reaction rate of methane were calculated via aforementioned equation (2-1) and equation (2-2), respectively:

$$\text{Reaction rate} = \frac{Conversion_{CH_4} \times CH_{4\,in}}{n_{Ni}}$$

(**Equation 2-1**)

$$\text{Conversion}_{\text{CH}_4} = \frac{CH_{4\,in} - CH_{4\,out}}{CH_{4\,in}} \times \frac{N_{2\,in}}{N_{2\,out}} \times 100\%$$

(**Equation 2-2**)

3.2.4. Catalyst characterization

The elemental composition of Ni was measured by atomic absorption spectroscopy (AAS) on a UNICAM 939 AA-Spectrometer. The BET specific surface area was determined by nitrogen adsorption-desorption isotherms measured at 77 K on a PMI automatic BET-Sorptometer. The sample was activated in vacuum at 473 K for 2 h prior to the measurement.

Transmission electron microscopy (TEM) images were taken by a JEM-2010 Jeol transmission microscope operating at 120 kV. The sample was firstly made suspension in ethanol by ultrasonication, and a drop of such suspension was deposited onto a carbon-coated Cu grid.

X-ray absorption measurements were performed at the Super XAS beamline at the SLS in Villigen, Switzerland recorded at the with a channel-cut Si(111) monochromator.[27] Data analysis was carried out with Athena and Artemis software from the IFEFFIT[28] package and with FEFF6.[29]

The amount of coke deposits on spent catalysts were quantified by thermogravimetric analysis (TGA) on a SETARAM Sensys Evo system. For these experiments, 10 mg of spent catalysts (SiC free) were loaded in the sample holder. The samples were pretreated in He (flow rate 16 $mL \cdot min^{-1}$) at 473 K (heating rate 10 $K \cdot min^{-1}$) to remove adsorbed H_2O and CO_2 before cooling to 303 K. Subsequently, the temperature was increased to 1073 K (heating rate 5 $K \cdot min^{-1}$) in air (flow rate 16 $mL \cdot min^{-1}$) and kept for 0.5 h. The amount of coke deposition were obtained from the weight loss of the spent catalysts.

^1H–NMR spectra were recorded at 500 MHz, using a Bruker AV 500 spectrometer. ^1H–NMR chemical shifts are given in ppm by using $CHCl_3$ as references (7.26 ppm).

3.3. Results and discussion

3.3.1. Estimation of particle size threshold for stable DRM catalysts

The fraction of perimeter nickel in total number of surface nickel as a function of Ni nanoparticle size was estimated using a hemispherical-shaped model for Ni nanoparticles on the ZrO_2. As shown in our previous work, CO_2 is activated at the oxygen vacancies at the interface between Ni and ZrO_2 to form surface oxygen species in the form of transient carbonates (Figure 3-3).[3-7]

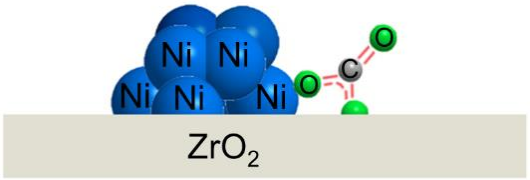

Figure 3-3. Schematic representation of the carbonate formation in the vicinity of Ni and ZrO_2 over DRM catalysts with metal particle size of 0.75 nm

This oxygen is on top of one interface Ni and can react with H or C atoms on its closest adjacent Ni, therefore the surface Ni in the bottom layer, i.e. the layer at Ni-ZrO_2 interface, and in the second layer from the bottom are accessible to oxygen from CO_2 and both are considered as perimeter Ni. Consequently, all the nickel atoms are perimeter Ni when the particle size is below 1 nm (Figure 3-3), while a fraction of the surface Ni was in the third layer from the bottom thus not accessible to oxygen when the particle size is above 1 nm (Figure 3-4).

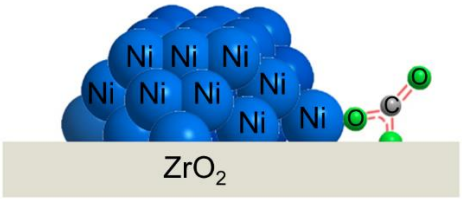

Figure 3-4. Schematic representation of the carbonate formation in the vicinity of Ni and ZrO_2 over DRM catalysts with metal particle size of 1.25 nm

Therefore, we hypothesize that the fractions of perimeter remains 1.0 for the Ni particles with size below 1 nm, however above this threshold this fraction decreased sharply with growing particle size (Figure 3-5). The above calculations show that an ideal Ni/ZrO_2 catalyst for DRM must have Ni particle size of below 1 nm on which every Ni is at the perimeter interface, where the CO_2 activation is faster than surface carbon formation, thus having a very slow coke deposition rate during DRM reaction.

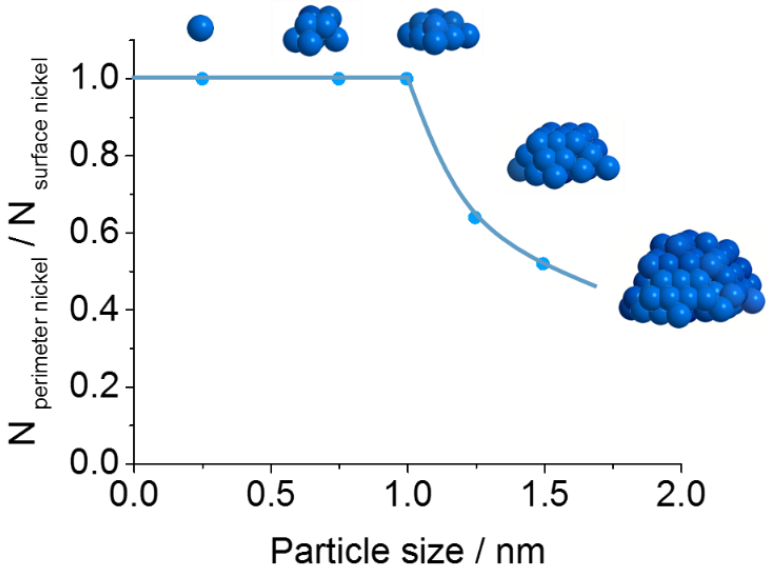

Figure 3-5. Estimation of impact of particle size on the fractions of perimeter nickel in total number of surface nickel.

3.3.2. Synthesis of small nickel and platinum particles via metal colloidal solution

To synthesize nano-sized nickel particles on oxide supports, a novel method using nanocapsules is presented in this work. The compound rccc-5,11,17,23-tetrahydroxy-2,8,14,20-tetra(n-ndecyl)resorc[4]arene (pyrogallol[4]arene) was synthesized according to a literature procedure[30,31], its structure was confirmed by NMR spectroscopy. The Ni colloid was prepared by adding $Ni(NO_3)_2 \cdot 6H_2O$ into a water saturated chloroform ($CHCl_3$) solution (Sigma, ≥ 99.9 %) and mixing by sonication as described in detail previously[26]. After 1 h the solution was added to pyrogallol[4]arene yielding a clear solution after gentle heating. The synthesis strategy is shown in Figure 3-6. The long alkyl chains on the outer surface of nanocapsules provide a large distance between the capsules and metal ions, which is essential for the stability towards aggregation in the colloidal solution and allows to achieve a good dispersion of Ni^{2+} in the precursor solution. The encapsulation of the Ni^{2+} ions by the host molecules was confirmed by the absence of unsolved metal salts in the synthesis mixture after overnight stirring (shown in Figure 3-6).

In a control experiment, $Ni(NO_3)_2 \cdot 6H_2O$ was added into the water saturated $CHCl_3$ solution without pyrogallol[4]arene, which led to sedimentation of Ni salt as it is not soluble in the organic phase. Furthermore, by the increase of the Ni concentration in the water saturated $CHCl_3$ solution from 3 mg/L to 71 mg/L after adding pyrogallol[4]arene confirmed the encapsulation of Ni^{2+}.

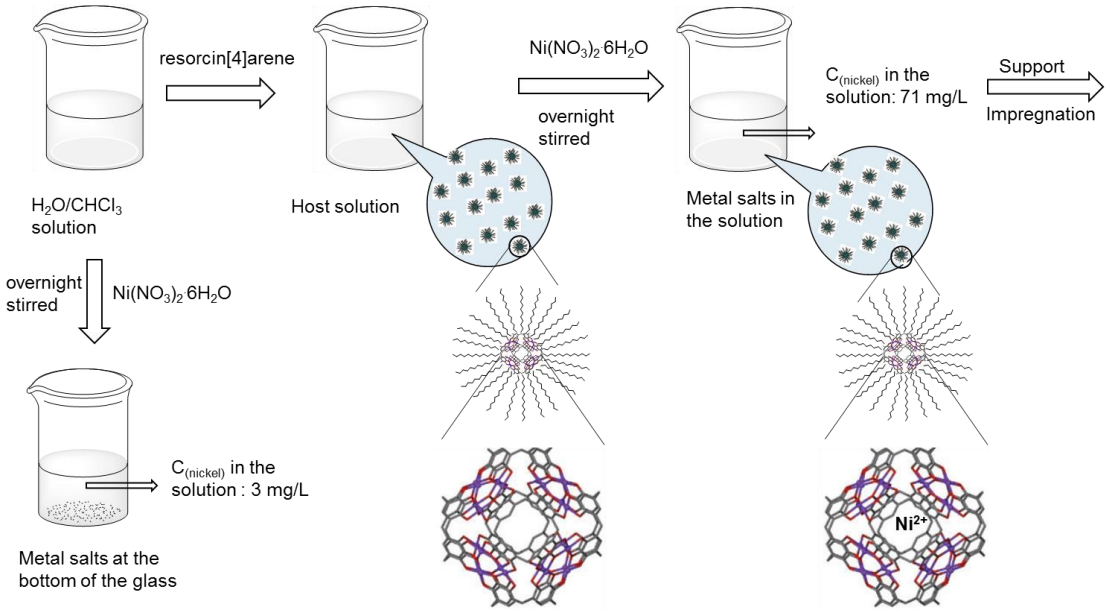

Figure 3-6. Encapsulation of Ni^{2+} during synthesis procedure with hexameric pyrogallolarene capsule.[32]

To investigate the location of Ni^{2+} in the metal-organic nanocapsule, increasing amounts of $Ni(NO_3)_2 \cdot 6H_2O$ were added to the hexameric pyrogallol[4]arene solution. The concentration of Ni species in the organic phase was measured by atomic absorption spectroscopy (AAS), showing an increasing amount of Ni species in the hexameric pyrogallol[4]arene solution from 71 mg/L to 365 mg/L (Table 1), while the nickel concentration did not change in the pure $H_2O/CHCl_3$ solution. This result indicated the transfer of Ni species from solid state to organic solution, which could be explained by the encapsulation of Ni^{2+} in the arene capsule or coordination of Ni^{2+} with pyrogallol[4]arene via Ni-O bonds.

Table 3-1. Concentration of Ni species in the water saturated $CHCl_3$ solution with increasing amount of $Ni(NO_3)_2 \cdot 6H_2O$ before and after involving pyrogallol[4]arene molecule. Ethanol was added to the capsule solutions to destruct the host molecules and Ni species was extracted with water before AAS measurement.

n ($Ni(NO_3)_2 \cdot 6H_2O$) : n (capsule molecule)	0	1	2	5
C_{Ni} in the $H_2O/CHCl_3$ (mg/L)	-	3.3	3.3	3.4
C_{Ni} in the capsule solution (mg/L)	-	71	150	365

According to the published literature, 2 possible structures of Ni colloidal molecule could be presented after encapsulating Ni species. Zhang et al. reported that cationic guests are bound inside the cavity via cation–π interactions (shown in Figure 2-7 (a)).[26] On the other side, metal ions insert into the hydrogen-bonding networks and substitute H_2O molecules by the formation of metal coordinated capsule molecule based on the same structural motif, which offers greater stability rigidity (shown in Figure 2-7 (b).[33]

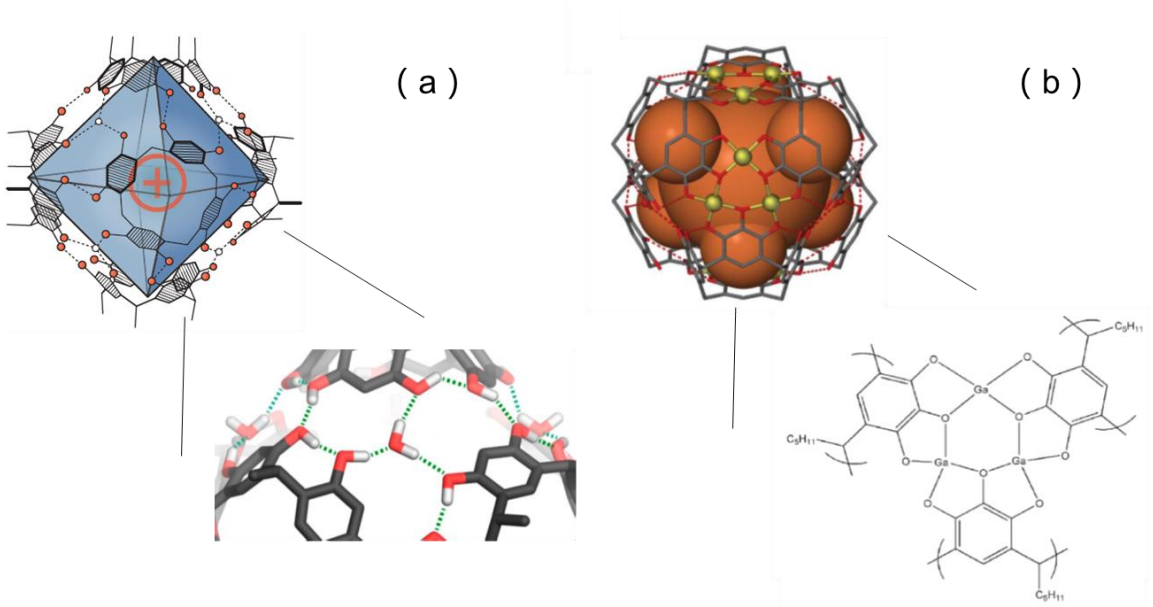

Figure 3-7. Schematic representation of possible structures of capsule molecule by the addition of metal salt in the host solution. (a) Cationic guests are encapsulated in the cavity[26] and (b) metal coordinated capsule molecule[33].

Hence, the total concentration of encapsulated $CHCl_3$ molecules in the cavity was determined from ^1H NMR spectra (Table 2 and Figure 3A-1). After adding $Ni(NO_3)_2{\cdot}6H_2O$, the number of encapsulated $CHCl_3$ (integral intensity of the H signal at 4.5ppm) did not decrease, suggesting that $CHCl_3$ inside the cavity were not replaced by other guest species (Ni^{2+} or NO_3^-). Note that the integral intensity of the peaks did not change, while the width of the peak increased from 0 to 5 eq, which could be explained by the faster relaxation of nearby protons after coordination with paramagnetic metal ion (Ni^{2+}).[34]

Table 3-2. Integral of the encapsulated $CHCl_3$ peaks with increasing amount of $Ni(NO_3)_2{\cdot}6H_2O$. The integral of the methanetriyl group (3.84 ppm, 24 H) of the assembly of pyrogallol[4]arene were used as references to determine the encapsulation ratio.

n ($Ni(NO_3)_2{\cdot}6H_2O$) : n (capsule molecule)	0	1	2	5
Integral of encapsulated $CHCl_3$ protons	10.09	10.24	10.80	10.16

Hence, Ni species were concluded to be located on the surface of the capsule molecules, which substitute H_2O molecules and insert into the hydrogen-bonding networks by the formation of Ni-O bonds. Compared to hydrogen bonded capsules on the same structural motif[24], the metal coordination increases the stability and rigidity of the structure.

In order to gain more insight into the structure of the nickel-organic nanocapsules during the synthesis procedure, *in situ* XAFS experiments at the Ni K-edge were carried out (Figure 3-7). ZrO_2 was used as support due to its higher oxygen storage capacity[1]. However, Ni/ZrO_2 could not be analyzed by XAFS due to the high

absorption cross section of the support[35], therefore, SiO_2 supported Ni catalysts were used as model catalysts for further XAS experiments. The strong white line at ca. 8350 eV confirmed the presence of oxidized Ni on the dried and *in situ* calcined samples. After reduction with H_2 at 873 K for 90 minutes, Ni was fully reduced, confirmed by the absence of the white line at 8350 eV in the XANES of Ni (Figure 3-8).

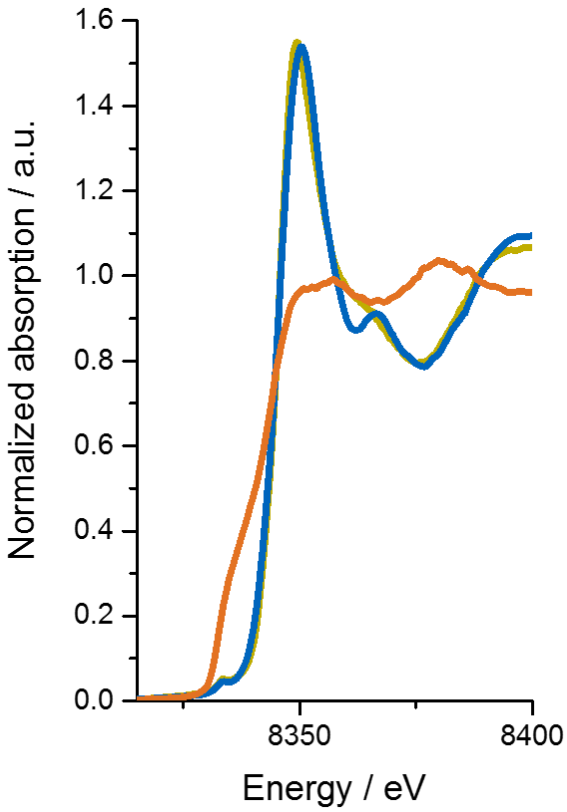

Figure 3-8. XANES at the Ni K-edge of dried (green), calcined (blue) and in situ reduced (orange) 1 wt% Ni/SiO_2.

The analysis of the EXAFS (Figure 3-9 and Table 3A-1) revealed the presence of Ni-O contributions and the absence a metallic Ni environment in the dried sample, which is in agreement with the formation of a nickel-organic nanocapsule via Ni-O coordinative bonds. After reduction an average coordination numbers for

Ni-Ni of 5.53 was observed for Ni/SiO_2, which indicates the presence of Ni particles with an average size of 1.1 nm[34].

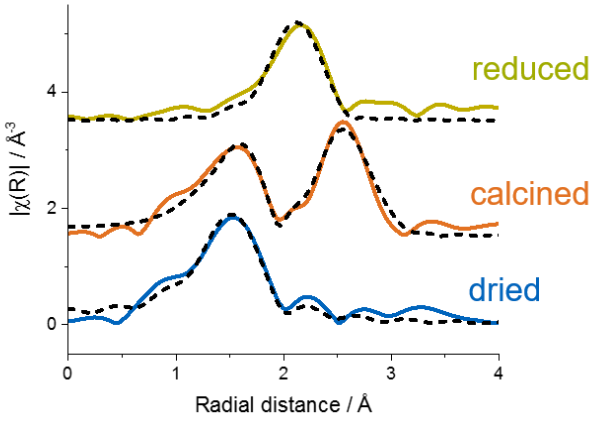

Figure 3-9. Fourier transformed EXAFS at the Ni K-edge recorded at room temperature 1 wt% Ni/SiO_2 after drying under vacuum at room temperature (blue line), *in situ* oxidation (orange line) and *in situ* reduction (green line). The dotted lines are the results of the EXAFS fits.

3.3.3. Characterization of particle size

The TEM pictures of the catalysts are shown in Figure 3-10. This method was also extended to Pt and Ni/Pt bimetallic catalysts. Note that TEM images do not allow to differentiate the Ni and the ZrO_2 due to the low difference in the contrast[36]. The average metal particle sizes of supported catalysts synthesized using metal colloidal precursors were below 2 nm. Therefore, long alkyl chains on the outer surface of these capsules provide large distances between each capsule and metal species and prevent metal-to-metal contact and reduce the tendency for sintering during calcination[15,37], which leads to small mean particle size after high temperature treatment.

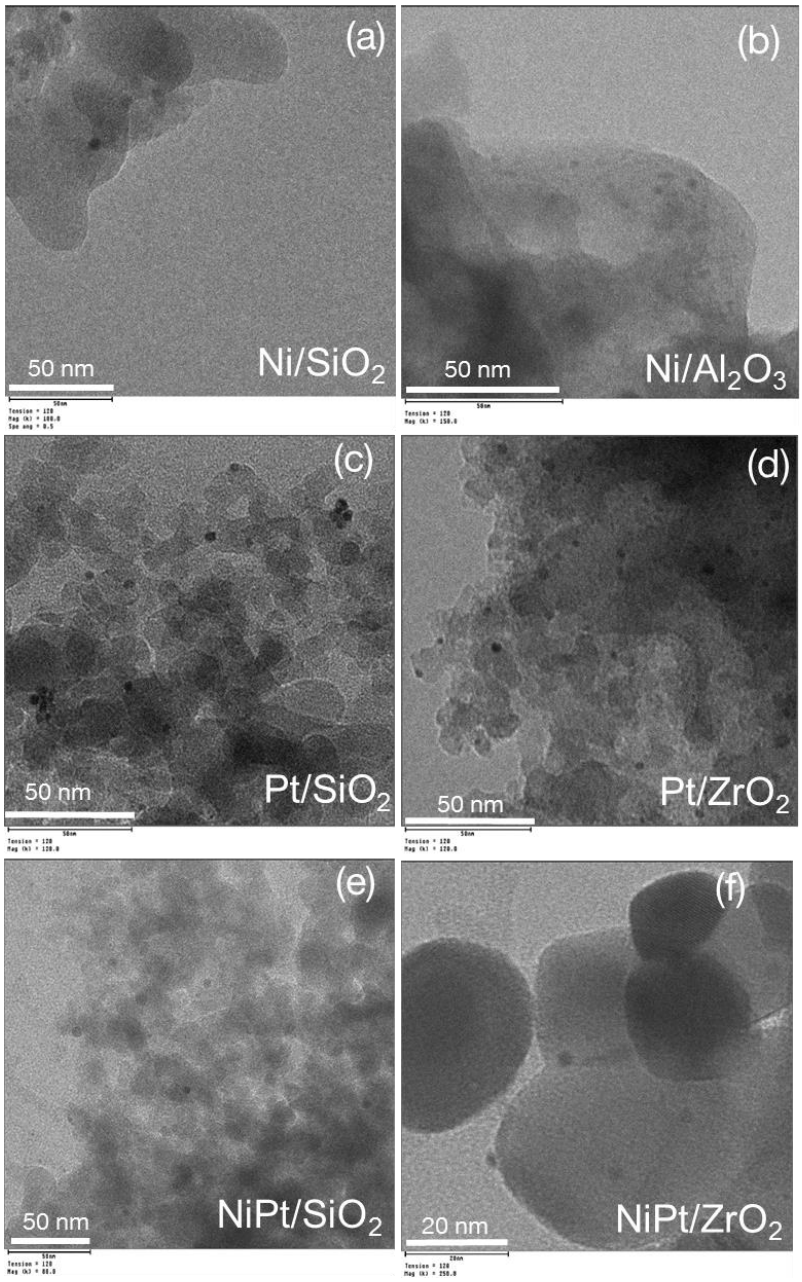

Figure 3-10. TEM images of reduced catalysts. (a) 1 wt% Ni/SiO_2 (b) 1 wt% Pt/ZrO_2 (c) 1 wt% Ni/ZrO_2 (d) 1 wt% Pt/ZrO_2 (e) 1 wt% $NiPt/SiO_2$ (f) 1 wt% $NiPt/ZrO_2$

To explore the influence of nickel loading on the final particle size, EXAFS of 1 wt%, 2 wt% and 5 wt% Ni/SiO_2 were analyzed after drying and *in situ* reduction (Figure 3-11 and table 3A-2). For the dried samples, Ni was present in oxidized form (as concluded above from the XANES) with the same coordination number (~4.7) for the three samples. After *in situ* reduction, the disappearance of the Ni-O contributions and a contraction of the Ni-Ni distances were observed. The 1 wt% Ni/SiO_2 showed the lowest Ni-Ni coordination number within these three catalysts, with Ni particle size of 1.1 nm. This is consistent with the results of TEM microscopy, taking into consideration the increases of molar volume upon oxidation.[15]

The nickel particle size of 2 wt% and 5 wt% Ni/SiO_2 are 1.5 and 1.9nm, respectively, which reveals that the concentration of Ni inside the nanocapsule determines the size of the final Ni particle on the support. We further assume that the nickel particles have the same size on the SiO_2 and ZrO_2 as Ni/ZrO_2 could not be analyzed by XAFS due to the high absorption cross section of the support[35]

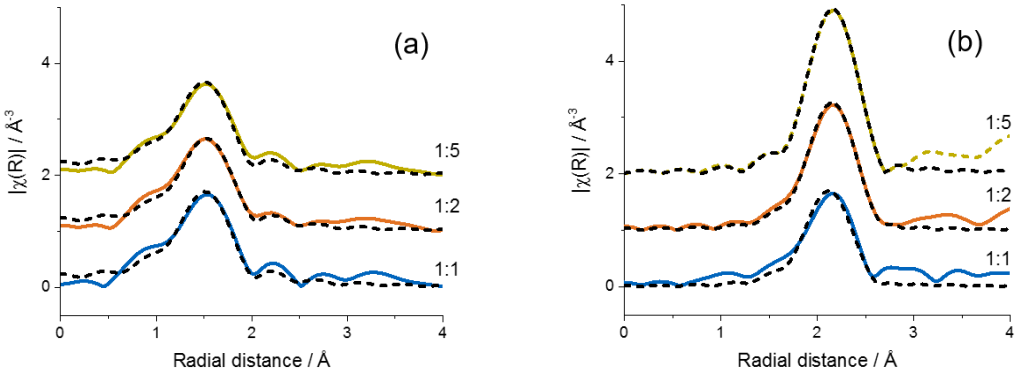

Figure 3-11: Fourier transformed EXAFS at the Ni K-edge recorded at room temperature of dried (a) and reduced (b) 1 wt% Ni/SiO_2 (blue line), 2 wt% Ni/SiO_2 (orange line) and 5 wt% Ni/SiO_2 (green line). The dotted lines are the results of the EXAFS fits.

3.3.4. Catalytic performance

The catalytic activities of Ni and Pt supported on ZrO_2 are shown in Figure 3-12. ZrO_2 supported Ni and Pt catalysts showed slight deactivations in the first 100 mins of reactions, followed by stable activities during further 3000 mins of DRM. In addition, the H_2/CO ratio remained constant over an extended reaction time, which indicates that the rate of carbon formation reaction is kinetically equal to the rate of carbon removal.

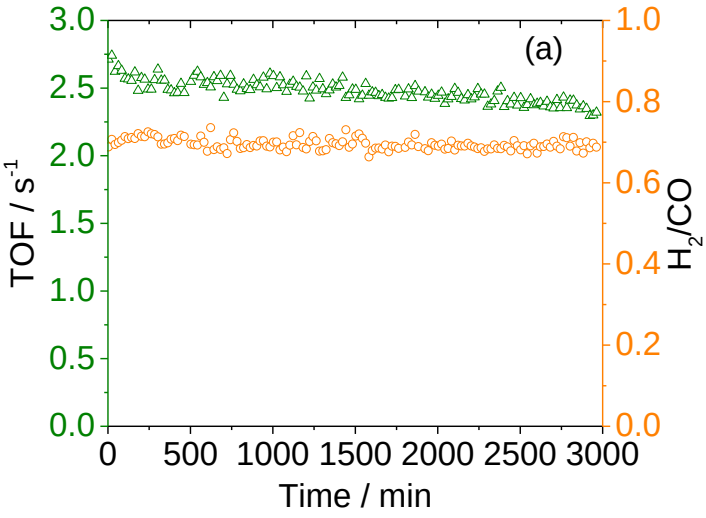

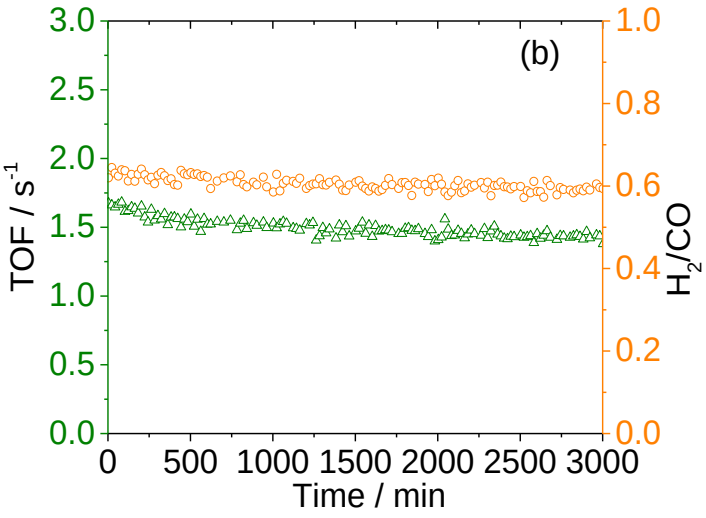

Figure 3-12. Reaction rate of CH_4 (△) and H_2/CO ratio (○) over (a) Pt/ZrO_2, (b) Ni/ZrO_2 at 873 K during DRM reaction.

The stable activities during DRM reaction were also consistent with the almost identical amount of coke deposited on the catalysts after a short period of DRM reaction. TGA measurements of spent catalysts after DRM reaction are shown in Figure 3-13. The amount of carbon deposition on the spent catalysts remained constant after 100 and 200 mins over Ni/ZrO_2 and Pt/ZrO_2 respectively, indicating that the rate of C-H bonds activation (formation of CH_x species) and coke removal via oxygen species (in form of carbonate) are equal. This results is consistent with our previously work showing that coke removal is carried out at the Pt-ZrO_2 perimeter[3] and small metal particle sizes enlarge the metal-support interface and could, thus, kinetically inhibit the deposition of inactive coke[4,5,8] on the catalysts, leading to stabilization of metallic catalysts under DRM condition.

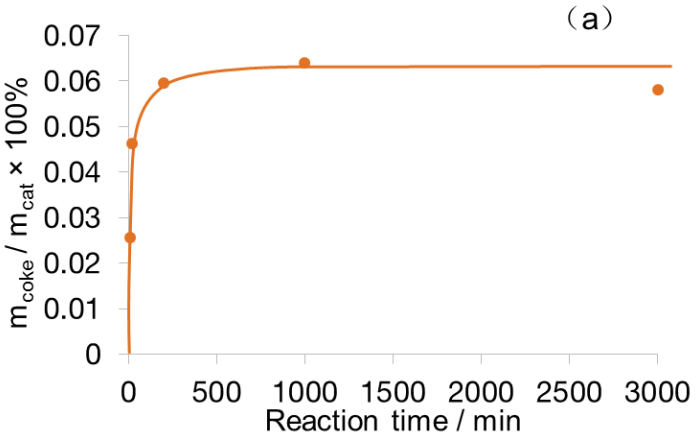

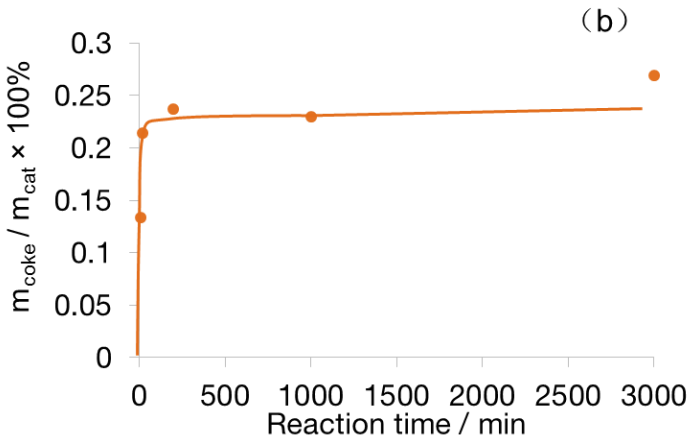

Figure 3-13. Total amount of coke accumulation over (a) Pt/ZrO_2, (b) Ni/ZrO_2 during DRM reaction.

3.3.5. Influence of particle size on the DRM activity and stability

The catalytic activities of the ZrO_2 and SiO_2 supported Ni catalysts for methane dry reforming are shown as the conversion rate of CH_4 in Figure 3-14. All the three Ni/ZrO_2 catalysts showed comparable initial rate per surface Ni, (0.63 ± 0.09) mol_{CH4} s^{-1} mol_{Ni}^{-1}, regardless of the Ni loading. The Ni/SiO_2 catalyst was the least active, with an initial rate of 0.19 mol_{CH4} s^{-1} mol_{Ni}^{-1}. However, 1 wt% Ni/ZrO_2 was much more stable against deactivation compared to other catalysts. During the first 200 minutes of reaction the 1 wt% Ni/ZrO_2 catalyst showed only a slight deactivation, followed by a period of 1000 mins with constant activity. In contrast, the catalysts with 2 and 5 wt% Ni on ZrO_2 (nanocapsule/$Ni(NO_3)_2{\cdot}6H_2O$ = 1:2 and 1:5) suffered from a fast and continuous deactivation during DRM reaction, which led to a loss of activity of 71 % and 84 % after 900 minutes, respectively. The 1 wt% Ni/SiO_2 showed the strongest deactivation, which led to an almost complete loss of activity after 50 min TOS.

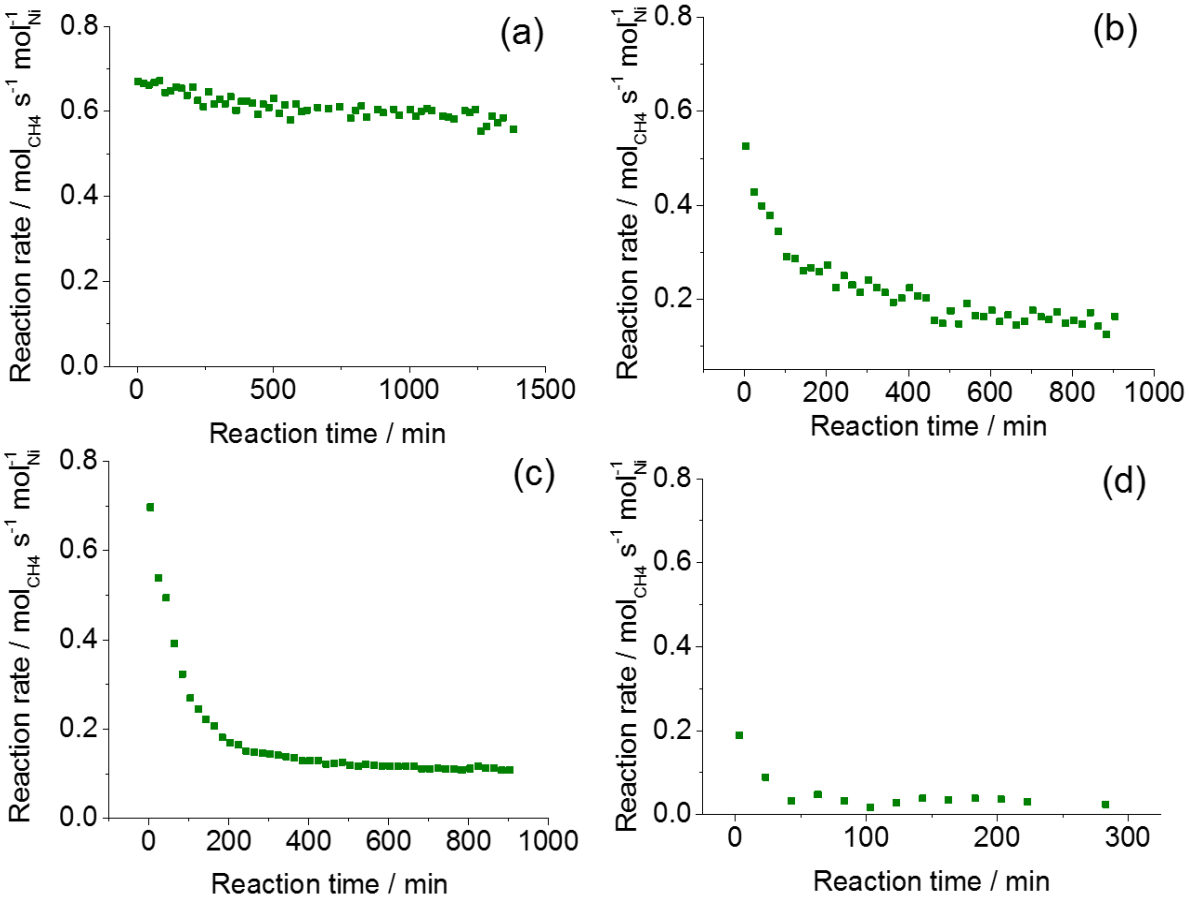

Figure 3-14 Reaction rate of CH_4 over (a) 1 wt% Ni/ZrO_2, (b) 2 wt% Ni/ZrO_2 (c) 5 wt% Ni/ZrO_2 and (d) 1 wt% Ni/SiO_2 at 873 K during DRM reaction.

The pattern of H_2 and H_2O formation rate with TOS during DRM reaction were shown in Figure 3-15, which decreased sharply for H_2 formation on 2 wt% and 5 wt% Ni/ZrO_2, while the rate was relatively stable on the 1 wt% Ni/ZrO_2 over a long period of time. This agrees well with the decreases in the CH_4 conversion activities (on the surface Nickel, SNi) over these 3 catalysts, suggesting the largely decreased number of accessible surface Ni on 2 wt% and 5 wt% Ni/ZrO_2 for methane activation. In contrast, the rate for H_2O formation was much more stable on all catalysts compared to H_2 formation rate.

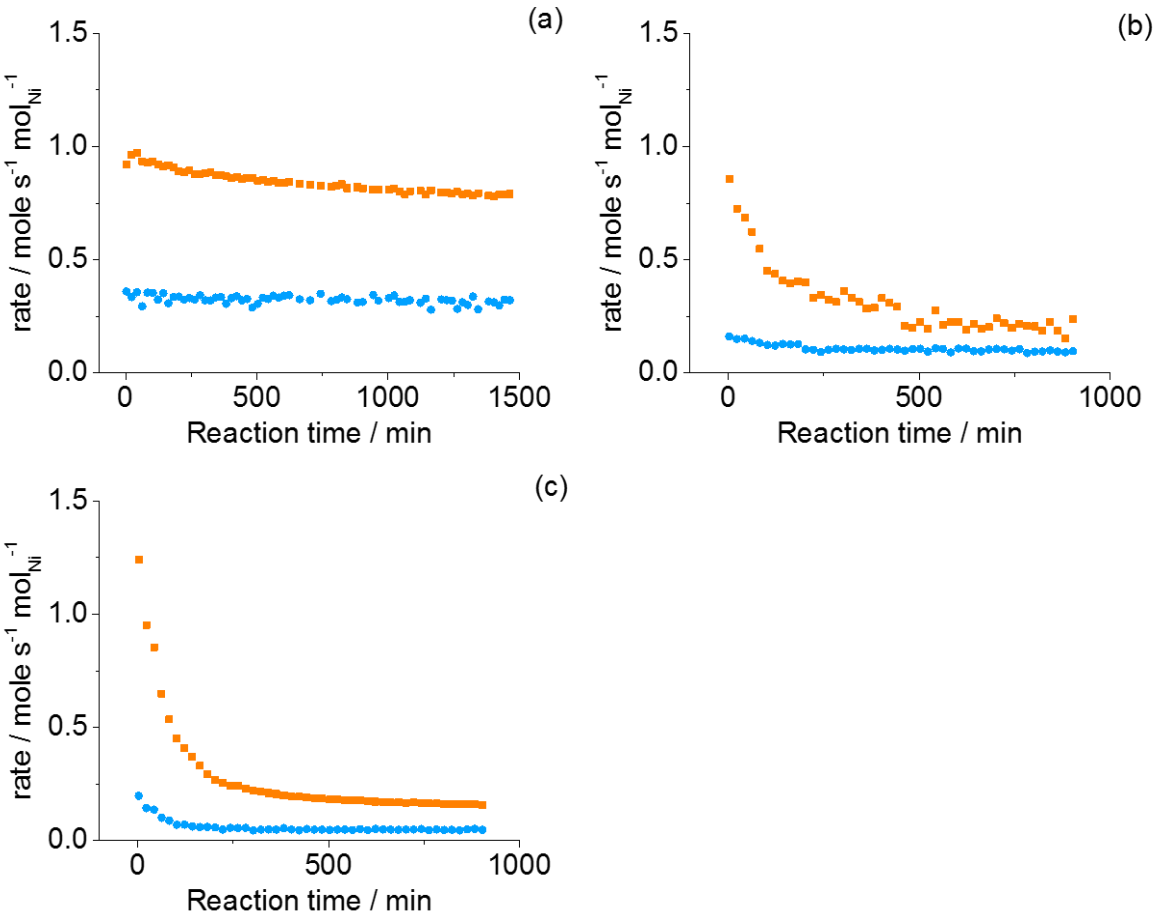

Figure 3-15. Rate of H_2 (orange) and H_2O (blue) formation over (a) 1 wt% Ni/ZrO_2, (b) 2 wt% Ni/ZrO_2 and (c) 5 wt% Ni/ZrO_2 at 873 K during DRM reaction.

To monitor the changes of active sites on DRM catalysts under DRM reaction conditions, we further compared the evolution of the rates of H_2O and H_2 formation with time on stream. The ratio between H_2 and H_2O formation rate over Ni/ZrO_2 catalysts at 873 K were shown as a function of time on stream in Figure 3-16. It is seen that the Ni/ZrO_2 catalysts had different initial r_{H2} / r_{H2O} values, e.g. 2.56 on 1 wt% Ni/ZrO_2, 5.30 on 2 wt% Ni/ZrO_2 and 6.27 on 5 wt% Ni/ZrO_2, which, however, approached and stabilized at the same level (2.5 ± 0.4) after a certain time on stream. This is further shown on two stable Ni/ZrO_2 catalysts (Zr6Ni3imp (2.7 wt% Ni/ZrO_2) and Zr82Ni3imp (3 wt% Ni/ZrO_2)) synthesized by impregnation with the concomitant addition of $NaHCO_3$ published in our previous work.[38] It is noteworthy

that all the stable catalysts (1 wt% Ni/ZrO_2, Zr6Ni3imp and Zr82Ni3imp) showed an initial r_{H2} / r_{H2O} value already around 2.5. This allows us in principal to differentiate the metal surface sites both undisturbed (NP Ni), which is far from the interface between Ni and ZrO_2 and have no reactive atomic oxygen transferred from the support, and in vicinity of the ZrO_2 support (perimeter Ni, P Ni). Here we assign this number (r_{H2} / r_{H2O} = 2.5), based on the results from our previous work, to the quantitative selectivity ratio between H_2O and H_2 formed on the perimeter Ni as the non-perimeter nickel (NP Ni) was completely covered by the coke deposition after deactivating to a stable level.[3]

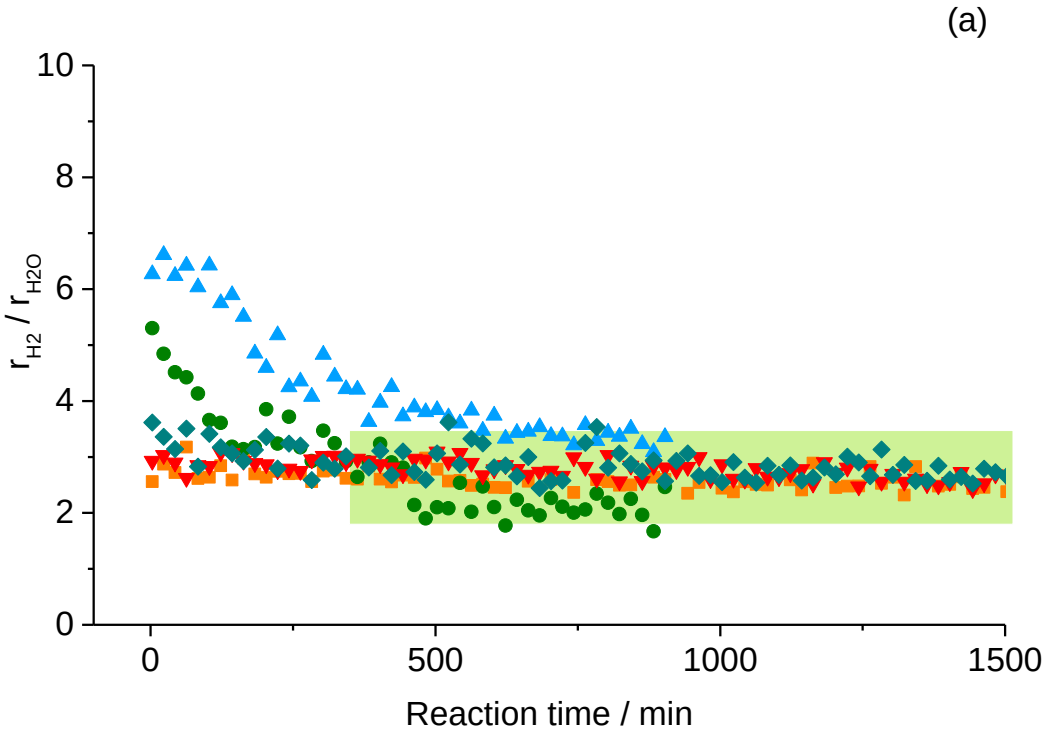

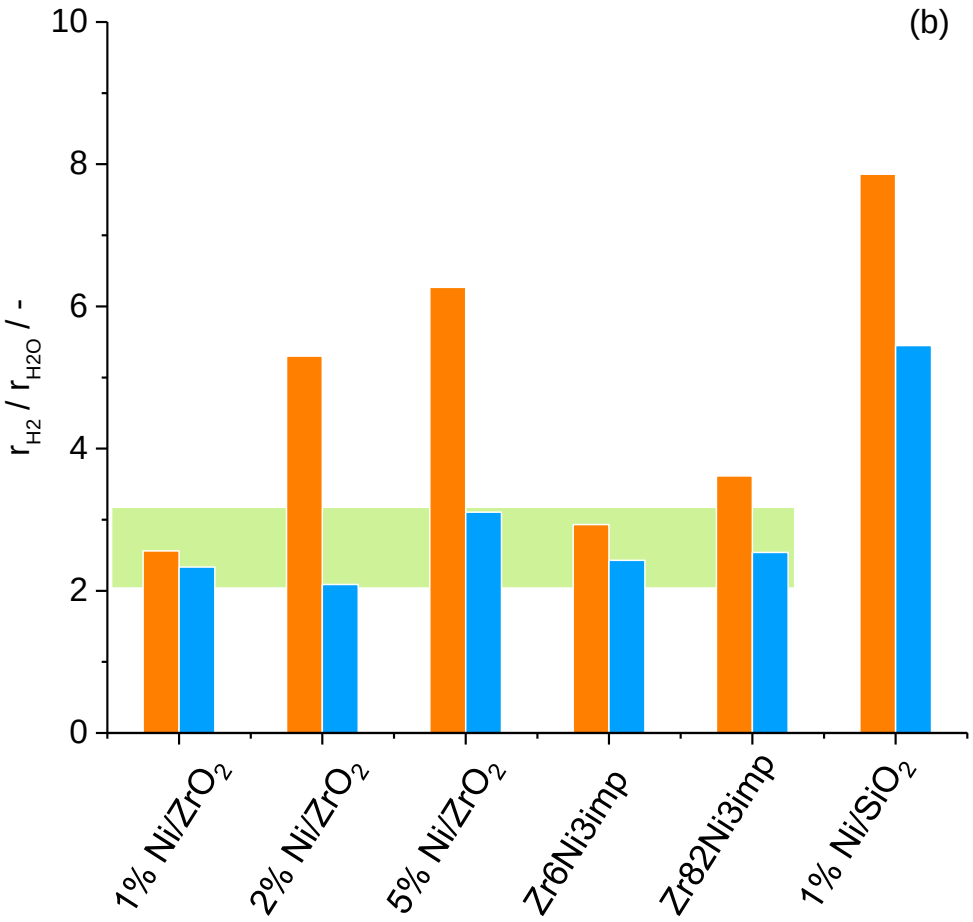

Figure 3-16. (a) ratios of H_2 and H_2O formation rate over (■) 1 wt% Ni/ZrO_2, (●) 2 wt% Ni/ZrO_2, (▲) 5 wt% Ni/ZrO_2 , (▼)Zr6Ni3imp and (◆)Zr82Ni3imp at 873 K during DRM reaction. (b) Initial (orange) and stable (blue) ratios of H_2 and H_2O formation rate over these Ni/ZrO_2 catalysts and 1 wt% Ni/SiO_2. The green horizontal bar in Figure (a) and (b) represents the interval of r_{H2} / r_{H2O} value under steady state.

Thus, as summarized in Figure 3-17, the Ni/ZrO_2 catalysts with an initial r_{H2} / r_{H2O} value of 2.5 showed much more stable DRM activities compared to the DRM over Ni/ZrO_2 catalysts with higher initial r_{H2} / r_{H2O} value. The Ni/SiO_2 showed the highest r_{H2} / r_{H2O} ratio and relatively lower reaction rate, which is due to the strongest deactivation in the initial reaction.

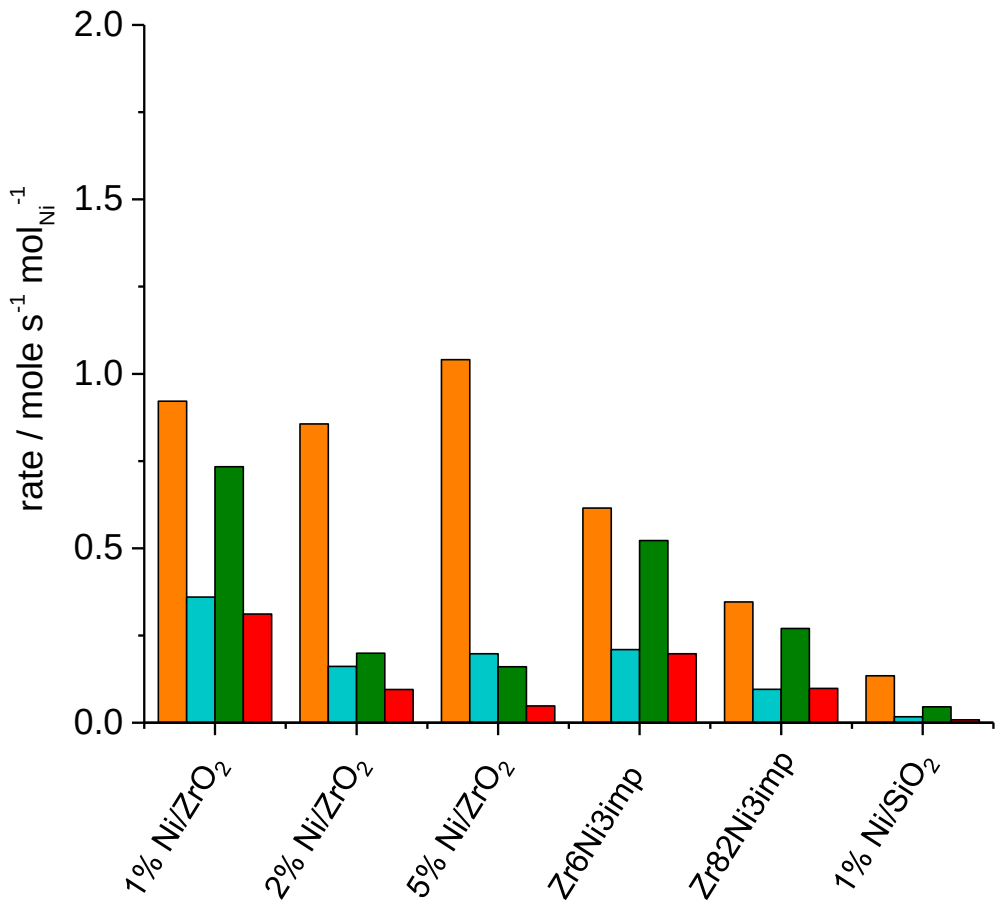

Figure 3-17. Rate of H_2 formation in the initial state (orange) and under stable condition (green) and rate of H_2 formation in the initial state (blue) and under stable condition (red).

As discussed, H_2 formation was formed on atomic nickel via dissociative adsorption of CH_4, forming surface C and H. In the absence of O, H leaves the surface via formation of H_2 while C accumulates and forms coke. With the accessibility to O, H and C could leave the surface in the form of H_2O and CO, thus coke formation and deactivation is alleviated. This means that the ratio of r_{H2} / r_{H2O} indicates the deficiency of surface O, and correlates with catalyst deactivation. Thus, we can use this value to estimate the DRM stability of ZrO_2 supported nickel

catalysts. The relation between deactivation rate and r_{H2} / r_{H2O} number are plotted in Figure 3-18. The deactivation rate of DRM catalysts is defined as

$$\text{Deactivation } rate = \frac{dr_{CH_4}}{d(TOS)} \times \frac{1}{r_{CH_4}}$$

(**Equation 3-6**)

It is remarkable that the deactivation rate increased exponentially with the r_{H2} / r_{H2O} ratio, which we assigned to the faster rate in forming surface carbon (Equation 3-1) than that removing the surface carbon (Equation 3-2), which lead to an accumulation of carbon deposits on the Ni and finally to cokes. This positive correlation indicates importance of perimeter nickel in the DRM reactions, which increases the rate of delivering surface oxygen to surface carbons, preventing coke formation.

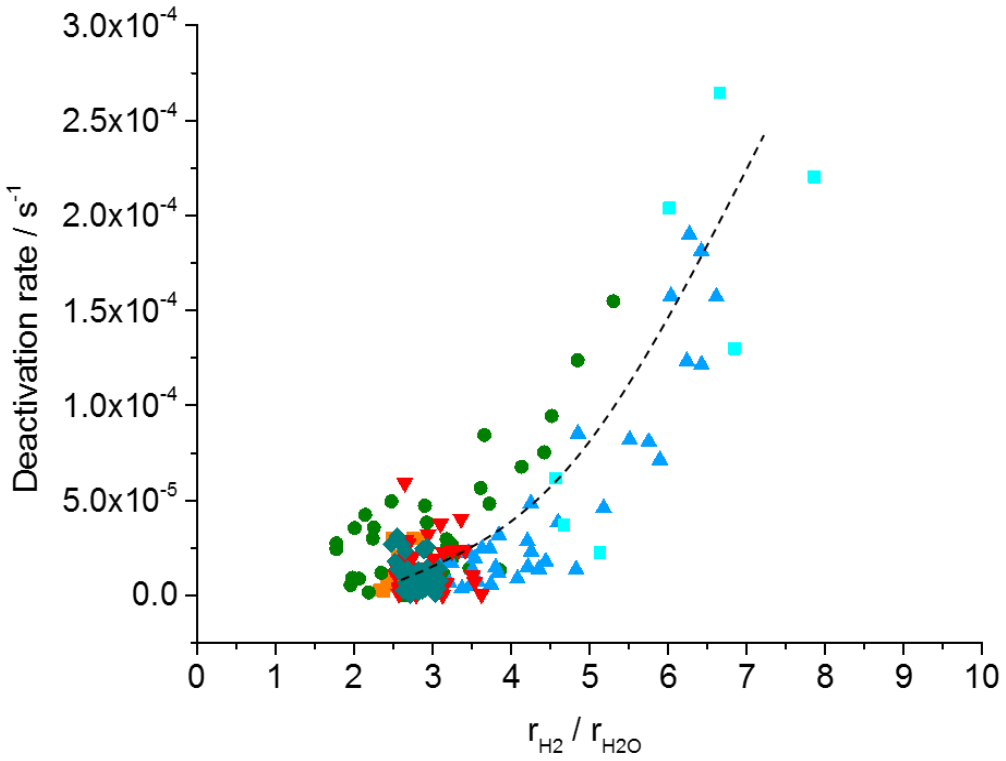

Figure 3-18. Deactivation rate against r_{H2} / r_{H2O} ratio over (■) 1 wt% Ni/ZrO_2, (●) 2 wt% Ni/ZrO_2, (▲) 5 wt% Ni/ZrO_2 , (▼)Zr6Ni3imp, (◆)Zr82Ni3imp and (■)1 wt% Ni/SiO_2 at 873 K during DRM reaction.

To quantitatively explain the stable activity of the 1 wt% Ni/ZrO_2 catalyst during DRM, the fractions of perimeter nickel in total number of surface nickel was quantified by the H_2 formation rate on the two types of Ni sites. The initial rate of H_2 formation on perimeter nickel *r* (initial H_2)$_{(P\ Ni)}$ was calculated using Equation 3-7:

$$r\ (\text{initial}\ \mathrm{H_2})_{\ (\mathrm{P\ Ni})} = r\ (\text{initial}\ \mathrm{H_2O})_{\ (\mathrm{P\ Ni})} \times 2.5$$

(**Equation 3-7**)

in which *r* (initial H_2O)$_{(P\ Ni)}$ is the initial rate of H_2O formation on perimeter nickel and an unchanged selectivity ratio of 2.5 between H_2O and H_2 formed on the nickel-ZrO_2 perimeter in the initial stage of reaction and under steady state is assumed. The *r* (initial H_2O)$_{(P\ Ni)}$ was calculated using Equation 3-8:

$$r\ (\text{initial}\ \mathrm{H_2O})_{\ (\mathrm{P\ Ni})} = r\ (\text{initial}\ \mathrm{H_2O})_{\ (\mathrm{S\ Ni})} - r\ (\text{initial}\ \mathrm{H_2O})_{\ (\mathrm{NP\ Ni})}$$

(**Equation 3-8**)

in which *r* (initial H_2O)$_{(S\ Ni)}$ is the overall H_2O initial formation rate obtained in DRM reaction, and *r* (initial H_2O)$_{(NP\ Ni)}$ is the rate contributed by NP Ni which was measured from the activity of the Ni/SiO_2 catalysts since CO_2 activation was not facilitated on the SiO_2 and thus gives the lower boundary for the rate in absence of the sites at the Ni-ZrO_2 perimeter.

Thus, the fractions of NP Ni to P Ni can be represented by their individual contribution in H_2 formation rate which is by the following expression

$$\frac{r\ (\text{initial}\ \mathrm{H_2})_{\ (\mathrm{NP\ Ni})}}{r\ (\text{initial}\ \mathrm{H_2})_{\ (\mathrm{P\ Ni})}} = \frac{r\ (\text{initial}\ \mathrm{H_2})_{\ (\mathrm{S\ Ni})} - r\ (\text{initial}\ \mathrm{H_2})_{\ (\mathrm{P\ Ni})}}{r\ (\text{initial}\ \mathrm{H_2})_{\ (\mathrm{P\ Ni})}}$$

(**Equation 3-9**)

Eventually, this fraction is calculated using the Equation 3-10 after rearrangement of Equation 3-9.

$$\frac{r\ (\text{initial } H_2)_{\ (\text{NP Ni})}}{r\ (\text{initial } H_2)_{\ (\text{P Ni})}} = \frac{r\ (\text{initial } H_2)_{\ (\text{S Ni})} - [r\ (\text{initial } H_2O)_{\ (\text{S Ni})} - r\ (\text{initial } H_2O)_{\ (\text{NP Ni})}] \times 2.5}{[r\ (\text{initial } H_2O)_{\ (\text{S Ni})} - r\ (\text{initial } H_2O)_{\ (\text{NP Ni})}] \times 2.5}$$

(**Equation 3-10**)

The fraction of H_2 formed on the NP Ni to that on P Ni was found to be dependent on the particle size (Figure 3-19), which decreased with reducing particle size. Therefore, a particle size threshold of 1 nm was found in the DRM reaction, below which all the surface nickels were on the perimeter thus no undisturbed nickel existed. As reported in our previous work,[3] the activation of CO_2 on the support is fast enough to remove surface carbon in the vicinity of perimeter. Thus, the 1 wt% Ni/ZrO_2 showed stable reactivity during DRM because of its small Ni size (1.1 nm). However, for 2 and 5 wt% Ni/ZrO_2, due to the larger Ni particle size, the disbalance between the reaction forming surface carbon and the reaction removing it leads to the coke accumulation and catalyst deactivation during DRM reaction. This is supported by the higher amount of coke on the spent catalysts with larger Ni particle size (Figure 3-19). All observations are consistent with the fact that nickel particles with size below 1 nm kinetically inhibit the formation of coke on the DRM catalysts.

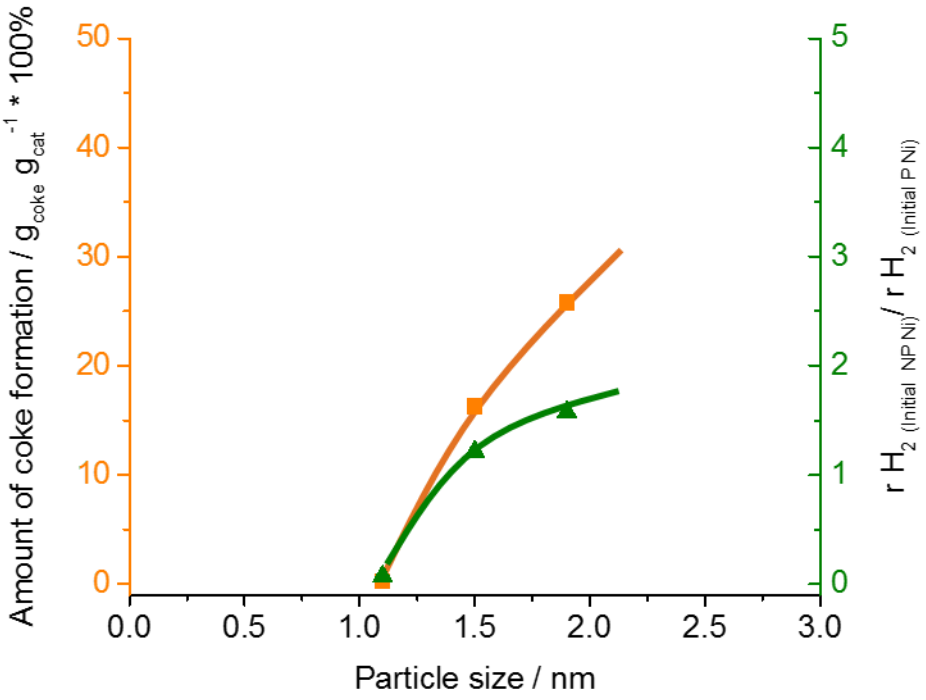

Figure 3-19. Amount of coke deposition (orange) and ratio of initial H_2 formation on the NP Ni to that on the P Ni (green) over 1 wt% Ni/ZrO_2, 2 wt% Ni/ZrO_2 and 5 wt% Ni/ZrO_2 at 873 K during DRM reaction.

3.4. Conclusions

The new synthesis method developed based on encapsulating Ni particles into molecular capsules via a spontaneous self-assembly process allows preparation of Ni/ZrO_2 catalyst with small to 1.1 nm particle size. In this approach the long alkyl chains on the outer surface of host capsules increase the distance between each capsule and the nickel ions, leading to a stabilization of nickel particles during calcination and reduction at elevated temperature. The smallest Ni particle size on 1 wt% Ni/ZrO_2 makes all the surface Ni on the perimeter interface, where Ni were highly accessible to surface O generated by CO_2 activation on the interface ZrO_2. This leads to a decrease of H_2 to H_2O ratio in the products and a faster removal of surface C via CO formation, and consequently a slow rate in coke formation and high stability against deactivation. Large Ni particles contains a lower fraction of perimeter nickel species, thus a deficiency in accessibility to O, making higher H_2 to H_2O and slower surface carbon removal, leading to a fast deactivation.

3.5. Associated Content

Publication

This chapter is based on the article of the same title as appeared which is prepared to be submitted. The content and structure of Chapter 3 is different from this manuscript.

Contributions

Yu Lou did the main contributions in experimental design, kinetic experiments, catalysts preparation, data analysis and manuscript preparation. Matthias Steib contributed with all EXAFS measurements. Anita Horvath is responsible for the synthesis of 2 stable Ni catalysts named Zr6Ni3imp and Zr82Ni3imp. Qi Zhang contributed with synthesis of pyrogallol[4]arene molecule. Andreas Jentys and Yue Liu supervised the topic of catalysts synthesis and kinetic measurements and was responsible for data analysis and manuscript preparation. Johannes A. Lercher is the principal investigator of this work.

Acknowledgments

This work was financially supported by the European Union under project ERA Chem and the BMBF under the project ZeitKatMat. The X-Ray absorption experiments were performed on the SuperXAS beamline at the Swiss Light Source, Paul Scherrer Institut, Villigen, Switzerland. The authors gratefully acknowledge the beamline scientists Maarten Nachtegaal and Ola Safonova for their help during the beamtime.

Copyrights

Figure 3-6 reprinted with permission from (Dalgarno, S. J.; Power, N. P.; Warren, J. E.; Atwood, J. L. *Chem Commun* **2008**, 1539). License number: 4047071239913

Figure 3-7 reprinted with permission from (Zhang, Q.; Tiefenbacher, K. *Journal of the American Chemical Society* **2013**, *135*, 16213.). Copyright (2013) American Chemical Society and from (McKinlay, R. M.; Thallapally, P. K.; Atwood, J. L. *Chem Commun* **2006**, 2956.) License number: 4047081183724

3.6. Appendix

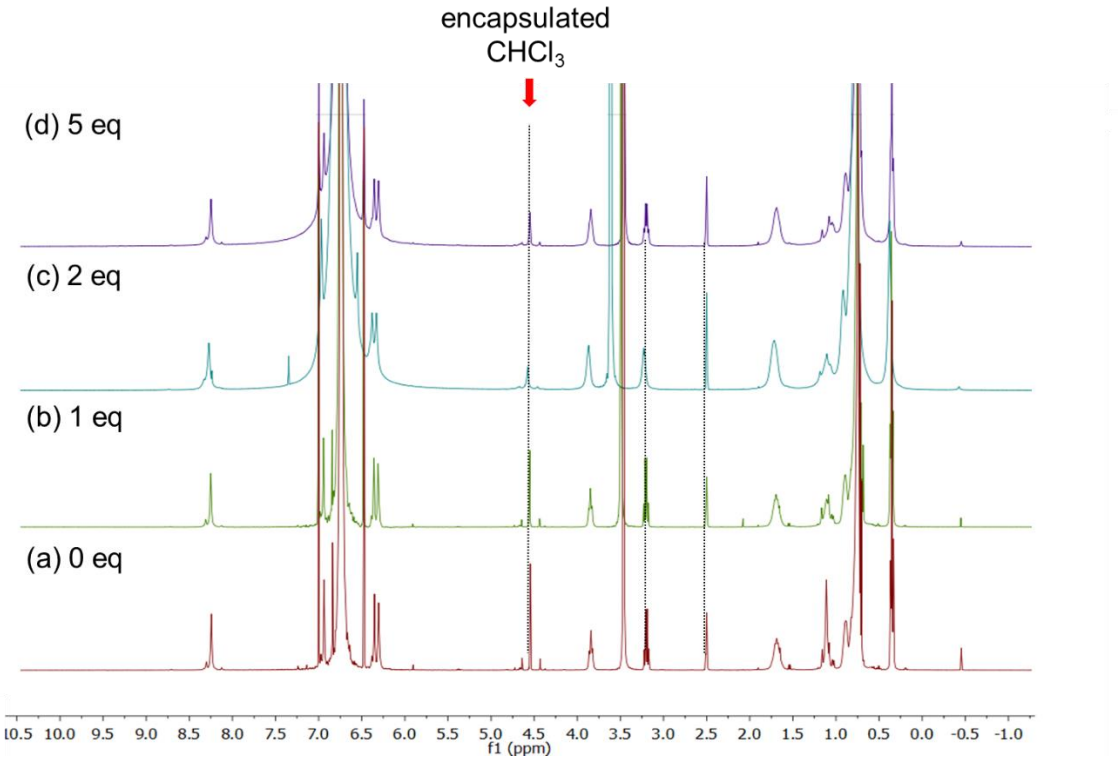

Figure 3A-1. ^{1}H NMR after adding $Ni(NO_3)_2 \cdot 6H_2O$ to the capsule solution with increasing amount of $Ni(NO_3)_2 \cdot 6H_2O$ (a-d)

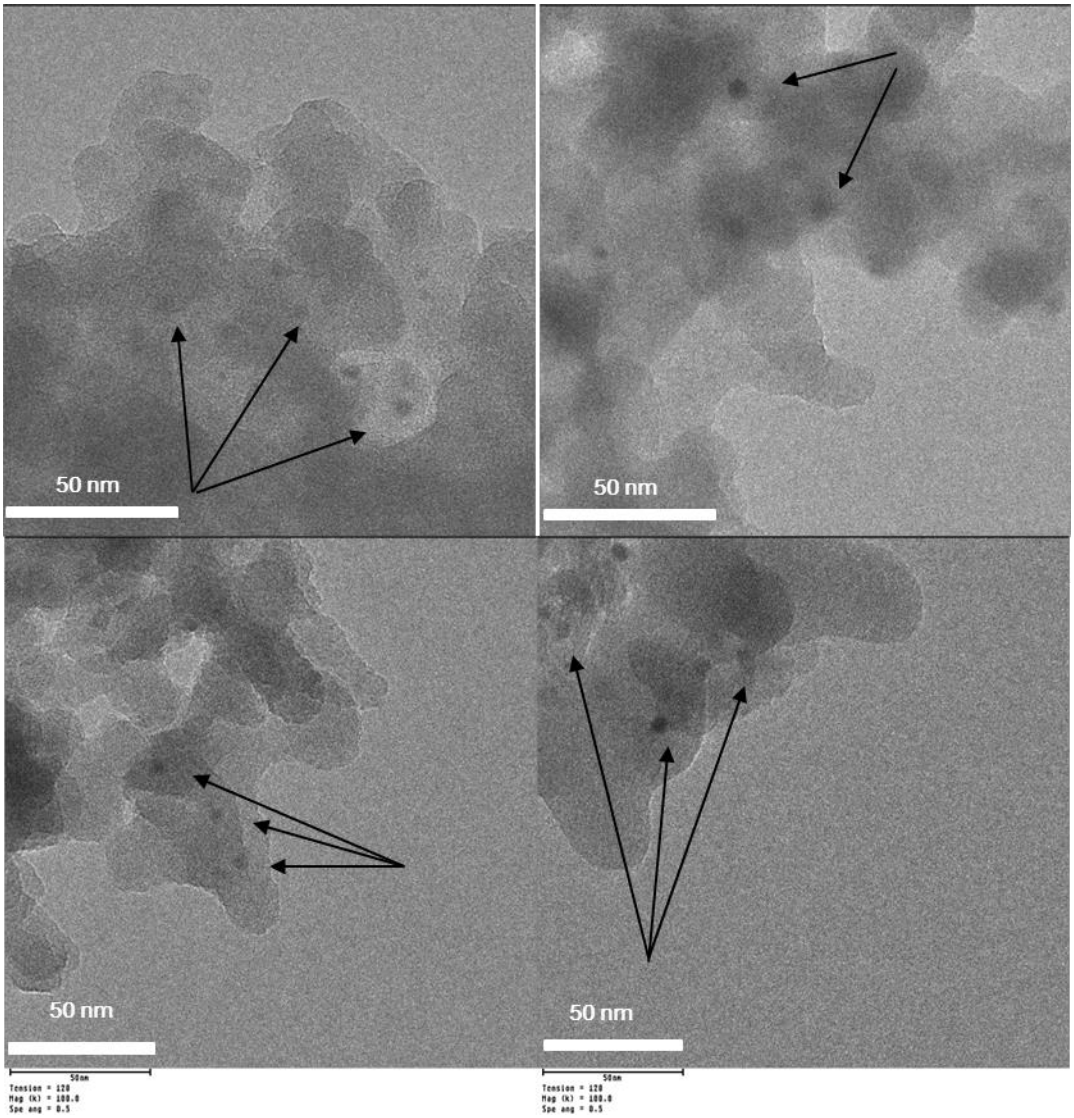

Figure 3A-2. TEM images of Ni/SiO_2

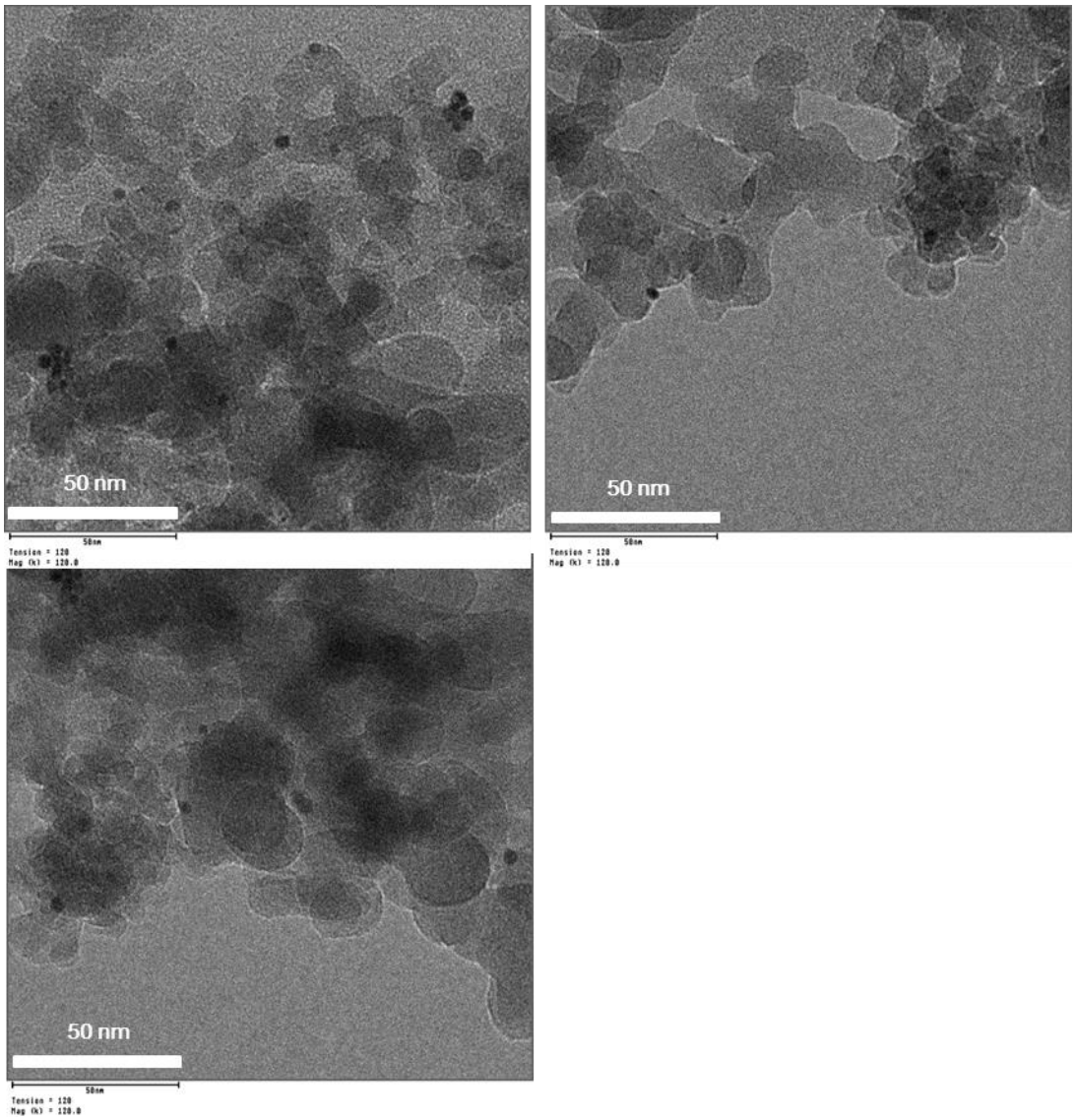

Figure 3A-3. TEM images of Pt/SiO_2

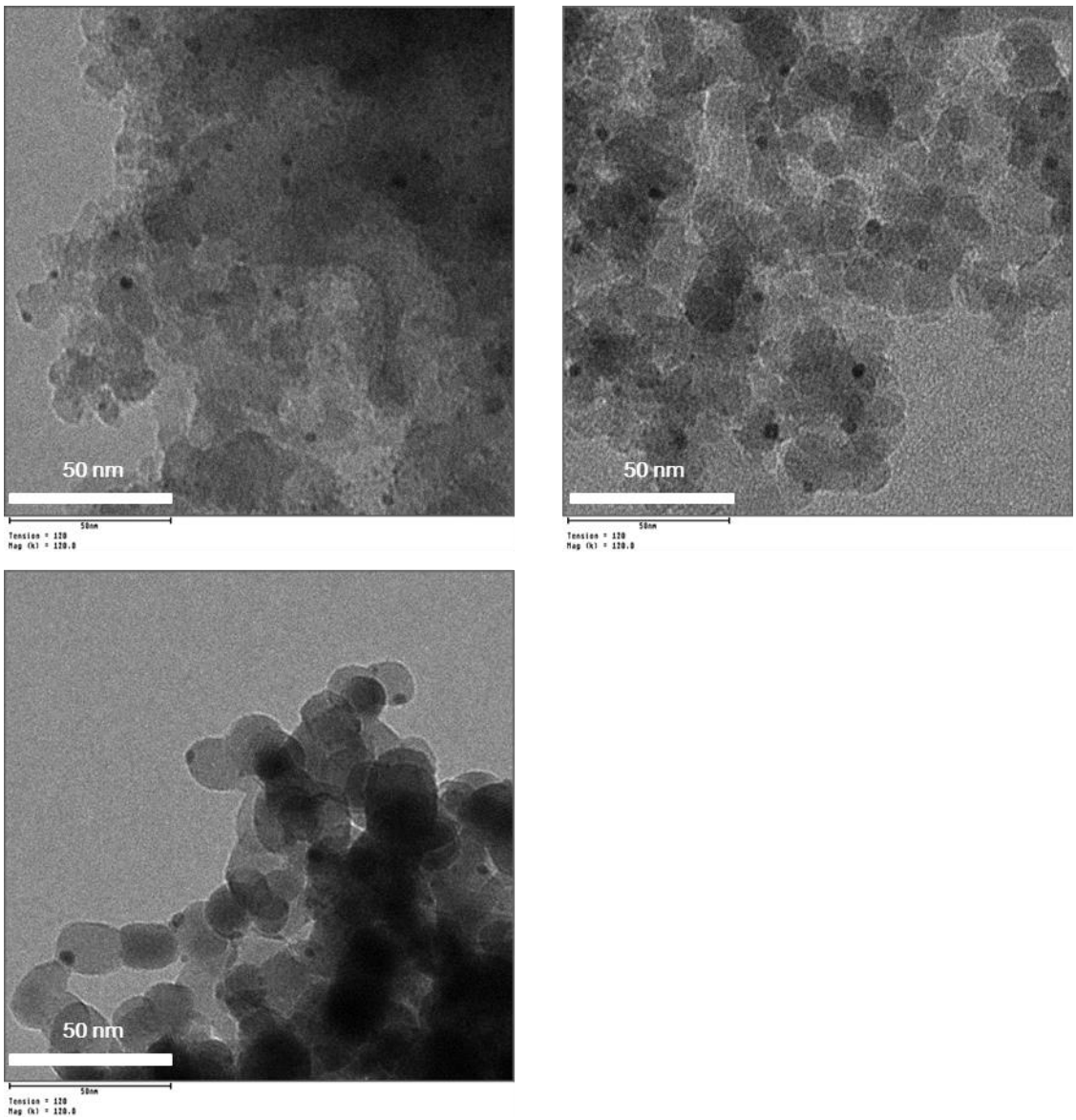

Figure 3A-4. TEM images of Pt/ZrO_2

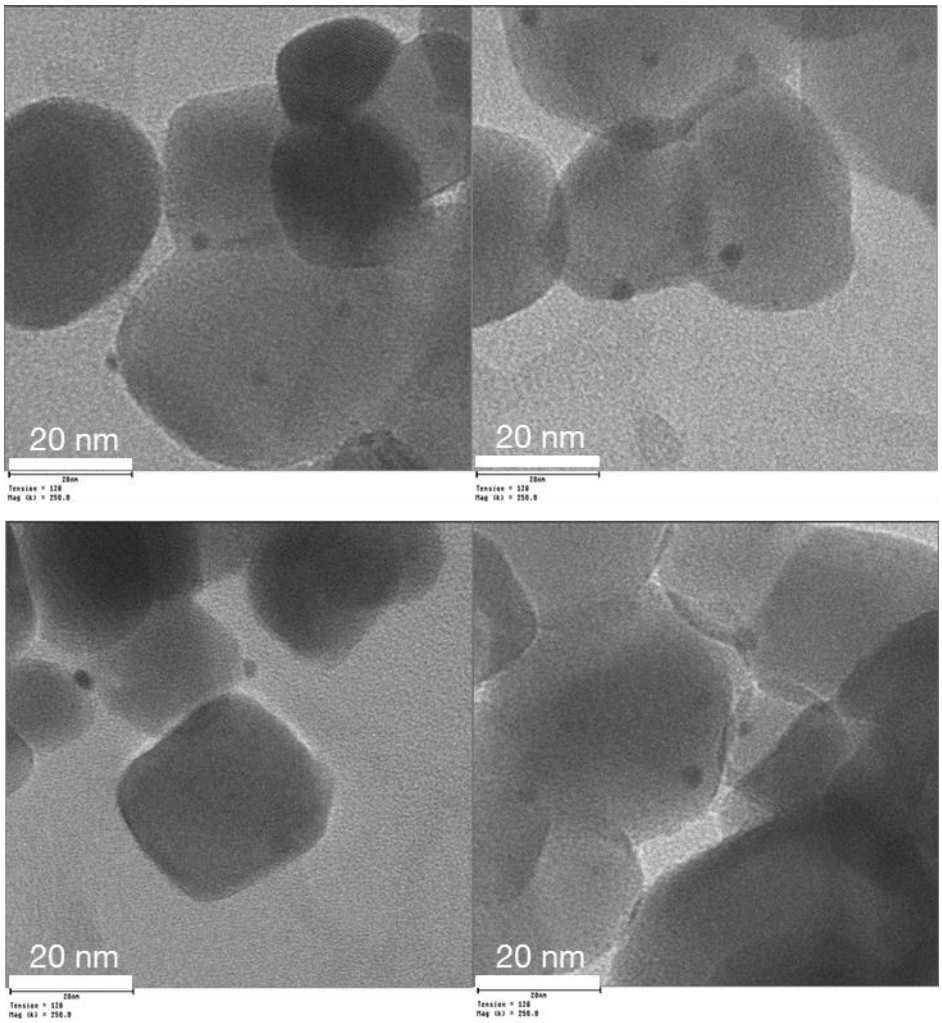

Figure 3A-5. TEM images of $NiPt/ZrO_2$

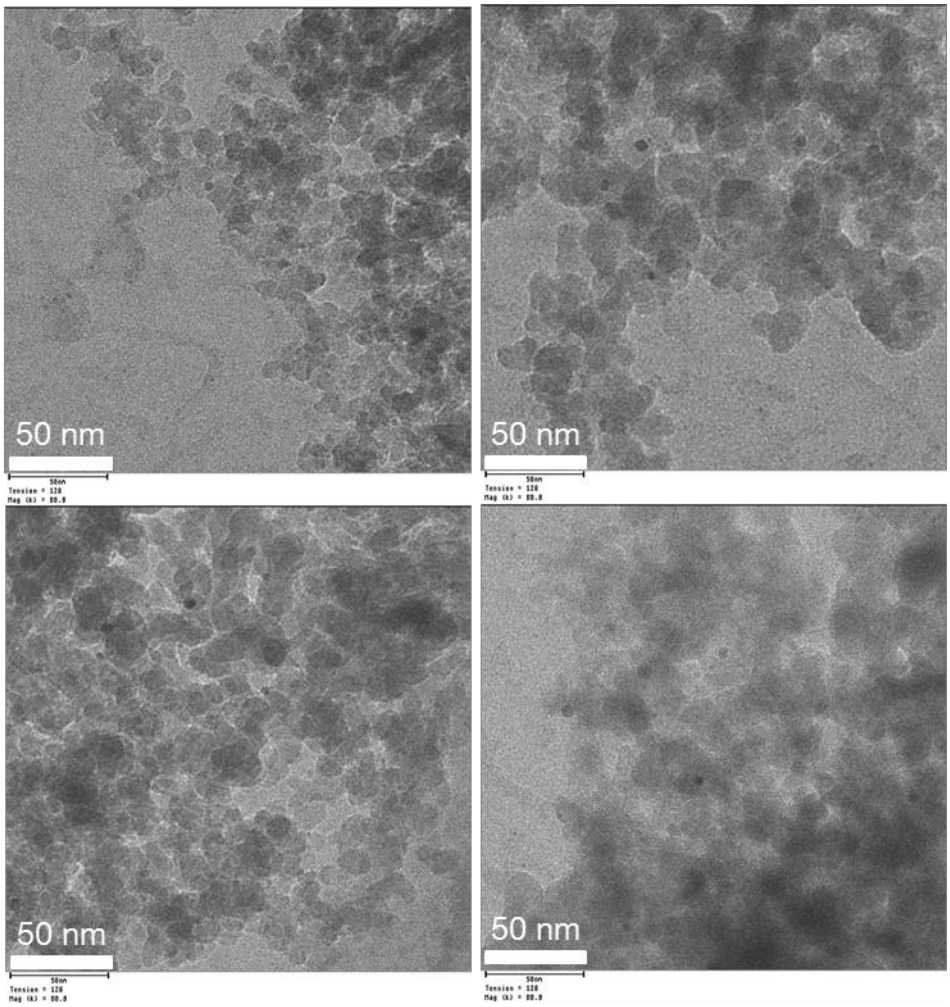

Figure 3A-6. TEM images of $NiPt/SiO_2$

Table 3A-1. EXFAS fitting parameters for dried, calcined and reduced 1 wt% Ni/SiO_2

	Ni-Ni				**Ni-O**			
	N (d)	ΔE_0 [eV]	r [Å]	σ^2 [Å²]	N (d)	ΔE_0 [eV]	r [Å]	σ^2 [Å²]
dried					4.81	-4.6	2.055	0.006
calcined	5.93	3.1	2.46	0.007	4.83	-4.5	2.057	0.008
reduced	5.53	2.6	2.46	0.008				

Table 3A-2. EXFAS fitting parameters for dried and reduced 1 wt% Ni/SiO_2, 2 wt% Ni/SiO_2 and 5 wt% Ni/SiO_2

Loading [wt%]	**Ni-O dried sample**				**Ni-Ni reduced sample**			
	N (d)	ΔE_0 [eV]	r [Å]	σ^2 [Å²]	N (d)	ΔE_0 [eV]	r [Å]	σ^2 [Å²]
1	4.81	-4.6	2.055	0.006	5.53	2.6	2.457	0.008
2	4.71	-3.4	2.060	0.007	8.62	5.7	2.475	0.009
5	4.54	-4.2	2.043	0.007	9.72	6.2	2.48	0.008

3.7. References

(1) Bradford, M. C. J.; Vannice, M. A. *Catal. Rev.-Sci. Eng.* **1999**, *41*, 1.

(2) Fan, M.-S.; Abdullah, A. Z.; Bhatia, S. *Chemcatchem* **2009**, *1*, 192.

(3) Nagaoka, K.; Seshan, K.; Aika, K.; Lercher, J. A. *Journal of Catalysis* **2001**, *197*, 34.

(4) Seshan, K.; Bitter, J. H.; Lercher, J. A. In *Recent Advances in Basic and Applied Aspects of Industrial Catalysis*; Rao, T. S. R., Dhar, G. M., Eds. 1998; Vol. 113, p 187.

(5) Bitter, J. H.; Seshan, K.; Lercher, J. A. *Journal of Catalysis* **1999**, *183*, 336.

(6) Bitter, J. H.; Seshan, K.; Lercher, J. A. *Journal of Catalysis* **1998**, *176*, 93.

(7) Bitter, J. H.; Seshan, K.; Lercher, J. A. *Journal of Catalysis* **1997**, *171*, 279.

(8) Hally, W.; Bitter, J. H.; Seshan, K.; Lercher, J. A.; Ross, J. R. H. *Studies in Surface Science and Catalysis*, 1994; Vol. 88.

(9) Bitter, J. H.; Hally, W.; Seshan, K.; vanOmmen, J. G.; Lercher, J. A. *Catalysis Today* **1996**, *29*, 349.

(10) Lercher, J. A.; Bitter, J. H.; Hally, W.; Niessen, W.; Seshan, K. *Studies in Surface Science and Catalysis*, 1996; Vol. 101.

(11) Kambolis, A.; Matralis, H.; Trovarelli, A.; Papadopoulou, C. *Applied Catalysis a-General* **2010**, *377*, 16.

(12) Montoya, J. A.; Romero-Pascual, E.; Gimon, C.; Del Angel, P.; Monzon, A. *Catalysis Today* **2000**, *63*, 71.

(13) Campbell, C. T.; Peden, C. H. F. *Science* **2005**, *309*, 713.

(14) Khajenoori, M.; Rezaei, M.; Meshkani, F. *Chem Eng Technol* **2014**, *37*, 957.

(15) Baudouin, D.; Szeto, K. C.; Laurent, P.; De Mallmann, A.; Fenet, B.; Veyre, L.; Rodemerck, U.; Coperet, C.; Thieuleux, C. *Journal of the American Chemical Society* **2012**, *134*, 20624.

(16) Xie, T.; Shi, L. Y.; Zhang, J. P.; Zhang, D. S. *Chem Commun* **2014**, *50*, 7250.

(17) Mirzaei, F.; Rezaei, M.; Meshkani, F. *Chem Eng Technol* **2014**, *37*, 973.

(18) Han, J. W.; Kim, C.; Park, J. S.; Lee, H. *Chemsuschem* **2014**, *7*, 451.

(19) Gould, T. D.; Izar, A.; Weimer, A. W.; Falconer, J. L.; Medlin, J. W. *Acs Catal* **2014**, *4*, 2714.

(20) Wu, T.; Cai, W. Y.; Zhang, P.; Song, X. F.; Gao, L. *Rsc Adv* **2013**, *3*, 23976.

(21) Newnham, J.; Mantri, K.; Amin, M. H.; Tardio, J.; Bhargava, S. K. *International Journal of Hydrogen Energy* **2012**, *37*, 1454.

(22) Liu, Z.; Zhou, J.; Cao, K.; Yang, W.; Gao, H.; Wang, Y.; Li, H. *Applied Catalysis B-Environmental* **2012**, *125*, 324.

(23) MacGillivray, L. R.; Atwood, J. L. *Nature* **1997**, *389*, 469.

(24) McKinlay, R. M.; Cave, G. W. V.; Atwood, J. L. *P Natl Acad Sci USA* **2005**, *102*, 5944.

(25) Pan, C.; Pelzer, K.; Philippot, K.; Chaudret, B.; Dassenoy, F.; Lecante, P.; Casanove, M. J. *Journal of the American Chemical Society* **2001**, *123*, 7584.

(26) Zhang, Q.; Tiefenbacher, K. *Journal of the American Chemical Society* **2013**, *135*, 16213.

(27) Muller, O.; Lutzenkirchen-Hecht, D.; Frahm, R. *Rev Sci Instrum* **2015**, *86*.

(28) Ravel, B.; Newville, M. *J Synchrotron Radiat* **2005**, *12*, 537.

(29) Rehr, J. J.; Kas, J. J.; Vila, F. D.; Prange, M. P.; Jorissen, K. *Phys Chem Chem Phys* **2010**, *12*, 5503.

(30) Letzel, M. C.; Agena, C.; Mattay, J. *J Mass Spectrom* **2002**, *37*, 63.

(31) Zhang, Q.; Tiefenbacher, K. *Nat Chem* **2015**, *7*, 197.

(32) Dalgarno, S. J.; Power, N. P.; Warren, J. E.; Atwood, J. L. *Chem Commun* **2008**, 1539.

(33) McKinlay, R. M.; Thallapally, P. K.; Atwood, J. L. *Chem Commun* **2006**, 2956.

(34) Cai, S.; Seu, C.; Kovacs, Z.; Sherry, A. D.; Chen, Y. *Journal of the American Chemical Society* **2006**, *128*, 13474.

(35) Xu, B. Q.; Wei, J. M.; Yu, Y. T.; Li, Y.; Li, J. L.; Zhu, Q. M. *Journal of Physical Chemistry B* **2003**, *107*, 5203.

(36) Zheng, W. T.; Sun, K. Q.; Liu, H. M.; Liang, Y.; Xu, B. Q. *International Journal of Hydrogen Energy* **2012**, *37*, 11735.

(37) Boualleg, M.; Basset, J.-M.; Candy, J.-P.; Delichere, P.; Pelzer, K.; Veyre, L.; Thieuleux, C. *Chemistry of Materials* **2009**, *21*, 775.

(38) Nemeth, M.; Schay, Z.; Sranko, D.; Karolyi, J.; Safran, G.; Sajo, I.; Horvath, A. *Applied Catalysis a-General* **2015**, *504*, 608.

Chapter 4

Summary and Conclusions

The aim of this thesis is to elucidate and understand the elementary reactions of DRM and to use this knowledge in developing highly active and stable catalysts for DRM. Two strategies were applied in this thesis, both focusing on improving the stability of the catalysts against coke formation via enhancing the supply of reactive oxygen species to remove coke form the metal surface.

In the first approach N_2 interruption test is applied to study the effect of coke deposition on the stability of DRM catalyst. Sintering of nickel particles has only slight effect on the reaction behavior, while the accumulation of inactive coke plays a role in the stability of DRM catalysts.

Then, we have studied the effect of nature and geometrical properties of metal particles and their interaction with the support on the dry reforming of methane (DRM) activity. The activity of Ni/ZrO_2 catalysts for DRM can be significantly enhanced and catalyst's thermal stability can be improved by activation and regeneration in presence of CO_2 above 873 K. After reduction in H_2, Ni particles are partly covered with Zr-suboxides. The exposure to CO_2 reduces the coverage by Zr-suboxides and creates a larger ZrO_2-Ni interface. Thus, compared to the direct CO_2 dissociation on metallic nickel, CO_2 treatment leads to an additional channel of CO_2 dissociation in addition to the direct CO_2 dissociation on Ni. The higher kinetically controlled availability of atomic oxygen on Ni is hypothesized to reduce the carbon concentration on the surface, leading to less refractory carbon deposition. In comparison to exposure to O_2, CO_2 treatment leads to a fast, but thermally less taxing oxidation of carbon deposits.

In the second approach, two pathways for H reactions were observed on ZrO_2 supported nickel catalysts, corresponding to the recombination of H species on metal surface to form H_2 and reaction of H species with surface oxygen species at the interface between Ni and ZrO_2 to form H_2O. It was shown that H_2 formation over Ni/ZrO_2 in DRM occurs on metallic Ni surface that easily blocked by cokes

while H_2O formation takes place dominantly on a different site that is hardly affected by cokes.

Subsequently, particle size threshold for stable DRM catalysts was estimated using hemispherical-shaped model. We hypothesize that the fractions of perimeter remains 100 % for the Ni particles with size of 1 nm. The carbon removal reaction can be thus facilitated by decreasing metal particle size.

Using this knowledge, a strategy was developed to synthesize stable catalysts for DRM reaction. The new method uses Ni and Pt colloids as metal precursor on a metal-oxide as support. Ni and Pt particles with size of 1-2 nm were dispersed on SiO_2, Al_2O_3 and ZrO_2. ZrO_2 supported Ni and Pt catalysts exhibited stable activities for more than 2 days of DRM reaction at 873 K, with only small amounts of coke deposited on the catalysts. ZrO_2 supported metal catalysts with small particle sizes, which have large metal-support interface, kinetically inhibit the deposition of inactive coke and allow to stabilize the catalysts during the DRM reaction.

Finally, the particle size threshold for stable DRM catalysts was proved by kinetic measurements. 1 wt% Ni/ZrO_2 has nearly 100 % of perimeter nickel and metallic nickel was highly accessible to surface O generated by CO_2 activation, leading to a fast removal of carbon deposition in the vicinity of Ni and ZrO_2.

Overall, the results show that (inexpensive) Ni can be also successfully used as catalyst in methane dry reforming, when metallic nickel are well dispersed on oxide supports with high oxygen storage capacity and oxygen species mobility.

In the future, we would like to further improve these methods to meet the requirement for industrial application including higher reaction temperature and pressure. Furthermore, combination of these two methods to synthesize a CO_2 treated catalyst with small metal particles to reach a higher activity and stability is under development.

Chapter 5

Zusammenfassung und Folgerungen

Das Ziel dieser Arbeit is es, die Elementarreaktionen von DRM aufzuklären und zu verstehen und anhand der erworbenen Erkenntnisse hochaktive und stabile Katalysatoren zu entwickeln. In dieser Arbeit wurden zwei Strategien angewendet, die sich beide auf die Verbesserung der Stabilität der Katalysatoren gegen die Koksbildung durch die Erhöhung der Zufuhr von reaktiven Sauerstoffspezies zur Entfernung von Koks auf der Metalloberfläche konzentrieren.

Im ersten Ansatz werden N_2-Unterbrechungstests angewandt, um den Einfluss der Koksablagerung auf die Stabilität des DRM-Katalysators zu untersuchen. Das Sintern von Nickelpartikeln hat nur eine geringe Auswirkung auf das Reaktionsverhalten. Die Anreicherung von inaktivem Koks spielt eine wichtige Rolle für die Stabilität von DRM-Katalysatoren.

Wir haben die Auswirkung der Beschaffenheit und Form der Metallpartikel und ihrer Wechselwirkung mit dem Träger auf die Aktivität der Trockenreformierung (DRM) untersucht. Die Aktivität und die thermische Stabilität des Ni/ZrO_2-Katalysators für DRM kann durch Aktivierung und Regeneration in Gegenwart von CO_2 bei einer Temperatur von über 873 K signifikant gesteigert und verbessert werden. Nach der Reduktion in H_2 werden die Ni-Partikeln teilweise mit Zr-Suboxiden bedeckt. Die CO_2-Behandelung reduziert die Bedeckung mit Zr-Suboxiden und führt zur einer größeren ZrO_2-Ni-Grenzfläche. Im Vergleich zur direkten CO_2-Dissoziation auf metallischem Nickel eröffnet die CO_2-Behandlung zu einem zusätzlichen Reaktionspfad der CO_2-Dissoziation über Ni. Es wird vermutet, dass die höhere kinetisch gesteuerte Verfügbarkeit von atomarem Sauerstoff auf Ni die Kohlenstoffkonzentration auf der Oberfläche reduziert, was zu weniger Kohlenstoffablagerungen führt. Im Vergleich zur Einwirkung von O_2 führt die CO_2-Behandelung zur einer schnellen, aber thermisch weniger strapazierenden Oxidation von Kohlenstoffablagerungen.

In einem weiteren Ansatz werden zwei Reaktionspfade für den Wasserstoffverbrauch auf ZrO_2-geträgerten Nickelkatalysatoren beobachtet, die der Rekombination von H-Spezies auf der Metalloberfläche unter Bildung von H_2

und der Reaktion der H-Spezies mit Oberflächen-Sauerstoffspezies an der Grenzfläche zwischen Ni und ZrO_2 unter Bildung von H_2O entsprechen. Es wurde gezeigt, dass die H_2-Bildung auf Ni/ZrO_2, die auf der metallischen Ni-Oberfläche auftritt, leicht durch Koks blockiert wird. Jedoch Die H_2O-Bildung erfolgt hauptsächlich an anderen Zentren, die kaum von Koks beeinflusst werden.

Anschließend wurde der Schwellenwert der Teilchengröße für stabile DRM-Katalysatoren unter Verwendung eines hemisphärischen Modells abgeschätzt. Wir nehmen an, dass der Anteil von Ni an der Grenzfläche 100 % beträgt, wenn die Ni-Partikelgröße einen Wert von 1 nm nicht überschreitet. Die Entfernung von Kohlenstoff kann somit durch die Verringerung der Metallpartikelgröße erleichtert werden.

Anhand dieser Erkenntnisse wurde eine Strategie entwickelt, um stabile Katalysatoren für die DRM-Reaktion zu synthetisieren. Die neue Methode verwendet Ni und Pt-Kolloide als Metallvorläuferverbindungen, die auf einem Metalloxid geträgert wurden. Ni und Pt-Partikeln mit einer Größe von 1-2 nm wurden auf SiO_2, Al_2O_3 und ZrO_2 dispergiert. ZrO_2-geträgerte Ni und Pt-Katalysatoren zeigten eine stabile DRM-Aktivität bei 873 K für mehr als 2 Tage, wobei nur geringe Mengen von Koks auf den Katalysatoren abgeschieden wurden. ZrO_2-geträgerte Metallkatalysatoren mit kleinen Teilchengrößen und einer großen Metall-Träger-Grenzfläche inhibieren die Abscheidung von inaktivem Koks kinetisch und ermöglichen die Stabilisierung der Katalysatoren während der DRM-Reaktion.

Schließlich wurde der Schwellenwert der Partikelgröße für stabile DRM-Katalysatoren durch kinetische Messungen nachgewiesen. Wenn der Anteil on Nickel an der Grenzfläche zwischen Ni und ZrO_2 100 % beträgt, ist das metallische Nickel für die Oberflächensauerstoffspezies, die durch die Aktivierung von CO_2 erzeugt wurde, sehr gut zugänglich, was zu einer schnellen Entfernung der Kohlenstoffablagerung in der Umgebung von Ni und ZrO_2 führt.

Insgesamt zeigen die Ergebnisse, dass (kostengünstiges) Ni auch erfolgreich als Katalysator in der Methan-Trockenreformierung eingesetzt werden kann, wenn metallisches Nickel fein dispergiert auf Oxidträgern mit hoher Sauerstoffspeicherkapazität und hoher Mobilität der Sauerstoffspezies vorliegt.

In Zukunft möchten wir diese Methoden weiter verbessern um den industriellen Anforderungen einschließlich höhere Reaktionstemperatur und –druck gerecht zu werden. Weiterhin befindet sich eine Kombination dieser beiden Methoden zur Synthese eines mit CO_2 behandelten Katalysators mit kleinen Metallpartikeln in der Entwicklung um eine höhere Aktivität und Stabilität zu erreichen.

Curriculum Vitae

Name: Yu Lou
Birth: 10.07.1986 in Zhejiang, PR China

Education

Since 11/2012 **PhD study** in faculty of technical chemistry II, Technical University of Munich (TUM)
Topic: „*Dry reforming of natural gas to produce synthesis gas*“

04/2009 - 05/2012 **Master's Degree** at the Technical University of Munich (TUM)
Major subject: Organic Chemistry
Secondary subject: Analytic Chemistry
Degree: Master of Science (Grade 1.7)

Master-Thesis at the Technical University of Munich (Grade 1.3)
Topic: „*Phenyl ether bond cleavage and hydrodeoxygenation of bio-derived phenolic dimer* “

08/2008 - 02/2009 **German course in China**
Certificate: German language examination for university entrance
Level 2 (DSH-2)

09/2004 - 07/2008 **Bachelor study** in the college of chemistry, Zhejiang University, China
Degree: Bachelor of Science (Grade 85 in 100)

Bachelor-Thesis: „*Regioselective routes to disubstituted dibenzo crown ether*“

Practical Experiences

Since 11/2012 **Scientific research assistant** in faculty of technical chemistry II, Technical University of Munich (TUM)
Activities:

- Preparation, testing and characterization of catalysts for dry reforming of methane with special laboratory and analytical devices (TPD, TPR, BET, XRD, IR and UV-Vis spectroscopy, GC, GCMS)
- Internal and external presentation of research results
- Supervision of laboratory practical course, individual research internships and dissertations of chemistry and chemical engineering students

- Responsibility for TPD measurements and maintenance of test equipment
- Successful participation in the "Fundamental Aspects and Common Principles of Catalysis" course of the South German Catalysis Institute

01/2013 - 12/2015 **Participation in the EU project** with the aim of converting natural gas into synthesis gas.

Activities:

- Cooperation with research groups from Vienna and Budapest
- Characterization and testing of new materials synthesized within the framework of EU project
- Discussion and planning of new strategies

04/2010 - 12/2010 **Research assistant** in faculty of technical chemistry II, Technical University of Munich (TUM)

Topic: Methanol to olefins (MTO) reaction over acidic zeolite (ZSM-5) or zeotype materials

List of Publications

Journals

M. Steib, Y. Lou, A. Jentys and J. A. Lercher * *"Carbon dioxide induced surface restructuring of Ni/ZrO_2 to enhance activity in methane reforming", to be submitted*.

Y. Lou, M. Steib, Y. Liu, Q. Zhang, K., A. Jentys and J. A. Lercher * *"Stable Nickel based catalysts for dry reforming of methane", to be submitted*

Oral Presentations

Y. Lou, M. Steib, A. Jentys and J. A. Lercher, Formation of highly active surface species induced by CO_2 on Ni/ZrO_2 in methane dry reforming, ACS Meeting 2016 (lecture).

A. Jentys, Y. Lou, M. Steib and J. A. Lercher, CO_2 induced formation of highly active surface species on Ni/ZrO_2 in methane dry reforming studied by operando XAFS, International Conference on Catalysis 2016 (lecture)

Poster presentations

Dry reforming – from understanding the elementary steps to better catalysts
Y.Lou, A. Jentys, J.A. Lercher, 47. Jahrestreffen Deutscher Katalytiker, Weimar 2014

Development of stable nickel and platinum catalysts for dry reforming of methane

Y.Lou, M.Steib, A. Jentys, J.A. Lercher, 48. Jahrestreffen Deutscher Katalytiker, Weimar 2015

Ni and Pt colloids as metal precursor for highly stable methane dry reforming catalysts
Y.Lou, A. Jentys, J.A. Lercher, 49. Jahrestreffen Deutscher Katalytiker, Weimar 2016